The Role of Sorcin in Excitation-Contraction Coupling

in Normal and Diseased Hearts

by

Xi Chen

A dissertation submitted in partial fulfillment
of the requirements for the degree of
Doctor of Philosophy
(Molecular and Integrative Physiology)
In the University of Michigan
2018

Doctoral Committee：

Professor Hector H. Valdivia, Chair
Associate Professor Justus M. Anumonwo
Associate Professor Anatoli N. Lopatin
Professor Leslie Satin
Associate Professor Margaret V. Westfall

Xi Chen

xichenum@umich.edu

ORCID iD: 0000-0002-9445-3240

ACKNOWLEDGEMENT

I would like to present my deepest gratitude to Professor Hector H. Valdivia, for his guidance and encouragement in my PhD period. Six years ago, Professor Valdivia welcomed me to his lab and opened the door of scientific research. Not only does he provide me strong technical and intellectual support in research, but also teaches me how to think critically and independently. Professor Valdivia's rigorous academic attitude will always inspire me in my future academic career.

I would like to thank my committee members (Drs. Anumonwo, Lopatin, Satin, and Westfall), who provide valuable guidance and feedback to my project. Their profound knowledge in cardiology and electrophysiology greatly improves the quality of the project, and sharpens my mind.

Thanks to the Department of Molecular & Integrative Physiology. The atmosphere of the department is active, free, and equal, which provides desirable environment for students to grow. The rigorous and well-structured training of the PhD program enables me to realize the frontiers of biology research in a variety of areas, and has greatly improved my presentation, writing, and critical thinking abilities. Thanks to the former and present chairs of the PhD program, Professor Scott Pletcher, Suzanne Moenter, and Daniel Michele, who always give me kind guidance and help.

My thanks also go to excellent collaborators of Valdivia lab and Center for Arrhythmia Research, including but not limited to Drs. Carmen Valdivia, Yanting Zhao, Jonathan Hernandez, Liang Xiao, Roberto Ramos, Emmanuel Camors, Cicero Willis, Yan Chen, Nulang Wang, and Jiang Jiang. Everyone is the expert in the field, and is kind to help.

Finally, I would like to express my deepest love to my parents (Wancheng Chen and Yuling Zhang), my husband (Ran Tao) and our daughter (Samantha JX. Tao). Thanks for your continuous support, encouragement, and love.

TABLE OF CONTENTS

LIST OF FIGURES

LIST OF ABBREVIATIONS

$[Ca^{2+}]_i$	intracellular Ca^{2+}
AP	action potential
APD	action potential duration
AW	anterior wall
BAPTA	1,2-bis(o-aminophenoxy)ethane-N,N,N’,N’-tetraacetic acid
BVT	bidirectional ventricular tachycardia
CaMKII	Ca^{2+}/calmodulin-dependent protein kinase II
CPVT	catecholaminergic polymorphic ventricular tachycardia
CRU	Ca^{2+} release unit
DAD	delayed afterdepolarization
EAD	early afterdepolarization
e-c coupling	excitation-contraction coupling
ECG	electrocardiogram
EGTA	ethylene glycol-bis(β-aminoethyl ether)-N,N,N',N'-tetraacetic acid
V_m	membrane potential
E_{NCX}	reversal potential of NCX

FDHM	full duration at half maximum
FWHM	full width at half maximum
KO	knock out
LTCC	L-type Ca^{2+} channel
NCX	Na^{+}-Ca^{2+} exchanger
PKA	protein kinase A
PKG	protein kinase G
PLN	phospholamban
P_o	open probability
PVC	premature ventricular contractions
PW	posterior wall
RyR2	ryanodine receptor type 2
SERCA	sarcoplasmic reticulum/endoplasmic reticulum Ca^{2+} ATPase
SR	sarcoplasmic reticulum
TAC	transverse aortic constriction
VT	ventricular tachycardia
WT	wild type
I-V curve	current-voltage relationship curve

ABSTRACT

Sorcin, a penta-EF hand Ca^{2+}-binding protein, is known to interact with cardiac ryanodine receptors type 2 (RyR2) and other Ca^{2+} regulatory proteins, including the L-type Ca^{2+} channel (LTCC), Na^{+}-Ca^{2+} exchanger (NCX), and sarcoplasmic/endoplasmic reticulum-Ca^{2+}-ATPase (SERCA). However, sorcin's influence on cardiac excitation-contraction coupling and its role in the development of cardiac malfunctions are not known. In this study, we generated a sorcin knockout (sorcin KO) mouse model to examine the role of sorcin in intracellular Ca^{2+} handling and its potential role in disease pathogenesis. Sorcin KO mice had no cardiac structural alterations, but had a shorter life span than WT. Chronic stress, which was induced by transverse aortic constriction, significantly decreased the survival rate of sorcin KO mice. Sorcin KO cardiomyocytes presented a high incidence of spontaneous sarcoplasmic reticulum (SR) Ca^{2+} release events under isoproterenol stimulation. As the result, isoproterenol-stimulated young (1-month-old) sorcin KO hearts/cardiomyocytes presented ventricular arrhythmia episodes, depleted SR Ca^{2+}, and impaired contractility. The impaired contractility, however, was rescued in adult (6-month-old) sorcin KO hearts. Sorcin KO hearts of adult, but not young mice developed overexpression of L-type Ca^{2+} channel and Na^{+}-Ca^{2+} exchanger, which enhanced I_{Ca} and I_{NCX}. Although the electrophysiological remodeling of I_{Ca} and I_{NCX} helped to retain SR Ca^{2+} load and heart contractility, it provided favorable substrate for DADs and EADs, leading to sustained ventricular arrhythmia, cardiac arrest, and sudden death in adult sorcin KO mice. Our study demonstrates that the loss of sorcin would impair contractility and further trigger lethal arrhythmias due to generalized Ca^{2+} disturbances and electrophysiological remodeling. The results evidenced the detrimental effect of sorcin's absence in the development of cardiac dysfunction.

CHAPTER I

Introduction: Cardiac excitation-contraction coupling

1.1 Ultrastructure of cardiomyocytes

The heart is a muscular organ which pumps blood throughout the body to meet the metabolic requirements of cells. In humans and mammals, the heart is divided into four chambers: upper left atria, upper right atria, lower left ventricle, and lower right ventricle. Through contraction, the heart pumps blood to the systemic circuit to provide the body oxygen and nutrients (1).

Arranging in organized layers, ventricular cardiomyocytes constitute the two lower ventricles of the heart. Ventricular cardiomyocytes are highly specialized, rod-shaped cells, typically 100~150 μm long and 20~35 μm in diameter. For an efficient coupling of electrical excitation and contraction, a delicate sarcolemma ultrastructural organization is developed in ventricular cardiomyocytes. Transverse tubules (T-tubules), which are finger-like membrane structures, penetrate deep into the cell as an extension of the surface plasma membrane (surface sarcolemma). This folding structure makes up 21-33% of the total sarcolemmal area (2, 3), thus greatly increasing the ratio of plasma membrane area to cell mass. T-tubules provide scaffold structures for anchoring of ion channels. The L-type Ca^{2+} channel, a voltage-gated channel that plays an important role in cardiomyocyte contraction, is highly concentrated in T-tubules. Formamide-induced

detubulation of rat cardiomyocytes leads to a 75% decrease of L-type Ca^{2+} current (I_{Ca}) (4). Considering the ratio of T-tubules to surface sarcolemma (21-33% of the total sarcolemmal area), it can be inferred that Ca^{2+} channel density in the T-tubule is ~9 times higher than that in the surface sarcolemma. Therefore, the structural specialization of T-tubules makes it a Ca^{2+} entry site of cardiomyocytes (Fig. 1A). Besides T-tubules, the sarcolemma also forms flask-shape invaginations called caveolae (5). Varieties of signaling molecules, including scaffolding protein caveolin-3, are enriched in caveolae. Therefore, caveolae serves as a place where incoming and outgoing messengers meet (6).

Another set of intracellular membrane system, the sarcoplasmic reticulum (SR), is present in the cytosol of cardiomyocyte. Serving as a "Ca^{2+} warehouse", the SR stores Ca^{2+} and provides majority of Ca^{2+} needed for myofilament contraction during excitation-contraction coupling (e-c coupling). According to differences in function, shape and location, SR can be classified into longitudinal SR and junctional SR. Longitudinal SR distributes along cardiomyocyte, forming a network that wraps around myofibrils. Highly expressed in longitudinal SR are SR Ca^{2+}-ATPase pumps (SERCA), which pump intracellular cytosolic Ca^{2+} ($[Ca^{2+}]_i$) back to the SR. Junctional SR, in contrast, localizes close to the sarcolemma. The enlarged terminal of the junctional SR, named subsarcolemmal cisterna, forms a junction with either the surface sarcolemmal or T-tubule as a dyad. Ryanodine receptors type 2 (RyR2s), the Ca^{2+}-gated SR Ca^{2+} release channel, are highly expressed in the junctional SR (Fig. 1B) as organized clusters. The narrow space between the surface sarcolemma and junctional SR (less than 15 nm) forms a functional correlation between LTCC and RyR2s during e-c

coupling. In cardiomyocytes, this arrangement usually comes with a stoichiometry of 1 LTCC to 4~10 RyR2s [6].

1.2 Ca^{2+}-induced Ca^{2+} release, Ca^{2+} sparks, and Ca^{2+} waves

The structure of the dyad favors an intimate communication between LTCC and RyR2s, the two key ion channels involved in Ca^{2+}-induced Ca^{2+} release. LTCC consists of four pore-forming α_1-subunits and β, α_2, δ, γ accessory subunits (7). The channel is named as L-type due to its **L**arge conductance (~25 pS in 110 mM Ba^{2+}, compared with ~8 pS of T-type Ca^{2+} channel) and **L**ong lasting activation status (8). I_{Ca} is activated at the membrane potential of -40 mV and reaches a peak at 0~10 mV. At more positive membrane potentials, the open probability (P_o) of LTCC increases but the Ca^{2+} driving force decreases so I_{Ca} is reduced. Therefore, I_{Ca} presents a bell-shaped current-voltage relationship (I-V curve). Under the sustained membrane depolarization, I_{Ca} gradually decreases due to the Ca^{2+}-and voltage-dependent inactivation. The Ca^{2+} entry through LTCC and SR Ca^{2+} release can greatly accelerate the inactivation of I_{Ca}, suggesting Ca^{2+}-dependent inactivation is much faster than voltage-dependent inactivation (9).

Facing the LTCC in the dyad structure are RyR2s, the Ca^{2+}-gated SR Ca^{2+} release channels. The channel gained its name due to its affinity for the plant alkaloid ryanodine, which has excitatory effect on RyR2s at concentration lower than 1 μM, but inhibitory effect at concentration higher than 100 μM (10, 11). As the largest known ion channel, RyR2 is a homotetramer with each subunit at the molecular size of 560 kDa. In electron micrographs, the RyR2 presents mushroom-shaped structure. The four S6 transmembrane segments of carboxyl-terminus form the ion conducting pore, allowing

Ca^{2+} to permeate from the SR lumen to the cytosol. The nine domains of each protomer in cytosol side form a superhelical assembly, which interacts with the neighboring super spiral to form the cytosolic region of RyR2 (12-14) (Fig. 2). Varieties of ligands, including Ca^{2+}, protein kinase A, Ca^{2+}/calmodulin-dependent protein kinase II, FKBP 12.6, S100A, and sorcin, bind to the cytosolic region of RyR2 to modulate the gating of the channel. Among those, Ca^{2+} is the most potent regulator by binding to the cytosolic or lumen side of RyR2. The RyR2 activity vs. Ca^{2+} concentration plot is bell-shaped: Ca^{2+} activates RyR2s at the range of 0.1 to 10 μM but inactivates RyR2s at the concentration higher than 100 μM. The affinity and cooperativity of Ca^{2+} binding to RyR2 sites are greatly influenced by the posttranslational modification of the channel (phosphorylation, oxidation, and nitrosylation) and the presence of other modulators (Mg^{2+}, ATP, H^{+}). For complete RyR2 inactivation, a supraphysiologic Ca^{2+} concentration (1~3 mM) is required (15-17), which makes the $[Ca^{2+}]_i$-dependent inactivation of RyR2 unlikely be a major mechanism for the termination of e-c coupling.

In each heartbeat, the action potential propagates to the T-tubules of ventricular cardiomyocytes and activates the voltage-gated LTCCs. The Ca^{2+} influx through the LTCCs raises the dyad $[Ca^{2+}]$ to a level high enough to activate at least one of RyR2s in the cluster. The release of Ca^{2+} through activated RyR2 further recruits neighboring RyR2s, leading to a local Ca^{2+} release event. Synchronized by the action potential, local Ca^{2+} release events turn to a global massive Ca^{2+} release from SR, which is observed as an overall Ca^{2+} transient. This Ca^{2+}-induced Ca^{2+} release process dramatically increases the whole cell $[Ca^{2+}]_i$ from 100 nM to ~1 μM, and leads to contraction of myofilaments.

The local Ca^{2+} release can also happen spontaneously without I_{Ca}. In an unstimulated cardiomyocyte loaded with the fluorescent Ca^{2+} indicator Fluo-4, local Ca^{2+} releases can be observed as "Ca^{2+} sparks" (Fig. 3A-B). The diameter of a Ca^{2+} spark is confined to ~2.0 μm. The fluorescence intensity of a spark peaks to ~2 fold of background level within 10 ms, and gradually decays within 20 ms (Fig. 3C). Due to the stochastic opening of RyR2s, Ca^{2+} sparks appear randomly in time and space. The frequency of Ca^{2+} sparks is positively correlated to RyR2-activity, thus the elevation of $[Ca^{2+}]_i$ and SR lumen Ca^{2+} ($[Ca^{2+}]_{SR}$), which increase RyR2 activity, significantly increase the Ca^{2+} spark frequency. Some RyR2 gain-of function mutations (e.g. V2475F (18), R4496C (19), R176Q (20)) could also significantly increase RyR2's sensitivity to cytosol and luminal Ca^{2+}, leading to increased Ca^{2+} sparks in the resting state.

In a normal situation, locally released Ca^{2+} in resting cell quickly dissipates in the cytosol, so Ca^{2+} sparks do not trigger cell-wide Ca^{2+} wave. However, when RyR2s are hyper-activated due to elevated $[Ca^{2+}]_i$, $[Ca^{2+}]_{SR}$, or due to gain of function mutations, Ca^{2+} spreads to the neighboring dyad and is more likely to recruit more RyR2s. Thus, the spatially discrete Ca^{2+} spark develops into a arrhythmogenic Ca^{2+} wave that can propagate along the cell (Fig. 3D).

1.3 Termination of Ca^{2+}-induced Ca^{2+} release and the removal of $[Ca^{2+}]_i$

Theoretically, Ca^{2+}-induced Ca^{2+} release is a self-regenerative process, in which increased $[Ca^{2+}]_i$ keeps stimulating RyR2s to allow more Ca^{2+} release. However, under physiological conditions, Ca^{2+} release during in e-c coupling is quickly terminated, suggesting mechanisms exist to stop the positive feedback. Fabiato et al. propose that

besides the Ca^{2+} activation site, a high-affinity but slow-action Ca^{2+} inactivation site exists in RyR2 (21). While a fast Ca^{2+} stimulus quickly evokes a burst of RyR2-activity, Ca^{2+} also gradually binds to the inactivation site, leading to a slow inactivation of the channel. The refractory period of RyR2s prevents further SR Ca^{2+} release until Ca^{2+} is removed from the dyad. The theory of Ca^{2+}-dependent inactivation, although straight forward and elegant, is not well supported by experiment results, as RyR2s under constitutive Ca^{2+} stimulation are able to be reactivated (22). Moreover, single channel recording shows that $[Ca^{2+}]_i$ needs to be 1~3 mM to inactivate RyR2s, which is hard to be reached during e-c coupling.

Another mechanism for termination of Ca^{2+}-induced Ca^{2+} release is the depletion of SR Ca^{2+}. It has been demonstrated that Ca^{2+} release through RyR2s is terminated once SR Ca^{2+} drops to ~50% of its total (23, 24), although the underlying mechanism is unknown. While some research suggests luminal $[Ca^{2+}]$ directly regulates RyR2 inactivation (25, 26), other work suggests that calsequestrin, a luminal Ca^{2+} binding protein, is required (27, 28). Besides these mechanisms, some Ca^{2+}-regulatory proteins, such as sorcin, also play an active role in the termination of Ca^{2+}-induced Ca^{2+} release. Details will be discussed later in the dissertation.

After Ca^{2+}-induced Ca^{2+} release, Ca^{2+} must be eliminated to drive cell relaxation. Four transporters work synchronously to bring $[Ca^{2+}]_i$ down: SR Ca^{2+} ATPase (SERCA), Na^+-Ca^{2+} exchanger (NCX), Ca^{2+} ATPase, and mitochondrial Ca^{2+} uniporter. Highly expressed in longitudinal SR membrane, SERCA pumps $[Ca^{2+}]_i$ back to the SR at the cost of ATP hydrolysis. The rate of Ca^{2+} pumping by SERCA is regulated by the protein

phospholamban (PLN), which exerts an inhibitory effect on SERCA function. When under β-adrenergic stimulation, phosphorylated PLN is dissociated from SERCA so SERCA pumps at a higher rate to meet the requirement of Ca^{2+} homeostasis. NCX is an antiporter protein driven by the electrochemical gradient across the cell membrane. When the membrane potential (V_m) is negative to the reversal potential of NCX (E_{NCX}= $E_{NCX}=3E_{Na}-2E_{Ca}$, which is ~-60 mV in resting state), NCX works in the forward mode to pump 1 Ca^{2+} out for 3 Na^{+} in. In rabbit (and in human) ventricular cardiomyocytes, the contribution of SERCA, NCX, Ca^{2+}-ATPase and mitochondrial Ca^{2+} uniporter to Ca^{2+} removal is 70%, 28%, 1% and 1% respectively. In rat and mice ventricular cardiomyocytes, the ratio is 92%, 7%, 0.5%, and 0.5%. In summary, SERCA and NCX play predominant roles in Ca^{2+} removal at the end stage of e-c coupling (29).

1.4 Excitation-contraction coupling

The contraction of myofilaments is initiated by the elevation of $[Ca^{2+}]_i$. At low $[Ca^{2+}]_i$, the binding site between actin and cross-bridge of myosin is blocked by troponin and tropomyosin of thin myofilament, so the muscle fiber is in a resting state. Once SR Ca^{2+} release is triggered, the binding of Ca^{2+} to the troponin C in the thin filament causes conformational changes that dissociate troponin from actin and adjust the position of tropomyosin to expose a site on actin which can strongly bind the cross-bridge of myosin. Strong cross-bridge binding to actin uses energy from ATP hydrolysis to initiate a power stroke, which generates a force and/or shortening via sliding of the thin filament within the sarcomere.

In summary, in each heartbeat, excitatory membrane depolarization spreads from the SA node to the ventricular cardiomyocytes. During membrane depolarization, the opening of voltage-gated Ca^{2+} channels allows the influx of a small amount of Ca^{2+}, which triggers massive SR Ca^{2+} release to the cytosol. By binding to the troponin C of the myofilament, free Ca^{2+} triggers the contraction of the myofilament. This process, called e-c coupling, converts the excitatory membrane depolarization originated from the SA node to the mechanical contraction of the cardiomyocyte (29). Because the contractility of the myofilament is sensitive to the concentration of surrounding $[Ca^{2+}]_i$, synchronized SR Ca^{2+} release during e-c coupling is required for efficient ventricular contraction.

1.5 Regulation of excitation-contraction coupling by sympathetic activation

During exercise or under emotional stress, the heart beats at a faster rate and strength to meet the increased metabolic requirements of the body. This process is mediated by the sympathetic stimulation-activated β-adrenergic pathway. During β-adrenergic stimulation, catecholamines (norepinephrine, epinephrine) released from sympathetic nerves and the adrenal medulla bind to β-adrenergic receptors in cardiomyocytes to trigger protein kinase A (PKA)-mediated phosphorylation of LTCC, PLN, RyR2, troponin I, and myosin binding protein C. The phosphorylation of LTCC significantly increases I_{Ca}, which increases Ca^{2+} entry during e-c coupling. Meanwhile, phosphorylation of PLN relieves the protein's inhibitory effect on SERCA, thus increasing SR Ca^{2+} uptake rate and SR Ca^{2+} content. The increased I_{Ca} and SR Ca^{2+} load greatly enhances Ca^{2+} transient amplitudes, exerting an inotropic effect on the

heart (29). The phosphorylation of troponin I accelerates the dissociation of Ca^{2+} from myofilament, exerting a lusitropic effect on heart.

RyR2 is also one of target proteins phosphorylated under β-adrenergic stimulation. It has been reported that β-adrenergic stimulation could accelerate and synchronize RyR2s' response to opening of a single LTCC (30). At least three phosphorylation sites of RyR2, Serine 2808 (S2808), Serine 2814 (S2814) and Serine 2030 (S2030), have been identified. S2814 is exclusively phosphorylated by Ca^{2+}/calmodulin-dependent protein kinase II (CaMKII), which is another downstream kinase activated by the Ca^{2+}/Calmodulin complex in the β-adrenergic signaling pathway. S2030 is exclusively phosphorylated by PKA, and S2808 can be phosphorylated by both PKA and CaMKII. During β-adrenergic stimulation, RyR2s response to extrinsic cues (enhanced I_{Ca} and SR Ca^{2+}) releases more Ca^{2+} into the cytosol. However, whether the direct phosphorylation of RyR2s will bring intrinsic changes to the channel gating is highly controversial. Marks et al. propose that exclusive PKA-phosphorylation at S2808 of RyR2 will dissociate the RyR2 stabilizer, named FKBP 12.6, from RyR2, rendering RyR2 hyperactive during β-adrenergic stimulation. In later studies, they report that mice harboring a non-phosphorylated S2808A mutation have blunted "fight or flight" responses to β-adrenergic stimulation, and are protected from heart failure and arrhythmias due to the prevention of diastolic SR Ca^{2+} leak (31-34). However, several laboratories failed to reproduce key experiments underlying this hypothesis by showing S2808A mice present a preserved response to β-adrenergic stimulation and a normal progression to heart failure as WT (35-37). In fact, single channel recording finds that while PKA stimulation increases the responsiveness of RyR2 to $[Ca^{2+}]_i$, it accelerates

adaptation of RyR2 and brings the channel to a lower steady state (38). In the cellular setting, the effect of RyR2 phosphorylation is reflected as an increased rising rate of the Ca^{2+} transient in response to a given Ca^{2+} entry (I_{Ca}) and SR Ca^{2+} load. Ca^{2+} transient amplitude, however, won't change (39). In contrast to Marks' hypothesis, Shannon and Bers propose that CaMKII, not PKA, mediates β-adrenergic stimulation-mediated SR Ca^{2+} leak (40, 41). Based on these facts, Valdivia proposes a "multi-phosphorylation site model". In this model, residues from 2804 to 2814 constitute a "phosphorylation hot spot" of RyR2, which is targeted by several kinases (PKA, CaMKII, PKG). The change of RyR2 gating is a combined effect of kinases on phospho sites in the hot spot, while the phosphorylation of a single residue has little influence on the channel gating property (42). Due to the divergent observations and controversy, more work is needed to illustrate the role of RyR2 phosphorylation in Ca^{2+} homeostasis.

1.6 Cardiomyocyte Ca^{2+} handles heart rhythm and contractility

Because myofilament contraction could happen as long as there are sufficient Ca^{2+} and ATP, the heart rhythm and contractility are directly influenced by the timing and amount of Ca^{2+} released from SR. When a spontaneous Ca^{2+} release appears between two normal beatings, extra contraction as well as decreased contractility will appear due to Ca^{2+} turbulence.

Role of Ca^{2+} in heart rhythm

Under normal conditions, SR Ca^{2+} release is precisely controlled by the rhythm of the sinus node. However, in some pathological conditions, spontaneous SR Ca^{2+} releases events (Ca^{2+} sparks and Ca^{2+} waves) could happen without an action

potential due to RyR2-hyperactivity and/or SR Ca^{2+} overload. An extra action potential, named delayed afterdepolarization (DAD), or early afterdepolarization (EAD), could be triggered by spontaneous Ca^{2+} release events. DAD happens when the cell is in a resting condition. The elevated diastolic $[Ca^{2+}]_i$ drives NCX to extrude Ca^{2+} out at the expense of letting 3 Na^+. The stoichiometry of the Ca^{2+}-Na^+ exchange (1:3) generates an inward current, which would depolarize the membrane potential and may further trigger an extra action potential once V_m reaches the threshold (43). EAD is more likely to appear in a cell with prolonged action potential duration. In the plateau phase of the action potential, the reactivation of I_{Ca} and I_{NCX} can depolarize the membrane potential and lead to another upstroke before the cell completely repolarizes (44) (Fig. 3E). Both DAD and EAD are able to trigger a synchronized Ca^{2+} wave, thus triggering an extra contraction between two normal beatings (Fig. 3D). The repetition of this altered focal Ca^{2+} turbulence could further lead to tachycardia and ventricular arrhythmias.

A typical example of Ca^{2+}-mishandling triggered arrhythmia is catecholaminergic polymorphic ventricular tachycardia (CPVT), which is an autosomal-dominant inherited cardiac syndrome. Patients with CPVT present no structural remodeling in the heart and have normal heart function in resting state. However when under physical exercise or dramatic emotional stress, patients suffer from polymorphic ventricular arrhythmias, which could develop into cardiac arrest and sudden death. Spontaneous SR Ca^{2+} release in diastole is considered to be the underlying mechanism. As referred above, in cardiomyocytes of CPVT patients,

the Ca^{2+}-activated I_{NCX} depolarizes V_m to the threshold to trigger an arrhythmogenic DAD. More than 160 mutations in *RyR2*, the RyR2 encoding gene, are known to be associated with CPVT. An underlying hypothesis for the hyperactivity of mutant RyR2s (RyR2 gain-of function) includes dissociation of the RyR2 stabilizer FKBP 12.6 (45, 46), a decreased threshold for store-overload induced calcium release (SOICR) (26, 43, 47), and defective interaction between RyR2 interdomains (48). Mutations in *CSQ2*, the calsequestrin encoding gene, could also generate CPVT. Calsequestrin is a luminal Ca^{2+}-binding protein in the SR. By forming a complex with triadin, junctin and RyR2, calsequestrin helps to inhibit RyR2 activity when SR Ca^{2+} concentration is low. When SR Ca^{2+} increases, polymerized calsequestrin dissociates from the complex and effectively binds to SR Ca^{2+} as a Ca^{2+} buffer. Mutations in *CSQ2* could abolish calsequestrin's inhibitory effect on RyR2s during diastole, and reduces its Ca^{2+} binding and buffering capacity. The higher RyR2 activity and SR Ca^{2+} overload, then, would trigger SOICR and arrhythmias in *CSQ2* mutant cardiomyocytes (49, 50).

Role of Ca^{2+} handling in heart failure

As the concentration of $[Ca^{2+}]_i$ surrounding the myofilament directly influences the contractility, $[Ca^{2+}]_i$ mishandling could lead to the syndrome of heart failure. Heart failure is a pathological condition in which the heart contractility is impaired thus cannot pump enough blood throughout the body to meet metabolic requirements. Research has found that there are increased subconductance openings of RyR2s and decreased SERCA function in heart failure cardiomyocytes, which

deplete SR Ca^{2+} and blunt Ca^{2+} transients in e-c coupling (51, 52). Marks' group proposes that the RyR2-S2808 phosphorylation is increased in the failing heart, as the heart is usually under chronic β-adrenergic stress to maintain efficiency and competence. The PKA-mediated RyR2 phosphorylation at S2808, however, could dissociate FKBP12.6 from RyR2, thus increasing the SR Ca^{2+} leak and further deteriorating heart function (33, 53, 54). Wehren's group also proposes that the prevention of CaMK II phosphorylation at S2814 has a protective effect on pressure overload-induced heart failure (55). Although the hypothetical relationship between heart failure and RyR2 phosphorylation is straight forward and attractive, some key tenets cannot be confirmed by other groups (42, 52, 56, 57).

Besides Ca^{2+}'s direct influence on heart contractility, Ca^{2+} mishandling also activates two cardiomyopathy-related signaling pathways, calcineurin-NFAT and CaMK-MEF2 pathway. The downstream gene transcription results in maladaptive structural remodeling, which eventually develops into hypertrophy and congestive heart failure (58, 59).

1.7 Summary

The ultrastructure of T-tubules provides great advantage for cardiomyocytes to convert the excitatory membrane depolarization to Ca^{2+}-triggered myofilament contraction. At the upstroke of the action potential, the opening of voltage-gated Ca^{2+} channels allows influx of a small amount of Ca^{2+}, which triggers massive SR Ca^{2+} release into the cytosol. By binding to troponin C in the myofilament, free Ca^{2+} triggers myofilament

contraction. This process, called e-c coupling, converts the excitatory membrane depolarization originated from the sinus node to mechanical contraction by the cardiomyocyte. After contraction, the majority of $[Ca^{2+}]_i$ is either extruded out of cell by NCX, or recycled back to SR by SERCA.

Ca^{2+} homeostasis determines heart rhythm and contractility. The β-adrenergic stimulation exerts positive inotropic and lusitropic effects on ventricular cardiomyocytes by enhancing Ca^{2+} homeostasis. Ca^{2+} mishandling could result in arrhythmias and heart failure.

As Ca^{2+} plays a crucial role in heart function, the tuning of Ca^{2+} release must be precisely regulated by varieties of proteins, such as FKBP 12.6 (60, 61), S100A1 (62, 63), calmodulin (64), and calsequestrin (27, 28). In this project, I focus on one of Ca^{2+} regulatory proteins, named sorcin.

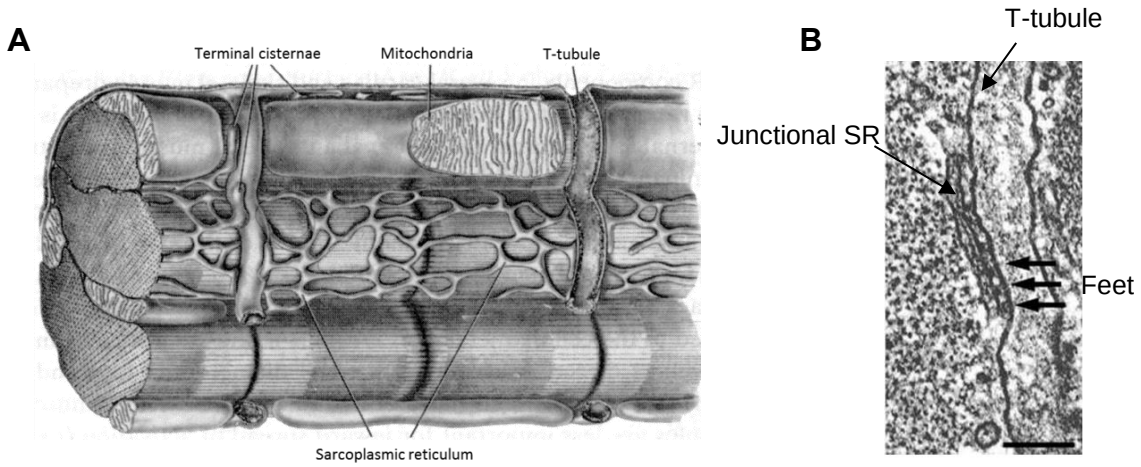

Figure 1.Ultrastructure of mammalian cardiac muscle (8) (65). (A) Surface sarcolemma, T-tubule, and sarcoplasmic reticulum. (B) Dyad formed by a T-tubule and a cisterna of junctional SR.

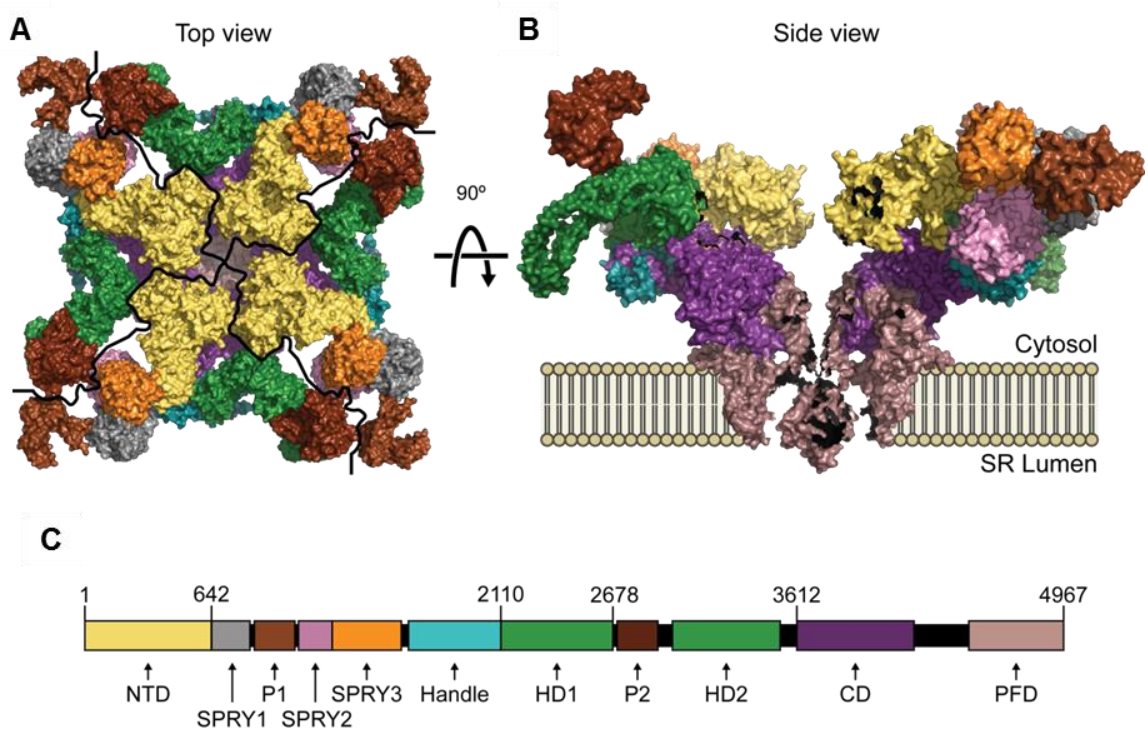

Figure 2. The electron microscopy map of closed RyR2 from porcine heart at resolution of 4.4 Å (12, 66). (A) Top view of closed RyR2. (B) Side view of RyR2. (C) Domain organization of a RyR2 protomer. NTD: amino-terminal domain; SPRY: SPla and the RYanodine Receptor domain; HD: helical domain; CD: central domain; PFD: pore-forming domain. The figure is the courtesy of Francisco J. Alvarado and is drawn based on *Peng, W., et al., Structural basis for the gating mechanism of the type 2 ryanodine receptor RyR2. Science, 2016. 354(6310).*

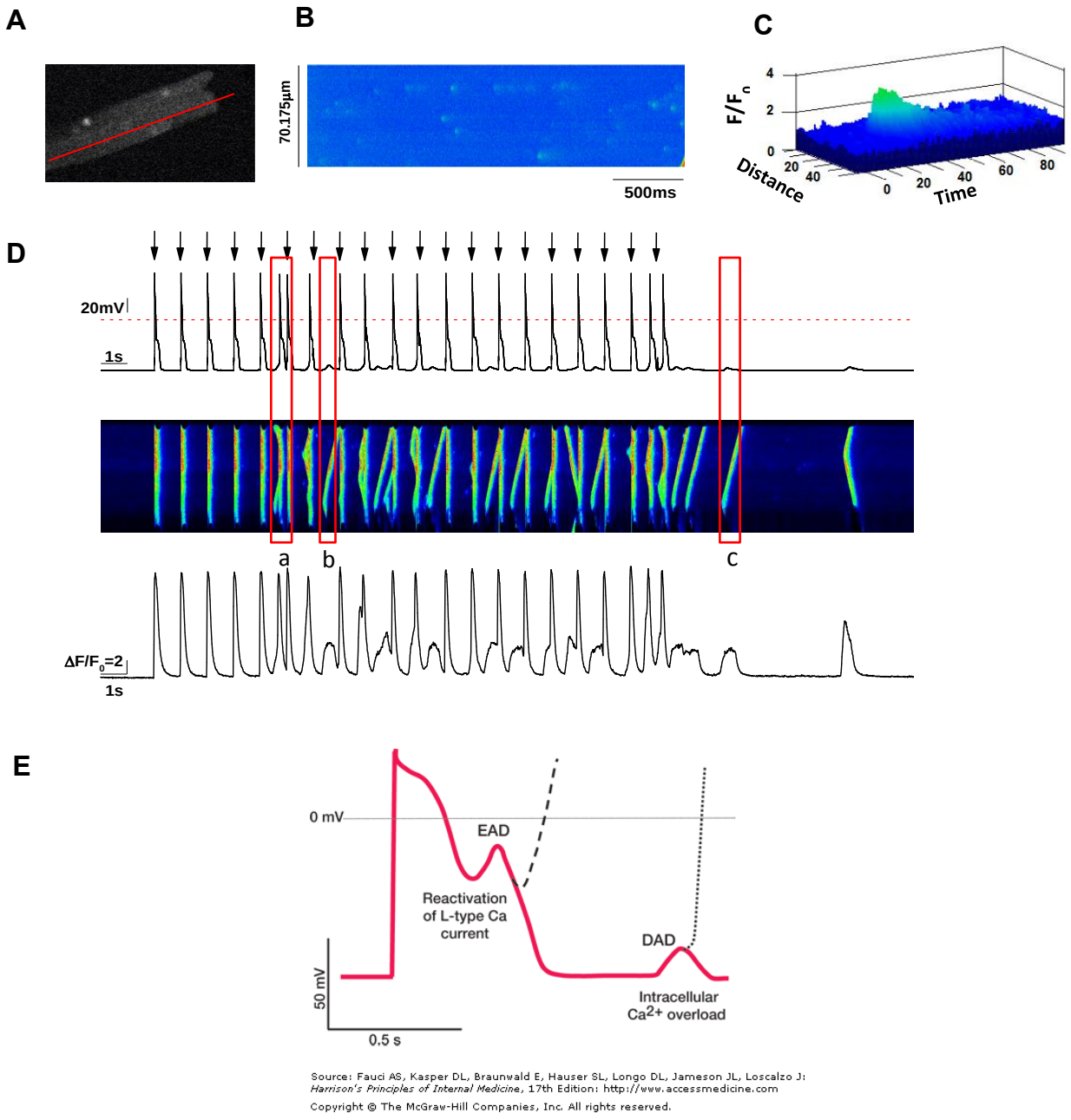

Source: Fauci AS, Kasper DL, Braunwald E, Hauser SL, Longo DL, Jameson JL, Loscalzo J: *Harrison's Principles of Internal Medicine*, 17th Edition: http://www.accessmedicine.com

Figure 3. Ca^{2+} sparks, spontaneous Ca^{2+} waves DADs and EADs. (A) Ca^{2+} sparks observed in a fluo-4 AM loaded cardiomyocyte by confocal microscopy. A line across the cell is chosen to observe Ca^{2+} activities. (B) Ca^{2+} sparks observed in line scan mode. A line is chosen across the cardiomyocyte (shown in figure A) and the Ca^{2+} activity across the line is observed. (C) 3D-plot of a representative Ca^{2+} spark. (D) Spontaneous Ca^{2+} waves and delayed afterdepolarizations observed in a cardiomyocyte with RyR2 CPVT mutation (R4496C+/-). The cell is under current clamp mode and is stimulated by current injection at 1Hz for 20 times (shown as arrow) to trigger action potentials and Ca^{2+} transients. Upper panel: action potential; middle panel: simultaneous fluorescent recording of Ca^{2+} transient; under panel: line plot of Ca^{2+} transient. Square a: a spontaneous Ca^{2+} wave triggers an extra action potential when the cell is fully repolarized (delayed afterdepolarization) (see section 1.6.1). Square b, c: spontaneous Ca^{2+} waves that fail to trigger action potentials during or after pacing. (E) The mechanisms for the generation of DAD and EAD (67). DAD happens when the cell is in resting condition. The elevated diastolic $[Ca^{2+}]_i$ drives NCX to

extrude Ca^{2+} out at the expense of letting Na^{+} in with a stoichiometry of 1:3, thus generating an inward current. The inward current depolarizes membrane potential and could trigger an extra action potential once V_m reaches to the threshold. EAD is more likely to appear in cell with prolonged action potential duration. In the plateau phase of action potential, the reactivation of I_{Ca} and I_{NCX} can depolarize membrane potential and lead to another upstroke before the cell completely repolarized.

CHAPTER II

Sorcin, a Ca^{2+} regulatory protein in cardiomyocytes

2.1 Introduction

Sorcin (soluble resistance-related calcium-binding protein) acquires its name because it is found to be overexpressed in several chemoresistant cell lines, and could be used as a biomarker of multidrug-resistance in several tumors (68-73). Silencing of sorcin by oligonucleotides in tumor cells could increase cell sensitivity to antitumor-drugs, suggesting sorcin is a promising target for reversing tumor multidrug-resistance (74, 75). However, further studies find a broad expression of sorcin in cardiomyocytes, neurons, pancreatic β–cells, and vascular smooth muscle (76-79), clearly transcending its role in multi-drug resistance. The following part will focus on sorcin's effect on cardiomyocytes and heart function. Sorcin's structure, target proteins and role in heart function will be reviewed in this chapter.

2.2 Structural basis of Ca^{2+}-dependent activation of sorcin

Sorcin is a 21.6 kDa protein that belongs to the penta-EF hand protein family (72, 80-82). Two domains, a glycine-rich N-terminal domain and a C-terminal Ca^{2+} binding domain, constitute the sorcin structure (80, 83). The Ca^{2+} binding domain is endowed

with five EF hands organized by eight α-helices (A-H). In physiological condition, sorcin forms a homodimer structure through interaction of EF4-5. EF1-3, which are more flexible than EF4-5, have high Ca^{2+} binding affinity (Kd_{Ca} ~1 μM) (84). The binding of Ca^{2+} to EF3 leads to the movement of three binding ligands, Asp113, Asp115 and Ser117, towards the E helix. As the result, the rigid and long D helix that connects EF2 and 3 undergoes a 21° shift away from the E-helix. EF1 and EF3 are widely opened, while EF2 displays minor movement (Fig. 4).

The opening of EF1 and EF3 upon Ca^{2+} binding makes an increase of 33% of solvent-accessible surface areas. The exposure of hydrophobic residues, including Tyr67, Ser80, Met81, Met86, Ile110, Arg116, Gly118, Ser143 and Ser197, enables sorcin to translocate from cytosol to cellular membranes. In accordance with the structural character, western blot of sorcin in permeabilized mouse cardiomyocytes shows that the percentage of membrane-bound sorcin significantly increases with the elevation of Ca^{2+} (ED_{50}=204 μM Ca^{2+}). Three hydrophobic pockets located in EF1 and EF3 (pocket 1: His108, Met132; pocket 2: Met81, Val101, Trp105, Val164; pocket 3: Ala26, Phe27, Pro28, Pro34, Leu35, Tyr36, Gly37, Tyr38, Ser61, Trp99) play important roles in mediating interactions between sorcin and its target proteins (81, 85).

2.3 Target proteins of sorcin in cardiomyocytes

In cardiomyocytes, sorcin is localized at z-lines that are in close proximity to T-tubules, which enables it to be regulated by the dynamic change of $[Ca^{2+}]_i$ during e-c coupling

(86, 87). Under resting conditions, $[Ca^{2+}]_i$ is at ~100 nM so most of sorcin is soluble in the cytosol close to T-tubules and is inactive. When Ca^{2+}-induced Ca^{2+} release is triggered, local $[Ca^{2+}]_i$ at dyad could theoretically rise to ~100 μM, leading to the binding of free Ca^{2+} to sorcin. The exposure of hydrophobic structure makes sorcin to translocate from cytosol to membrane-bond ion channels, pumps and exchangers, including RyR2, SERCA, NCX, and LTCC.

Sorcin's effect on RyR2

In 1995, Meyers et al. firstly found sorcin is localized at SR of cardiomyocytes. The immunoprecipitation of sorcin pulls down a >500 kDa protein band, which is indistinguishable from the 565 kDa RyR2. The mutation of Trp 105 (W105G) at D-helix of sorcin impairs the binding of sorcin to RyR2 (85), which further confirms the direct interaction of sorcin to RyR2 in cardiomyocytes (76). In single channel recording of a swine cardiac RyR2, recombinant sorcin added in the *cis* (cytosolic) side can significantly decrease the bursting frequency and increase the mean closed time of RyR2 in a dose dependent manner (EC_{50}=480 nM) (Fig. 5A) (88). The binding of radio-labeled ryanodine ([^{3}H]ryanodine) to RyR2s, which only happens when RyR2 is in the open state, is dampened by the appearance of 1 μM sorcin at various $[Ca^{2+}]_i$ concentrations (10^{-4}-10^{-7} M Ca^{2+}), suggesting sorcin prevents open of RyR2s (Fig. 5B) (88). The onset of this inhibitory effect is less than 20ms, which enables sorcin to exert the inhibitory effect on RyR2s on a beat-to-beat basis (86).

Sorcin's effect on SERCA

Sorcin can increase the oxalate-facilitated $^{45}[Ca^{2+}]$-uptake rate of SR vesicle in a dose dependent manner (EC_{50}=520 nM), implying a stimulatory effect of sorcin on SERCA function. In accordance with this observation, SR Ca^{2+} load and decay rate of Ca^{2+} transient are significantly increased in adenovirus-mediated sorcin overexpression rat heart, reflecting higher SR Ca^{2+} pumping rate in appearance of sorcin (89). The exact binding site of sorcin to SERCA, however, is not determined yet.

Sorcin's effect on NCX

The C-terminal Ca^{2+} binding domain of sorcin interacts with Ca^{2+} binding domain 1 and 2 of NCX. The presence of Ca^{2+} binding domain of sorcin could significantly increase the NCX activity, suggesting the importance of this structure in the stimulation of NCX activity and formation of sorcin-NCX complex. The silence of sorcin in rabbit cardiomyocytes by sorcin mRNAi virus transfection leads to significantly lower I_{NCX} compared with control. Also, exogenous sorcin overexpressed in rabbit cardiomyocytes significantly increases I_{NCX}. These results suggest sorcin has stimulatory effect on NCX (90, 91).

Sorcin's effect on LTCC

Sorcin is proposed to have direct interaction with α_{1c} subunit of LTCC via its C-terminal domain. (92). However the effect of sorcin on LTCC is complex and

controversial: while Meyers et al. find that sorcin accelerates Ca^{2+}-dependent inactivation of I_{Ca}, leading to decreased I_{Ca} integral for a given membrane depolarization in mouse cardiomyocytes, Fowler et al. report that sorcin stimulates voltage-dependent inactivation but slows Ca^{2+}-dependent inactivation in rabbit cardiomyocytes (87, 93). It seems that the regulation of sorcin on LTCC is influenced by prevailing recording conditions (use Ca^{2+} or Ba^{2+} as charge carriers; use HEK cells or ventricular cardiomyocytes).

2.4 Sorcin's role in e-c coupling in intact cardiomyocytes and whole heart

The above *in vitro* experiments illustrate sorcin's influence on four important proteins involved in cardiac e-c coupling: RyR2, LTCC, SERCA, and NCX. As RyR2 directly determines Ca^{2+} release from SR, it might be the most prominent molecular target of sorcin during e-c coupling. By influencing the pumping rate of SERCA and NCX, sorcin could alter the SR Ca^{2+} load, thus, indirectly influencing SR Ca^{2+} release. The alter of I_{Ca} inactivation by sorcin could change Ca^{2+} entry, which may have further influences on $[Ca^{2+}]_i$, SR Ca^{2+} release and SR Ca^{2+} load. Due to the complex relationship between sorcin and its target proteins, sorcin's overall effects on e-c coupling in intact cardiomyocytes remain unclear. Previous research tries to answer the question by using sorcin-overexpression animal or cardiomyocytes, but results are highly divergent. Suarez et al. claim a positive role of sorcin in maintaining heart contractility, as adenovirus-mediated 5-fold sorcin overexpression in mice significantly increases the contractility in normal hearts and rescues impaired contractility in diabetic heart (94). In

support of this conclusion, Frank et al. find that adenovirus-mediated 1.7-fold sorcin overexpression in cultured cardiomyocytes and rat heart leads to increased peak force of contraction and fractional shortening (95). However, on the contrary, Farrell et al. find sorcin (3 μM) dialysed into the cell via pipette significantly decreases Ca^{2+} transient amplitude and e-c coupling gain (ratio of Ca^{2+} transient amplitude to I_{Ca}) (86). Meyers el al. observe that the 20-fold sorcin overexpression mouse model decrease the Ca^{2+} transient amplitude compared with WT (87). Seidler et al. show adenovirus-mediated sorcin overexpression in rabbit cardiomyocytes leads to decreased Ca^{2+} transient amplitude and fractional shortening (90). Therefore, it seems that the method, time, and concentration used to expose sorcin to target proteins are critical determinants in the results obtained, and a high concentration of sorcin or its long-term exposure may be deleterious for cell function (94).

2.5 Sorcin's role in the development of heart diseases

As Ca^{2+} triggers contraction of myofilaments, and plays a role in two hypertrophy-related signaling pathways as second messenger, dysfunction of key Ca^{2+}-handling proteins could break the delicate $[Ca^{2+}]_i$ homeostasis and result in impaired heart contractility, hypertrophic cardiomyopathy, or arrhythmia (50, 96-100). Therefore, it is reasonable to suspect sorcin, a potent Ca^{2+} regulator during e-c coupling, can be an important factor in the development of heart diseases. Smith et al. and Matsumoto et al. find decreased sorcin expression in animal models of myocardial infarction and heart failure (89, 101). Meyers et al. observe that in mouse with spontaneous hypertensive

heart failure, the co-localization of sorcin with RyR2s at z-line is greatly disrupted (87). Moreover, a sorcin missense mutation, F112L, is found in two different families with familial hypertrophic cardiomyopathy and hypertension. Located at the end of D-helix, F112 residue is next to three crucial Ca^{2+} binding ligands in EF3, which are D113, D115 and S117. The replacement of larger phenylalanine (7 carbons) to smaller leucine (4 carbons) destabilizes EF3 and tilts EF1. As the result, sorcin with F112L mutation produces a 6-fold decrease of Ca^{2+}-binding ability (102, 103) . In summary, the observations above imply sorcin dysfunction *per se* may associate with cardiac pathologies. However, it is still unknown whether sorcin dysfunction prevents or deteriorates the development of heart diseases.

2.6 Summary

By having RyR2, LTCC, NCX and SERCA as primary targets, sorcin helps to terminate Ca^{2+} release from the SR, and facilitates the re-uptake and extrusion of $[Ca^{2+}]_i$. Thus, we propose a role of sorcin as a cytosolic Ca^{2+} "sweeper" during e-c coupling. However, due to the limitations of research approaches, sorcin's role in e-c coupling in intact cardiomyocytes and its role in heart function of normal and diseased hearts are still unknown.

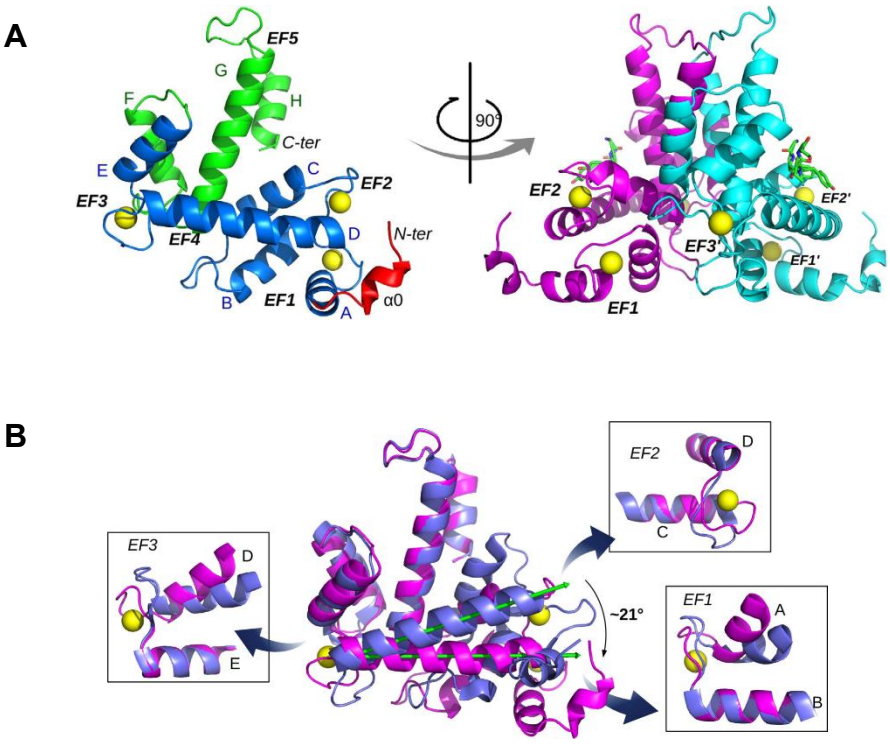

Figure 4. Overall X-ray crystal structure of sorcin (81). (A) A sorcin monomer (left) consists of a glycine-rich N-terminal domain (red) and a C-terminal Ca^{2+} binding domain. The Ca^{2+} binding domain is endowed with five EF hands organized by eight α-helices (A-H). EF1-3 (blue) have high Ca^{2+} (yellow) binding affinity. EF4-5 (green) have interaction of another sorcin and form a sorcin dimer structure (right). (B) The binding of Ca^{2+} to EF1-3 leads to a 21° shift of D helix away from the E-helix. EF1 and EF3 are widely opened in this situation, while EF2 displays minor movement.

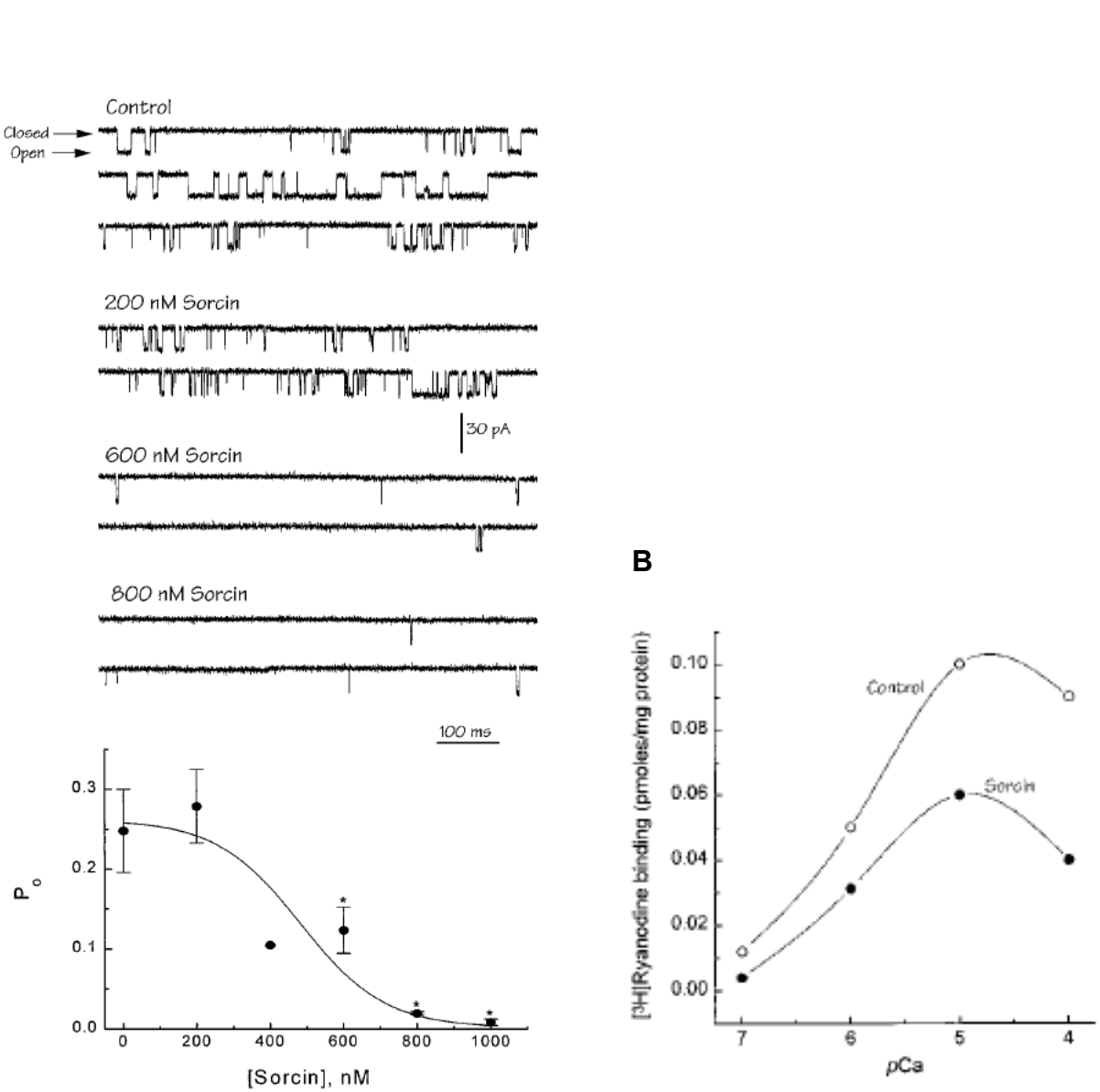

Figure 5. Sorcin inhibits open of RyR2s (88). (A) Sorcin's effect on single RyR2 inserted in artificial lipid bilayer. Recombinant sorcin added in the cis (cytosolic) side of the channel significantly decrease the open probability of RyR2. (B) Sorcin (1 μM) significantly decreases the binding of ^{3}[H]ryanodine to RyR2 at different Ca^{2+} concentrations.

CHAPTER III

Using sorcin knockout mouse model to investigate the role of sorcin in e-c coupling in normal and diseased hearts

3.1 Introduction

Sorcin, a 21.6-kDa Ca^{2+} binding protein originally discovered in multi-drug resistance cells, is also expressed in ventricular cardiomyocytes of mammalian species, including humans (81, 104). We have found that the majority of sorcin is localized in bands of high intensity running along the width of the cardiomyocyte, interspaced at about ~1.7 μm, and overlapping with RyR2 located in *z*-lines (86, 87). Thus, a great portion of sorcin appears localized in the dyadic junction, where crucial steps of e-c coupling occur. Also, using single RyR2 channels or isolated ventricular cells, we have found that sorcin rapidly binds to RyR2 and directly inhibits single channel activity, translocates from soluble to membrane-bound protein targets in a Ca^{2+}-dependent manner, and attenuates Ca^{2+} sparks and Ca^{2+} transients in saponin-permeabilized cardiomyocytes (86). By having RyR2s the as primary target, sorcin helps terminate Ca^{2+} release from the SR, and facilitates the re-uptake and extrusion of $[Ca^{2+}]_i$. Thus, we propose a role of sorcin as a cytosolic Ca^{2+} "sweeper" during e-c coupling in ventricular myocytes. However, there are still two important questions

that remain to be answered. (1) How does sorcin influence e-c coupling in intact cells? As sorcin not only regulates RyR2 channels, but also influences Ca^{2+} entry and SR Ca^{2+} load by interacting with LTCC, SERCA2a and NCX, it is difficult to predict sorcin's global effects in intact systems. Previous research attempted to answer this question by using sorcin-overexpressing animals or cardiomyocytes, however, this approach may not be optimal because the method, time, and concentration used to expose sorcin to target proteins are critical determinants of its function. Also, a high concentration of sorcin or its long-term exposure is shown to be detrimental for cell function (87, 90, 94, 95). Thus, an alternative model is desired to provide novel critical insight into the role of endogenous sorcin in e-c coupling and heart function; (2) What is sorcin's role in the development of heart diseases? As Ca^{2+} triggers contraction of myofilaments, and is linked to two hypertrophy-related signaling pathways as a second messenger, any dysfunction of key Ca^{2+}-handling proteins will break the delicate $[Ca^{2+}]_i$ homeostasis and result in impaired heart contractility, hypertrophic cardiomyopathy (99, 105), or arrhythmia. Therefore, it is reasonable to suspect sorcin, a potent Ca^{2+} regulator during e-c coupling, can be an important factor in the development of heart diseases.

To investigate the role of sorcin in e-c coupling in intact cardiomyocytes and its role in the development of heart diseases, we have generated a sorcin knockout (sorcin KO) mouse by ablating the exon 3 of *Sri*, the sorcin-encoding gene (106, 107). The sorcin KO mouse model enables us to study the role of endogenous sorcin on e-c coupling in intact cardiomyocytes, and to mimic the sorcin loss-of-function mutations

found in patients/models with heart diseases (102). By subjecting the sorcin KO mice to acute and chronic stress, we could explore the role of sorcin in the development of some heart diseases and their underlying mechanisms. In the project, I am exploring: (1) whether the ablation of sorcin will alter the expression and function of other Ca^{2+} regulatory proteins, including RyR2, LTCC, NCX, and SERCA; (2) whether the ablation of sorcin will lead to increased spontaneous Ca^{2+} releases (Ca^{2+} sparks and Ca^{2+} waves), and whether the spontaneous Ca^{2+} releases could influence Ca^{2+} transient amplitude and trigger arrhythmogenic EADs and DADs in sorcin KO cardiomyocytes; (3) heart function and rhythm of sorcin KO mice in normal and stressed condition.

3.2 Generation of sorcin KO mouse

Sorcin KO mouse was generated by ablating the exon 3 of *Sri*, the sorcin-encoding gene (Fig. 6). Portions of the murine *Sri* were obtained by screening the 129SV CITB BAC library (Invitrogen Inc.). A DNA fragment of *Sri* exon 1, 2, 3, 4 was cloned into pBluescriptSK (Stratagene Inc.) that contained the MC1-HSV-TK cassette. To remove exon 3, which is present in both sorcin isoforms (accession no. NM_001080974.2 and NM_025618.3), a mini targeting vector containing a loxP-flanked exon 3 and a loxP-flanked phosphoglycerol kinase (PGK) promoter-driven NEO-pGHpA cassette was generated. The mini targeting vector was transformed into the recombination-competent DY380 bacteria cells that previously transformed pBluescript-Sri-MC1-HSV-TK. Recombinants integrated the loxP-flanked exon 3 and

loxP-flanked pGK promoter-NEO-pGHpA cassettes were selected as targeting vectors. The homologous integration of the mini targeting cassette into pBluescript-Sri-MC1-HSV-TK was confirmed by DNA sequencing.

The targeting vector was electroporated into mouse 129S1/SvImJ ES cells. ES cells integrated the targeting vector were selected by growth on G18. Neor, GANCr clones were picked, expanded, and genomic DNA were isolated from each clone. Correctly targeted colonies, 1C4, 1D12, 1E1, 2B7, 2F5, 2H11, were identified by the appearance of a 2.6k-bp band by using the 32P autoradiogram 5' probe. One euploid clone, 1D12, was microinjected into the blastocyst to produce a chimeric founder. The male chimera was mated with 129S1/SvImJ female (F_0). The FloxNeo-/+ mouse in F1 generation was selected to mate with EIIa-Cre transgenic mice to excise Neo cassette as well as *Sri* exon 3 (F2). Three primers: sorIn3Rev 5'-GAA GGC TGG CAT GGA GTG AAA GCA-3', sorIn2For 5'-CTG ACC TCA GTC AAC CAG TAA GTA GG-3', and Neo 5'-CGT TGG CTA CCC GTG ATA TT-3' were used to determine genotyping of mice. 820-bp from *Sri*, which include exon 3 and neighboring introns, were excised by Cre-Lox recombination. The excision of *Sri* exon 3 as well as Neo cassette was confirmed by a 453-bp band in PCR, which included a 3' loxP site, a remnant 168-bp insertion from the targeting vector and neighboring intron, while WT DNA containing exon 3 presented a 1070-bp band (Fig. 7A). The $Sri^{+/-}$ mice was backcrossed to 129S1/SvImJ mice for 10 generations to eliminate Cre recombinase. Finally two $Sri^{+/-}$ mice were crossed to get the $Sri^{-/-}$ mice. western blot using a sorcin antibody demonstrated complete absence of the 21.6

kDa sorcin band in sorcin KO hearts (Fig. 7B). Crossbreeding of sorcin heterozygous mice yielded offspring with the expected Mendelian ratios of WT (sorcin 22%), heterozygous (sorcin 52%) and homozygous (sorcin 26%) mice.

3.3 Acknowledgement

Dr. Patricia Powers and Emily Farrell (Biotechnology Center of the University of Wisconsin) provided technical support for the generation of sorcin KO mouse colony.

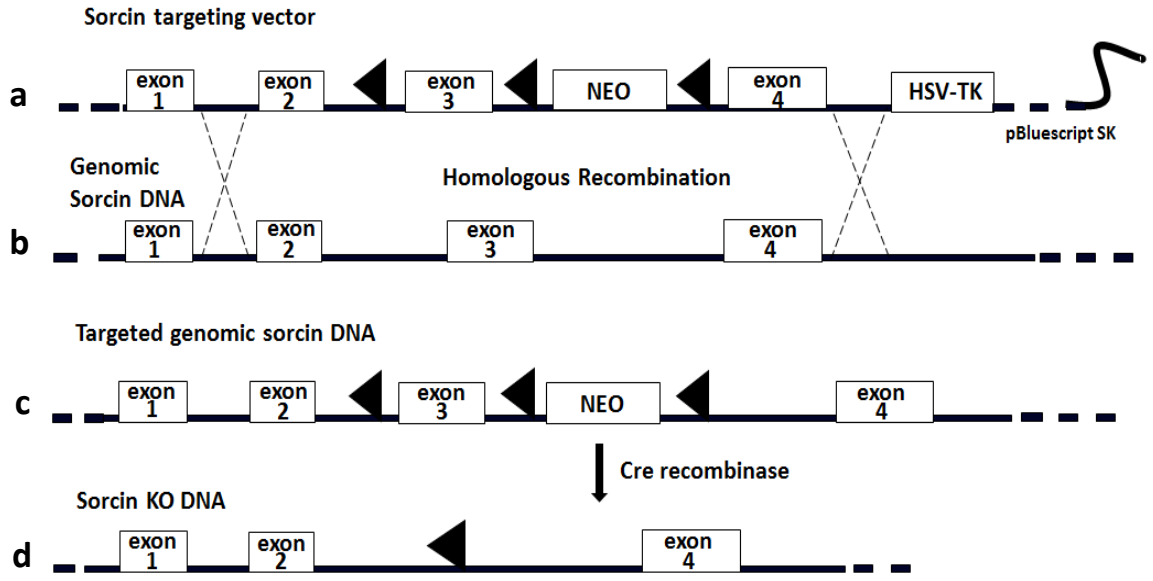

Figure 6. Strategy for the generation of sorcin KO mice by homologous recombination. a. The sorcin targeting vector containing *LoxP*-flanked exon 3 of *Sri*, *LoxP*-flanked Neo-cassette and the HSV-TK cassette; b. WT *Sri* containing seven exons (four exons are shown in graph); c. Homologous recombination between the endogenous *Sri* and sorcin targeting vector results in a DNA carrying *LoxP*-flanked *Sri* exon 3 and Neo-cassette. d. Sorcin KO DNA is created by the Cre-excision of *Sri* exon 3 and Neo-cassette.

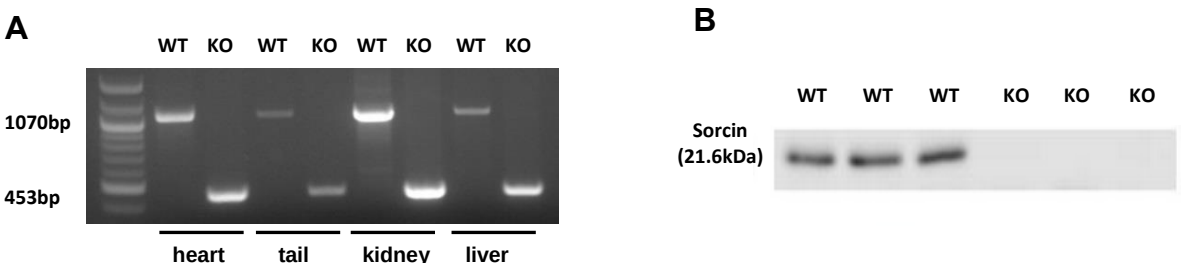

Figure 7. Confirmation of sorcin KO mice. (A) PCR confirmation of WT and sorcin KO mice. Instead of the 1070-bp band seen in WT, a 453-bp band is detected in sorcin KO allele. (B) Western blot with sorcin antibody confirms the presence of sorcin in 3 WT hearts (first three bands) and its absence in 3 sorcin KO hearts.

CHAPTER IV

Arrhythmias and sudden death in sorcin KO hearts and mice under acute or chronic stress

4.1 Introduction

The crossbreeding of sorcin heterozygous mice yielded offspring with the expected Mendelian ratios of WT, heterozygous and homozygous mice, suggesting the ablation of sorcin is not lethal for embryonic development. However, the ablation of sorcin may lead to change of heart rhythm and heart function after the mice are born, as $[Ca^{2+}]_i$ homeostasis is closely associated with heart rhythm and contractility (Chapter I, 1.6). To investigate the role of sorcin in heart function, in Chapter IV and V, I examined the heart structure, life span, electrocardiography (ECG), and heart contractility of sorcin KO mice. Considering the potential influence of age on heart function, both adult (6-month-old) and young (1-month-old) sorcin KO mice are used in the study.

4.2 Normal structure of adult sorcin KO heart

Vertical planes of hearts indicate no structural alterations in adult sorcin KO hearts compared with WT (Fig. 8).

4.3 Lower survival rate of freely-fed and stressed sorcin KO mice

Lifespan of non-manipulated, freely-fed sorcin KO mice was shorter than WT littermates (18-month survival rate: KO 70% vs. WT 92.5%, N=40 in each group; Kaplan-Meier test $p<0.05$) (Fig. 9A), suggesting some problems of adaptation or fragile subsistence in the absence of sorcin. To assess whether the fragility of sorcin KO mice could be exacerbated by chronic stress, we conducted transverse aortic constriction (TAC) to induce pressure overload in adult mice (108). After surgery, the survival rate in sorcin KO mice was significantly lower than that of WT (KO 52% vs. WT 88% after 3 weeks, N=24 in each group, Kaplan Meier test $p<0.01$,) (Fig. 9B). The substantial difference in survival rate indicates that the fragility of sorcin KO mice is exacerbated by TAC

4.4 Ventricular arrhythmias and sudden death in sorcin KO hearts and mice under acute or chronic stress

As both freely-fed and TAC sorcin KO mice presented significantly lower survival rates than WT, we assessed whether cardiac arrhythmias were part of the underlying mechanisms leading to accelerated death. ECG of anesthetized adult mouse was recorded in control state and stressed state, which was induced by intraperitoneal injection of epinephrine 2 mg/kg + caffeine 120 mg/kg (109). Continuous recording of ECG activity showed that, whereas the WT group had few arrhythmic events, 5 out of 6 adult sorcin KO mice presented higher incidence of premature ventricular contractions (PVCs), bidirectional ventricular tachycardia (BVT), and ventricular tachycardia (VT) within 5 min after injection (Fig. 10A-C). One third of sorcin KO mice, but no WT, experienced sudden cardiac arrest during recording (Fig. 10D). The duration of

ventricular arrhythmia was significantly longer in adult sorcin KO mice (356±151 s) than WT (16.6±6.9 s, $p<0.05$). (Fig. 10E), and two sorcin KO mice presented BVT for longer than 1000 s. In agreement with *in vivo* test, freshly explanted and Langendorff-perfused adult sorcin KO hearts displayed increased incidence of PVCs and bigeminy/trigeminy compared to WT hearts (Fig. 11).

Like adult ones, young sorcin KO mice also presented a higher incidence of premature contractions, bigeminy, and bidirectional ventricular tachycardia than WT littermates (Fig. 12A-C). Nonetheless, unlike adult sorcin KO mice that presented stable, long-lasting ventricular tachyarrhythmias (356±151 s), young sorcin KO mice presented short ventricular arrhythmia episodes (19.15±4.44 s, rank-sum test $p<0.05$ vs. adult ones). (Fig. 12D). These results show that sorcin KO mice, while apparently normal under basal conditions, are thrown into ventricular arrhythmias under acute sympathetic stimulation and fare worse than WT when subjected to chronic stress. Therefore, the shorter lifespan and increased TAC mortality of global sorcin KO mice may be due to cardiac alterations.

4.5 Summary

Sorcin KO mice were propagated at the expected Mendelian ratio, presented normal heart structure (Fig. 8), and had normal ECG as WT in resting condition. However, when under acute/chronic stress, sorcin KO hearts/mice presented high incidence of premature ventricular contractions, bidirectional ventricular tachycardia, ventricular tachycardia, and lower survival rate. Therefore, sorcin KO mice are in a delicate but precarious equilibrium under basal conditions. During β-adrenergic stimulation, the

greatly enhanced kinetic of $[Ca^{2+}]_i$ (Chapter I, 1.5) brakes the delicate equilibrium of sorcin KO mice, leading to arrhythmias and sudden death. Sorcin, a potent Ca^{2+} regulator, may play a prominent role in maintaining stable $[Ca^{2+}]_i$ homeostasis in this situation. In the following study, I will investigate the change of $[Ca^{2+}]_i$ homeostasis in sorcin KO cardiomyocytes and its correlation to ventricular arrhythmia.

4.6 Acknowledgement

This chapter includes data generated by Dr. Francisco Alvarado, University of Michigan (ECG recording) and Timothy Hacker, University of Wisconsin (TAC experiments).

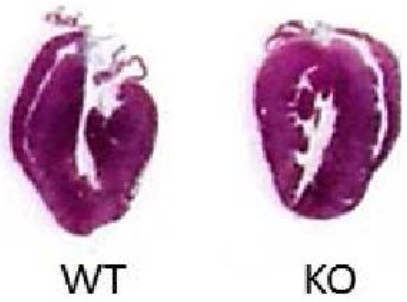

Figure 8. Vertical planes of hearts indicate no structural alterations in sorcin KO heart compared with WT. Left: WT heart; right: sorcin KO heart.

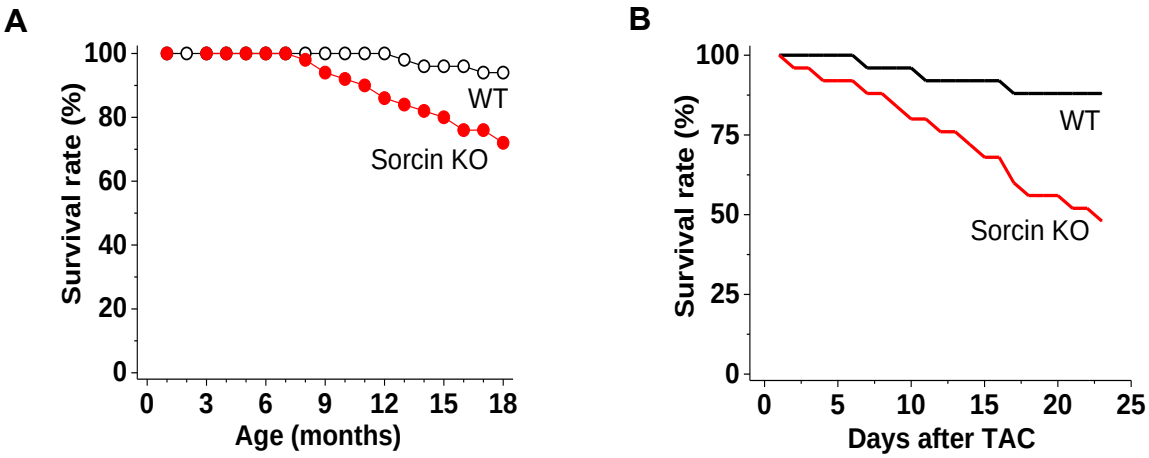

Figure 9. Life span and survival rate of mice. (A) Long-term follow up of lifespan of sorcin KO and WT mice. N=40/group. Kaplan-Meier test $p<0.05$. (B) Survival rate of 6-montho-old mice after the conduction of transverse aortic constriction (TAC) N=24/group. Kaplan-Meier test $p<0.01$.

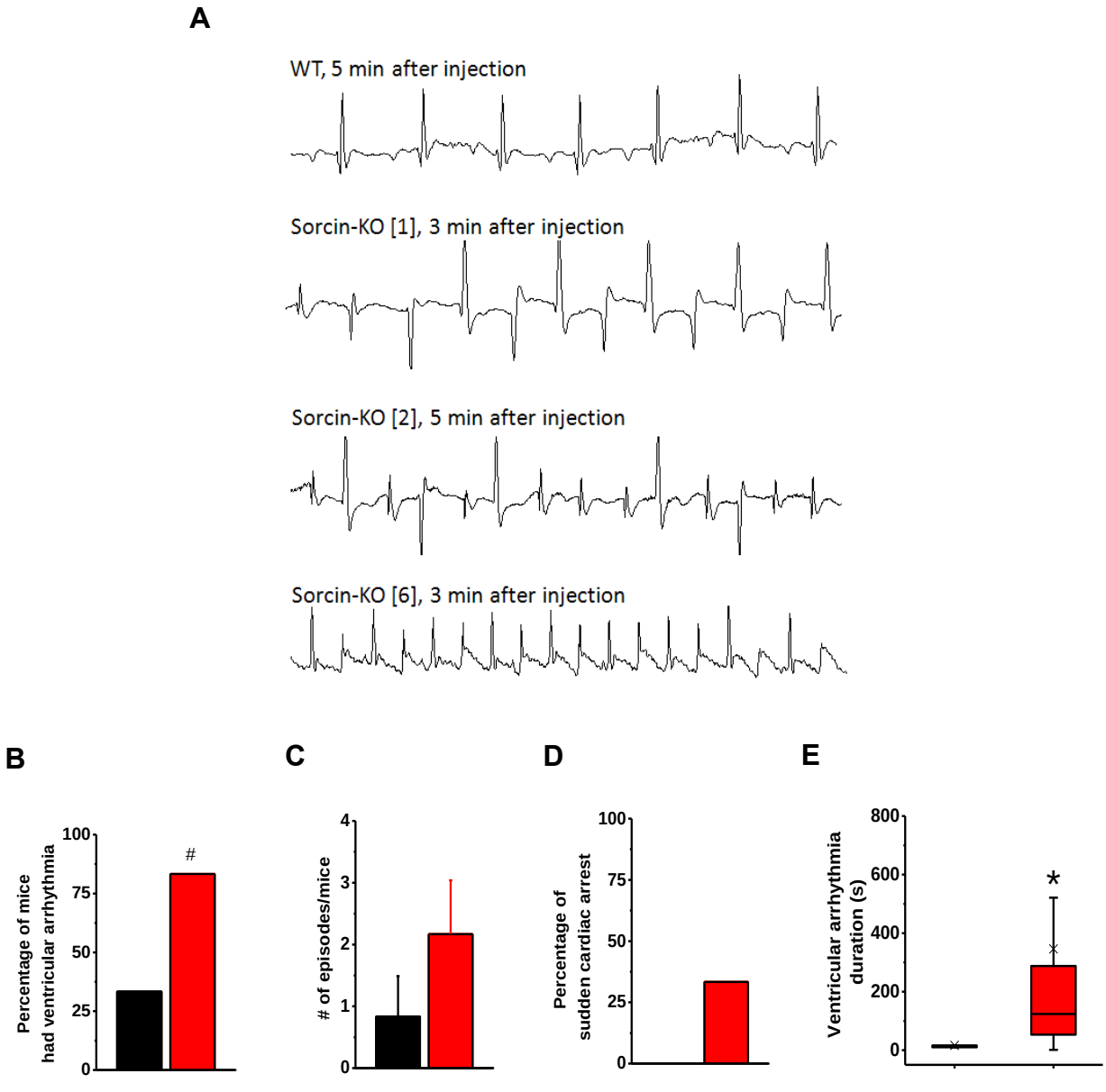

Figure 10. ECG recordings of 6-month-old anesthetized mice after the administration of epinephrine (2 mg/kg) + caffeine (120 mg/kg). (A) First trace: representative ECG of a WT mouse after 5 min of injection; second trace: bidirectional ventricular tachycardia (BVT) in a sorcin KO mouse after 3 min of injection; third trace: premature ventricular contractions (PVCs) in a sorcin KO mouse after 5 min of injection; fourth trace: ventricular tachycardia (VT) in a sorcin KO mouse after 3 min of injection. Each trace is 1s recording. (D) Percentage of mice that had ventricular arrhythmia after injection. (E) Number of ventricular arrhythmia episodes in WT and sorcin KO mice, per arrhythmia cocktail challenge. (F) Percentage of mice that presented sudden cardiac arrest after injection. (G) Duration of arrhythmias in WT and sorcin KO mice. N=6 in each group. ×, average value; *, p<0.05 vs. WT, #, p=0.051 vs. WT (t-test, rank-sum test, χ^2 test).

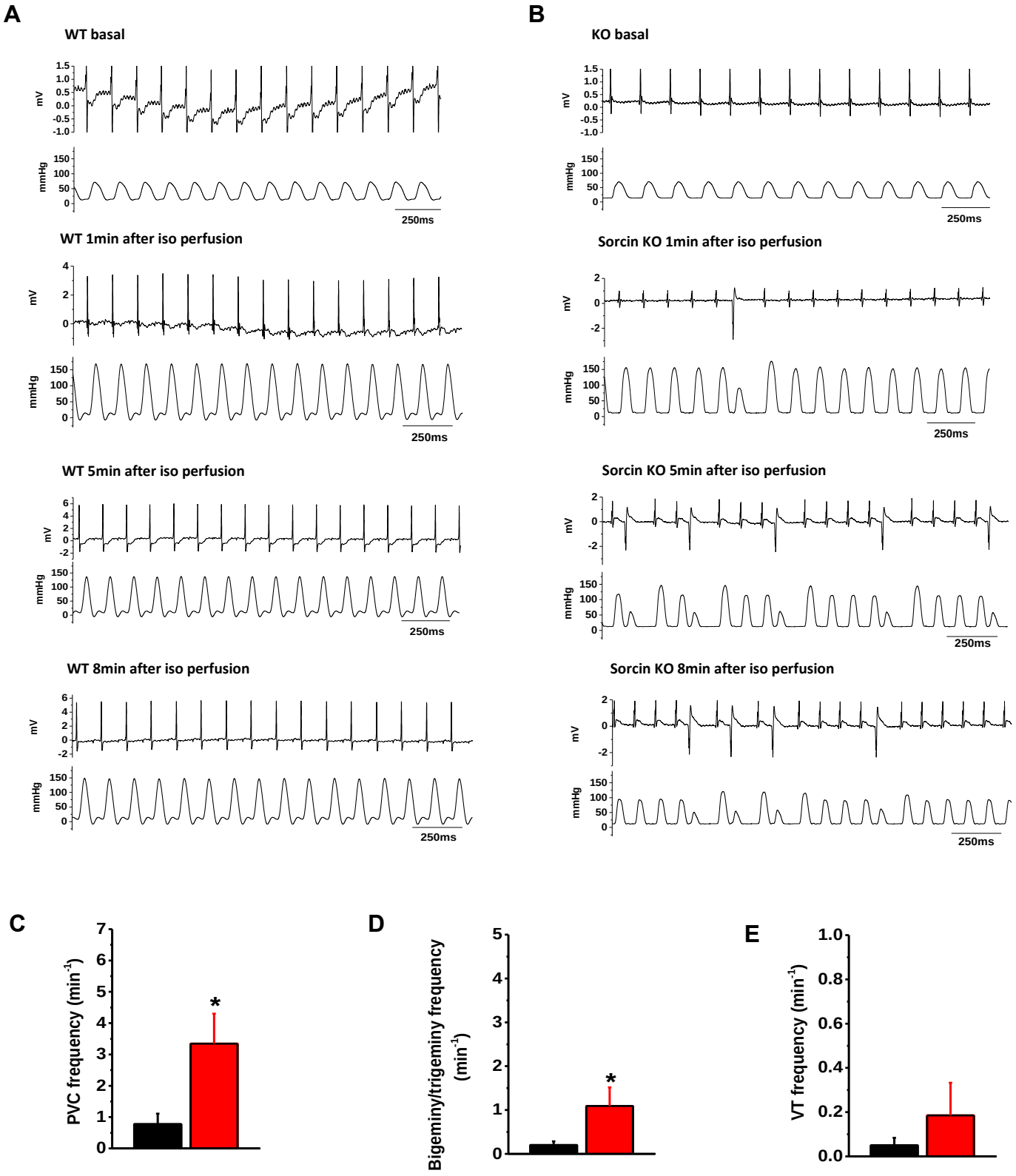

Figure 11. ECG and left ventricular pressure of 6-month-old mice recorded by Langendorff-perfusion. (A-B) Representative ECG and left ventricular pressure of WT (A) and sorcin KO hearts (B) at basal condition and 1, 5, 8 min after isoproterenol perfusion. (C) Frequency of premature ventricular contraction (PVC). (D) Frequency of ventricular bigeminy/trigeminy. (E) Frequency of ventricular tachycardia. N=12 in each group. *, p<0.05 vs. WT (t-test, rank-sum test).

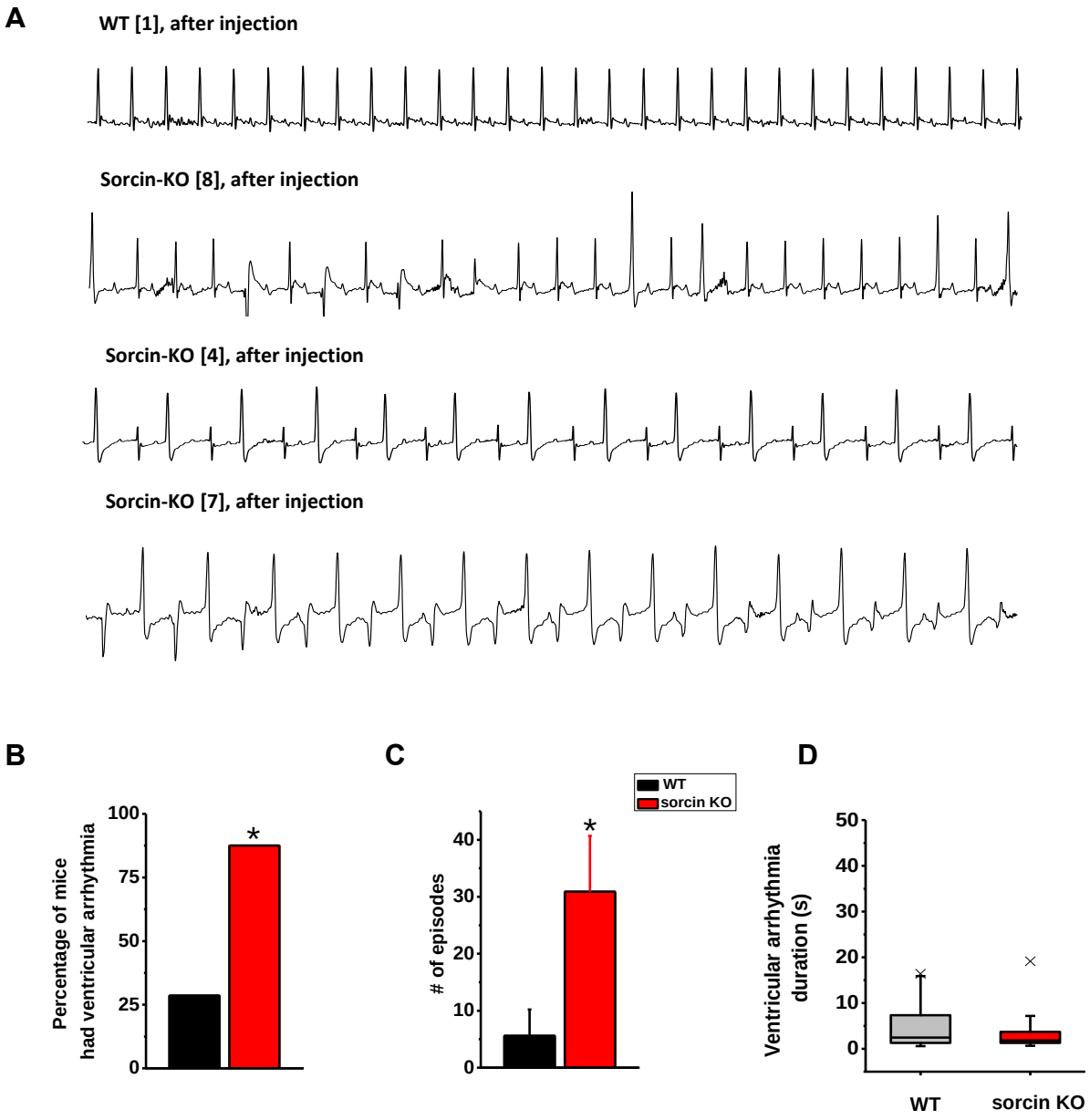

Figure 12. ECG recordings of 1-month-old anesthetized mice after the administration of epinephrine (2 mg/kg) + caffeine (120 mg/kg). (A) First trace: representative ECG of a WT mouse after injection; second trace: premature ventricular contractions in a sorcin KO mouse after injection; third trace: bigeminy in a sorcin KO mouse after injection; fourth trace: bidirectional ventricular tachycardia in a sorcin KO mouse after injection. (B) Percentage of mice that had ventricular arrhythmia after injection. (C) Number of ventricular arrhythmia episodes in WT and sorcin KO mice, per arrhythmia cocktail challenge. (D) Duration of arrhythmias in WT and sorcin KO mice. WT N=7, sorcin KO N=8. ×, average value; *, $p<0.05$ vs. WT (t-test, rank-sum test, χ^2 test).

CHAPTER V

Contractility of sorcin KO hearts

5.1 Introduction

As discussed in Chapter I, $[Ca^{2+}]_i$ homeostasis in cardiomyocytes is closely associated with heart contractility. For efficient heart contraction, synchronized Ca^{2+} release and quick Ca^{2+} sequestration during and after e-c coupling are desired. Therefore, heart contractility is greatly influenced by the activity of LTCC (determines Ca^{2+} entry), RyR2 (determines SR Ca^{2+} release), NCX and SERCA (determine Ca^{2+} reuptake and extrusion). Spontaneous Ca^{2+} release events (Ca^{2+} sparks and Ca^{2+} waves), which happen during diastole due to RyR2-hyperactivity and/or SR Ca^{2+} overload, may also influence heart contractility by influencing SR Ca^{2+} load. As sorcin regulates Ca^{2+} entry (by regulating LTCC), Ca^{2+} release (by regulating RyR2s), and Ca^{2+} reuptake and extrusion (by regulating SERCA and NCX), it may play crucial role in maintaining heart contractility. In this chapter, I evaluated the heart contractility of adult (6-month-old) and young (1-month-old) sorcin KO mice by Langendorff perfusion and echocardiographic recording.

5.2 Preserved heart contractility of 6-month-old sorcin KO mice

Heart contractility was measured by Langendorff perfusion. Hearts from adult WT or sorcin KO mice were quickly excised and cannulated on a Langendorff-perfusion system via the aorta. Hearts were perfused with oxygenated KH solution at 37℃, the heart kept beating during recording. Left ventricular pressure was measured by a pressure transducer-connected balloon placed in the left ventricle (Fig. 13A). Under basal conditions, adult WT and sorcin KO hearts had comparable left ventricular developed pressure, systolic rate (maximum dp/dt) and diastolic rate (minimum dp/dt). When β-adrenergic stimulation was triggered by adding 300 nM isoproterenol, a non-selective β-adrenoreceptor agonist, in KH solution, both adult WT and sorcin KO heart presented significant increases in left ventricular developed pressure, systolic rate, and diastolic rate. As time passed, the contractility gradually went down to a steady level due to the adaptation of RyR2 to isoproterenol. However, the difference between adult WT and sorcin KO hearts before and after (for 10 mins) isoproterenol stimulation was not significant (Fig. 13B-E).

Besides Langendorff perfusion, echocardiography was conducted to measure heart function (Fig. 14) of adult WT and sorcin KO mice before and after TAC surgery. LV mass, posterior wall (PW) thickness, anterior wall (AW) thickness, heart rate, stroke volume and fractional shortening were not significantly different between non-banded WT and sorcin KO mice (Fig. 14, non-banded). After TAC surgery, sorcin KO mice still presented comparable heart function as WT (Fig. 14, banded).

5.3 Decreased heart contractility of 1-month-old sorcin KO mice after isoproterenol stimulation

Then I conducted Langendorff perfusion on 1-month-old WT and sorcin KO hearts. WT and sorcin KO hearts had comparable left ventricular developed pressure, systolic and diastolic rate under basal conditions. At the moment being stimulated by 300 nM isoproterenol, both WT and sorcin KO hearts presented enhanced contractility. However, young sorcin KO hearts gradually presented decreased contractility and slower diastolic rate than WT, and the difference was significant after ~5min of isoproterenol stimulation (Two-way RM ANOVA $p<0.05$ after 5 min of isoproterenol stimulation) (Fig. 15).

5.4 Summary

The Langendorff perfusion reveals that at early age (1-month-old), sorcin KO hearts have decreased contractility when under isoproterenol stimulation. However, as sorcin KO mice grow up, the impaired heart function was rescued by some compensatory mechanisms, so adult sorcin KO hearts presented comparable left ventricular developed pressure and systolic/diastolic rate as WT ones. To confirm the change of heart contractility in sorcin KO hearts at cellular level, I also measured Ca^{2+} transients and SR Ca^{2+} load of adult and young sorcin KO cardiomyocytes, which will be introduced in Chapter VIII. In following chapters, I will investigate the reason that leads to decreased heart contractility in young sorcin KO mice, and the possible compensatory mechanisms that rescue this deficiency.

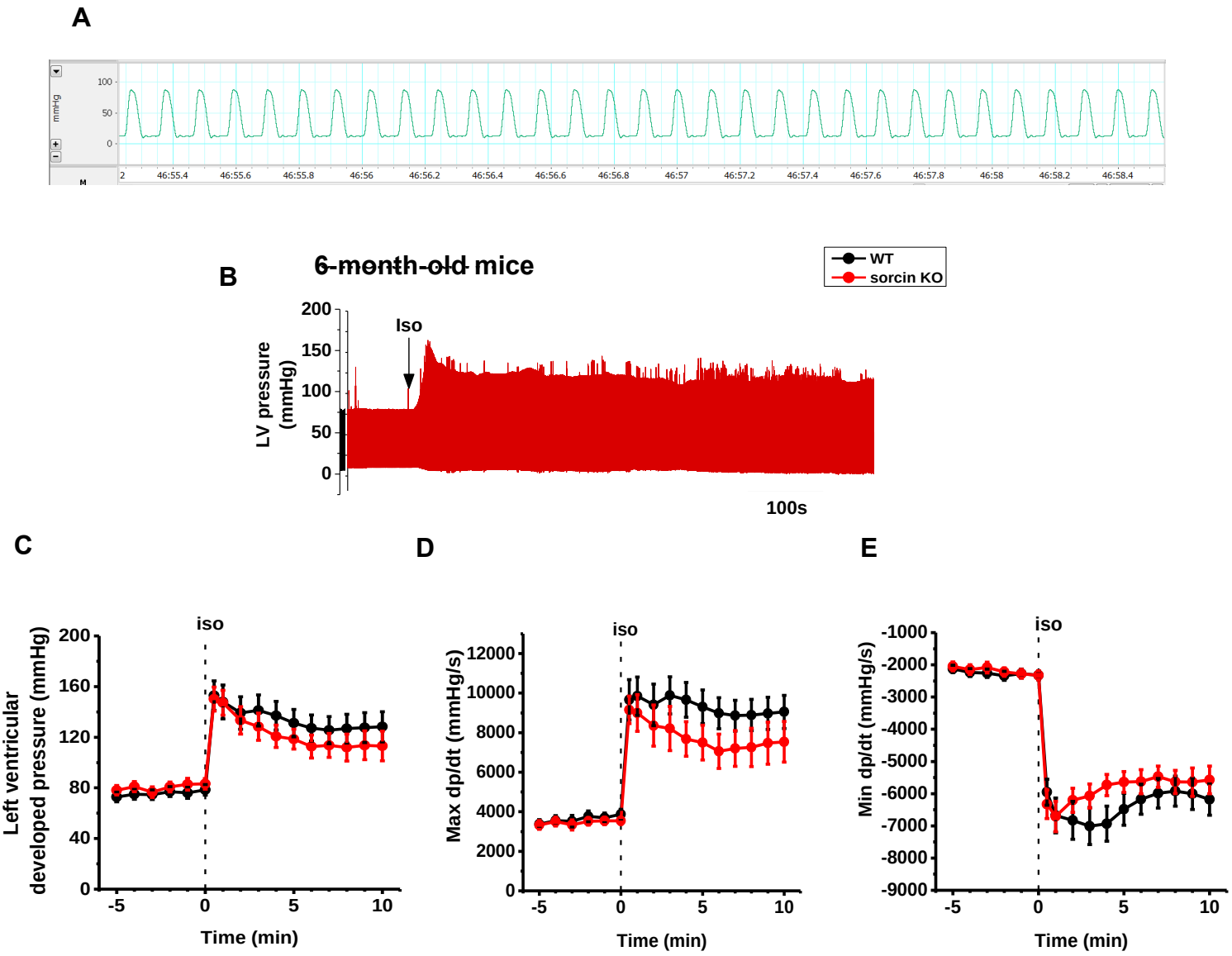

Figure 13. Left ventricular pressure of 6-month-old WT and sorcin KO mice recorded by Langendorff perfusion. (A) A representative 3-secend-recording of left ventricular (LV) pressure. (B) Representative 15-min-recording of LV pressure traces of a 6-month-old WT (black) and a sorcin KO (red) heart. Arrow indicates the time when isoproterenol reached the heart. (C) Left ventricular developed pressure (systolic pressure-end diastolic pressure) of Langendorff-perfused WT and sorcin KO hearts before (-5~0 min) and after (0~10 min) isoproterenol perfusion. (D-E) Systolic rate (maximum dp/dt) (D) and diastolic rate (minimum dp/dt) (E) of WT and sorcin KO hearts before and after isoproterenol perfusion. N=11 in each group (Two-way RM ANOVA).

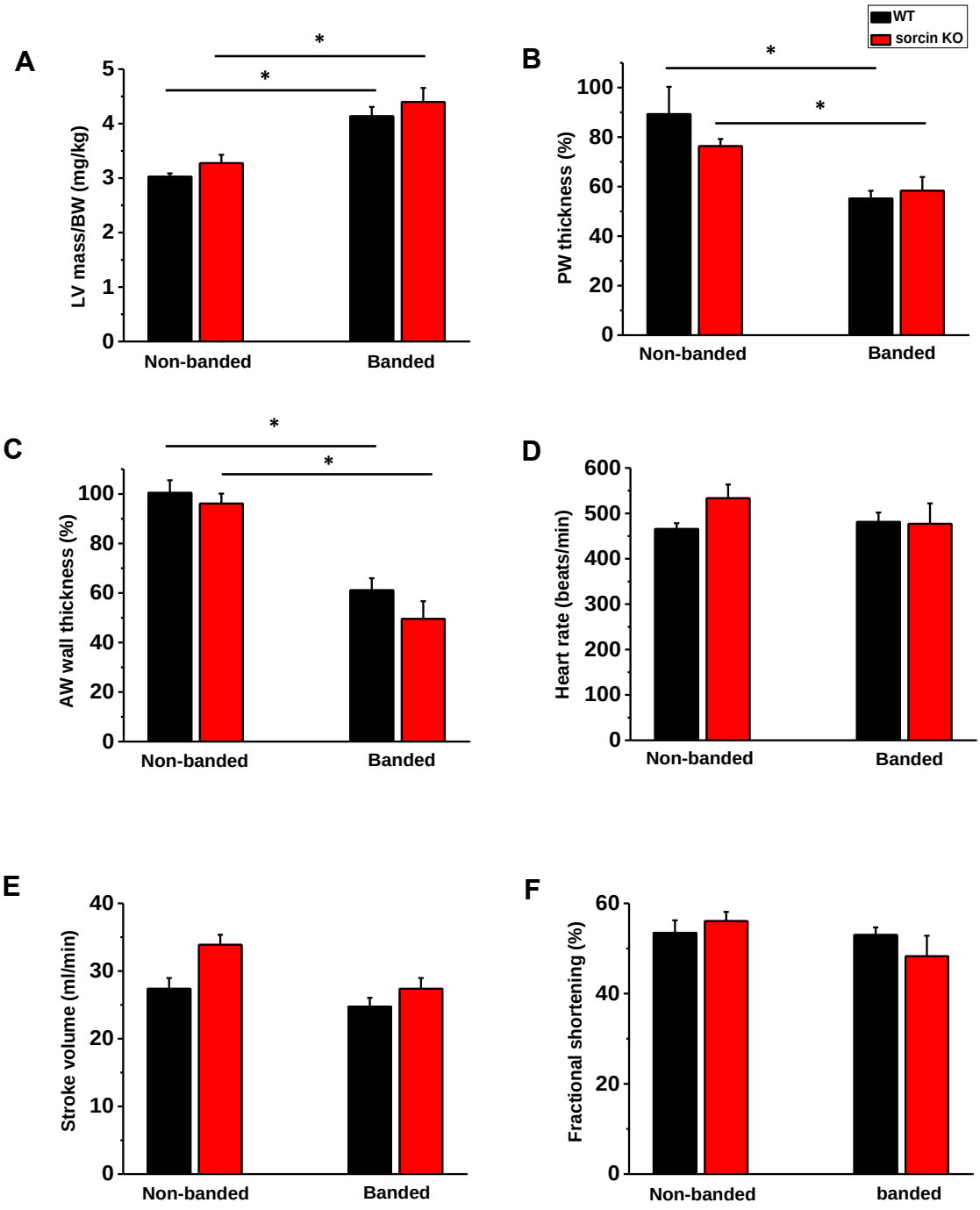

Figure 14. Echocardiography measured heart function before (non-banded) and after TAC (banded). (A-F) Echocardiography measured LV mass (A), posterior wall (PW) thickness (B), anterior wall (AW) thickness (C), heart rate (D), stroke volume (E) and fractional shortening (F) before and after TAC. *, $p<0.05$ vs. non-banded hearts (t-test).

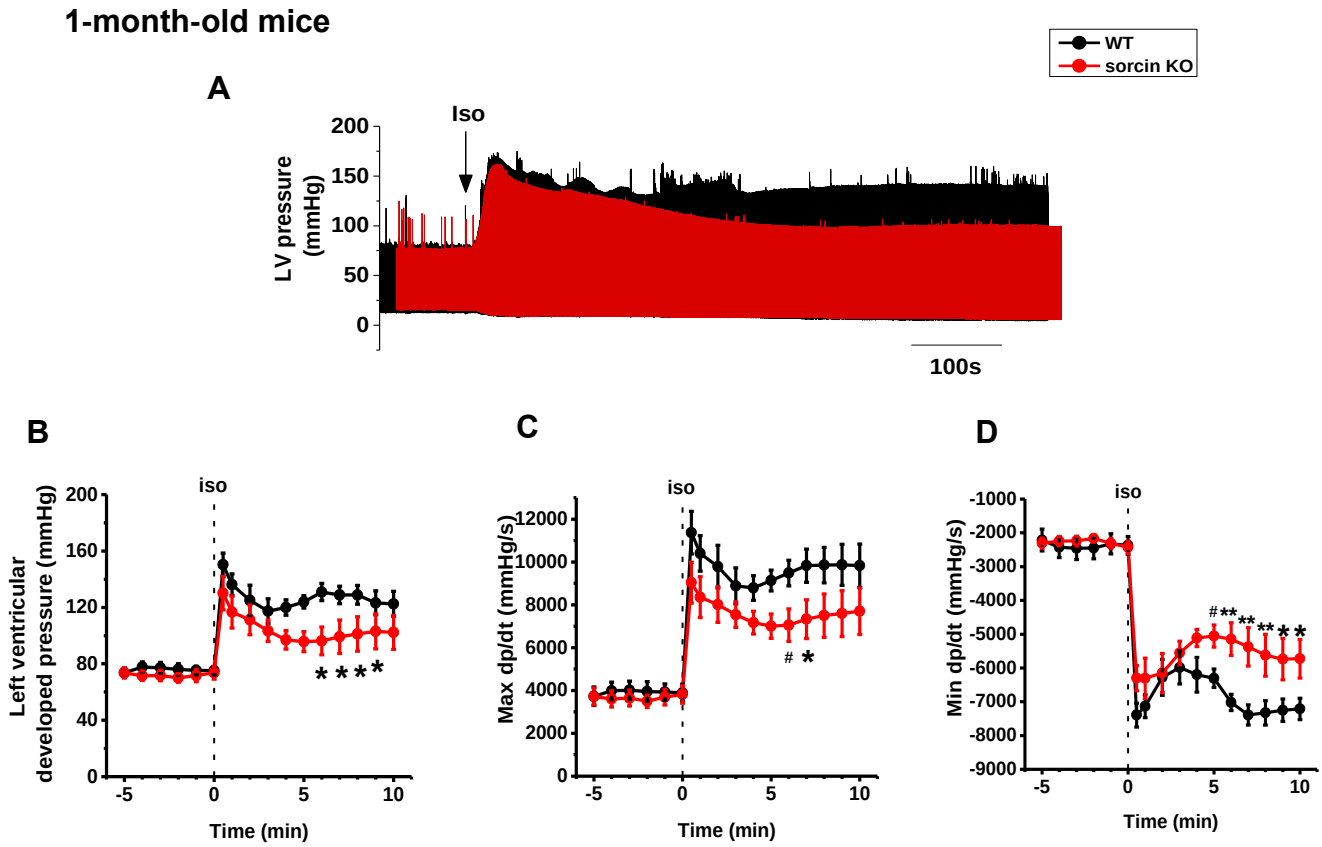

Figure 15. Left ventricular pressure of 1-month-old WT and sorcin KO mice recorded by Langendorff perfusion. (A) Representative 15-min-recording of LV pressure traces of a 1-month-old WT (black) and a sorcin KO (red) heart. Arrow indicates the time when isoproterenol reached the heart. (B) Left ventricular developed pressure of Langendorff-perfused WT and sorcin KO hearts before (-5~0 min) and after (0~10 min) isoproterenol perfusion. (C-D) Systolic rate (maximum dp/dt) (D) and diastolic rate (minimum dp/dt) (E) of WT and sorcin KO hearts before and after isoproterenol perfusion. N=8 in each group. * p<0.05, ** p<0.01, # p=0.051 (Two-way RM ANOVA).

CHAPTER VI

Progressive electrophysiological remodeling in sorcin KO hearts

6.1 Introduction

In the Langendorff recording, 1-month-old sorcin KO hearts developed decreased contractility ~5 min after isoproterenol stimulation. However, this phenotype was rescued in adult sorcin KO hearts, suggesting the KO heart has developed compensatory mechanisms to respond to the ablation of sorcin. To test the hypothesis, we measured the expression and function of other proteins involved in e-c coupling in WT and sorcin KO cardiomyocytes, including LTCC, NCX, SERCA, and RyR2.

6.2 Increased LTCC (Cav 1.2) and NCX expression in 6-month-old sorcin KO hearts

We tested the expression of LTCC (by testing the Cav 1.2 subunit), NCX, SERCA, and RyR2 of hearts from WT and sorcin KO mice using western blots. NCX and LTCC (Cav1.2) were ~2.2-fold and 2.4-fold, respectively, increased in 6-month-old sorcin KO hearts compared to WT, while the expression of SERCA and RyR2 was unaltered (Fig. 16A, B).

Interestingly, 1-month-old sorcin KO hearts did not present overexpression of LTCC and NCX as adult hearts. Instead, the expression of NCX in young KO hearts was lower

than WT (p<0.05, N=5) (Fig. 16C, D). The difference is modest so we may need to increase the N number to confirm whether the difference is due to random variation. No other changes were noted.

The result suggests that in response to the sorcin ablation, sorcin KO hearts develop a progressive overexpression of LTCC and NCX, which is observed in 6-month-old but not 1-month-old sorcin KO hearts.

6.3 Increased NCX activity in 6-month-old sorcin KO cardiomyocytes

To assess whether the overexpression of NCX and LTCC in 6-month-old sorcin KO hearts had a functional correlation, I measured NCX and LTCC activities respectively. NCX activity was first determined from the decay rate of the caffeine-induced Ca^{2+} transient ($K_{caffeine}$). Cardiomyocytes were loaded with 10 μM Fluo-4 AM, a cell-penetrating Ca^{2+} indicator with Ca^{2+} binding affinity (K_d) of 335 nM. Upon binding to Ca^{2+}, the indicator presented an increase in fluorescence, which was excited at the wavelength of 488 nm and recorded at wavelength >505 nm. Ca^{2+} images were collected by the unidirectional line scan of the long axis of cell, at the speed of 3.072 ms/line. The cardiomyocyte was paced by field stimulation for 20 times. After pacing, 10 mM RyR2 agonist, caffeine, was quickly perfused to the cell. By fully opening RyR2, caffeine releases SR Ca^{2+} to cytosol and prevents Ca^{2+} accumulation in SR. In this situation, the decline of $[Ca^{2+}]_i$ only depended on NCX, so the decay rate of caffeine-induced Ca^{2+} transients can be used to evaluate the NCX activity (Fig. 17). In analysis, the decay of caffeine-induced Ca^{2+} transients (shown as $\Delta F/F_0$) was fitted to the formula

$Ca(t) = A + Ca_0 \cdot e^{-\frac{t}{\tau}}$, in which Ca_0 was the apex of Ca^{2+} transient. K, defined as $1/\tau$, was used to describe the pumping rate of NCX (K_{NCX}).

In recording, adult sorcin KO cardiomyocytes had comparable decay of caffeine-induced Ca^{2+} transient as WT under basal conditions, but exhibited faster decay rate when under 300 nM isoproterenol stimulation (Fig. 18A, B). The calculated K_{NCX} was significantly higher in sorcin KO cardiomyocytes under isoproterenol stimulation, reflecting faster NCX rate (Fig. 18C).

To directly evaluate NCX activity, I recorded NCX current (I_{NCX}), which is generated by the exchange of 3 Na^+ ions for 1 Ca^{2+} ion, by patch clamp. NCX current is the forward-mode inward depolarizing current (Ca^{2+} out, Na^+ in) at membrane potential lower than E_{NCX} ($E_{NCX}=3E_{Na}-2E_{Ca}$, which is ~-60 mV in experiment setting), and turns to reverse-mode (Ca^{2+} in, Na^+ out) during depolarization. Cardiomyocytes were incubated in bath solution containing LTCC blocker (0.01 mM Nifedipine), Na^+-K^+-ATPase blocker (1 mM Ouabain·$8H_2O$), and Cl^- channel inhibitor (0.01 mM Niflumic Acid). Free $[Ca^{2+}]_i$ was set at ~210 nM by adding 6 mM Ca^{2+} and 10 mM ethylene glycol-bis(β-aminoethyl ether)-N,N,N',N'-tetraacetic acid (EGTA) in the pipette solution. The cell was depolarized to -40 mV to inactivate I_{Na} and went through a ramp from +70 mV to -140 mV. After the first recording, the cell was perfused by 2.5 mM $NiCl_2$ for 30 s, and went through the recording protocol again. NCX current—a Ni^{2+} sensitive current, was obtained by subtracting the second current from the first one (90, 91) (Fig. 19).

Adult sorcin KO cardiomyocytes presented comparable I_{NCX} as WT under basal conditions (Fig. 20B). However, when under isoproterenol stimulation, sorcin KO

cardiomyocytes presented significantly larger outward (clamped at 50~80 mV) and inward (clamped at -120~-80 mV) I_{NCX} compared with WT (Fig. 20A, C). The increased K_{NCX} as well as I_{NCX} in sorcin KO cardiomyocytes suggests that although the stimulatory effect of sorcin on NCX (90, 91) is not present in sorcin KO cells, NCX activity is enhanced under isoproterenol stimulation. It is likely that the overexpression of NCX protein detected by western blots allows for a more robust $[Ca^{2+}]_i$ extrusion, resulting in enhanced NCX activity observed in isoproterenol-stimulated sorcin KO cardiomyocytes.

6.4 Increased LTCC activity in 6-month-old sorcin KO cardiomyocytes

I then measured L-type Ca^{2+} current (I_{Ca}) of 6-month-old sorcin KO and WT cardiomyocytes. Cardiomyocytes were incubated in bath solution containing 30 μM I_{Na} inhibitor TTX and 10 mM I_{to} inhibitor 4-aminopyridine. The cell was clamped at -50 mV and depolarized from -50 mV to +70 mV with an increment of 10 mV. Under basal conditions, sorcin KO cardiomyocytes presented a modest but statistically significant increase in peak I_{Ca} compared to WT (Two-way RM ANOVA $p<0.05$) (Fig. 21, 23A). The robust stimulating effect of 300 nM isoproterenol blurred most of the difference in peak I_{Ca}, although at -20 mV sorcin KO cardiomyocytes still displayed significantly higher I_{Ca} than WT (Holm-Sidak test $p<0.05$) (Fig. 22, 23B). As ours and other group's research have shown sorcin does not influence amplitude of I_{Ca} (86, 87), the increased peak I_{Ca} in sorcin KO cardiomyocytes corresponds to LTCC overexpression.

Although I_{Ca} peak increased in adult sorcin KO cardiomyocytes under basal conditions, the Ca^{2+}-dependent fast inactivation of I_{Ca} (τ_{fast}) significantly accelerated at the same time (Fig. 24A, C) so the total I_{Ca} (Σ_{ICa}) was not significantly changed. On the other

hand, under isoproterenol stimulation, τ_{fast} of I_{Ca} in adult sorcin KO cardiomyocytes was slower than that of WT, which favors more Ca^{2+} entry during e-c coupling (Fig. 24B, D).

6.5 Unchanged NCX and LTCC activities in 1-month-old sorcin KO cardiomyocytes

As 1-month-old sorcin KO hearts did not present overexpression of NCX and LTCC, I recorded I_{NCX} and I_{Ca} in 1-month-old cardiomyocytes to observe if NCX and LTCC still presented enhanced activities. Unlike adult cardiomyocytes, young sorcin KO cardiomyocytes did not present significant increase in I_{NCX} (Fig. 25) and I_{Ca} (Fig. 26) under basal conditions and isoproterenol stimulation.

Although 1-month-old sorcin KO cardiomyocytes presented a slightly lower NCX expression than WT, and no longer had sorcin's stimulatory effect on NCX, we did not observe a significant lower I_{NCX} in 1-month-old sorcin KO cardiomyocytes (although there was a tendency). This may because I_{NCX} in mouse cardiomyocytes is relatively small (~5 times smaller than rabbit cardiomyocytes) so subtle changes in current amplitude are hard to observe. However this does not influence our conclusion that the increased I_{NCX} and I_{Ca} observed in adult sorcin KO cardiomyocytes are due to protein overexpression

6.6 Summary

In experiment, we found adult, but not young sorcin KO hearts presented increased expression of LTCC and NCX, while the expression of RyR2 and SERCA were unaltered. In accordance with protein overexpression, NCX and LTCC activities were

significantly enhanced in adult, but not young sorcin KO hearts. The result suggests the enhanced LTCC/NCX activities observed in adult cardiomyocytes are more likely due to protein overexpression. Combining results of protein expression, current amplitude and Ca^{2+} decay rate, we postulate that the sorcin KO heart presents a progressive electrophysiological remodeling of I_{Ca} and I_{NCX} with increase of age. The increased Ca^{2+} entry through LTCC and NCX (works in reverse mode to let Ca^{2+} in) during the upstroke of action potential could trigger more SR Ca^{2+} release and reload SR Ca^{2+}, which may play a key role in rescuing the impaired contractility observed in young sorcin KO heart.

6.7. Acknowledgement

This chapter includes data generated by Dr. Francisco Alvarado, University of Michigan and Craig Weber, Department of Physiology, University of Arizona College of Medicine (western blot).

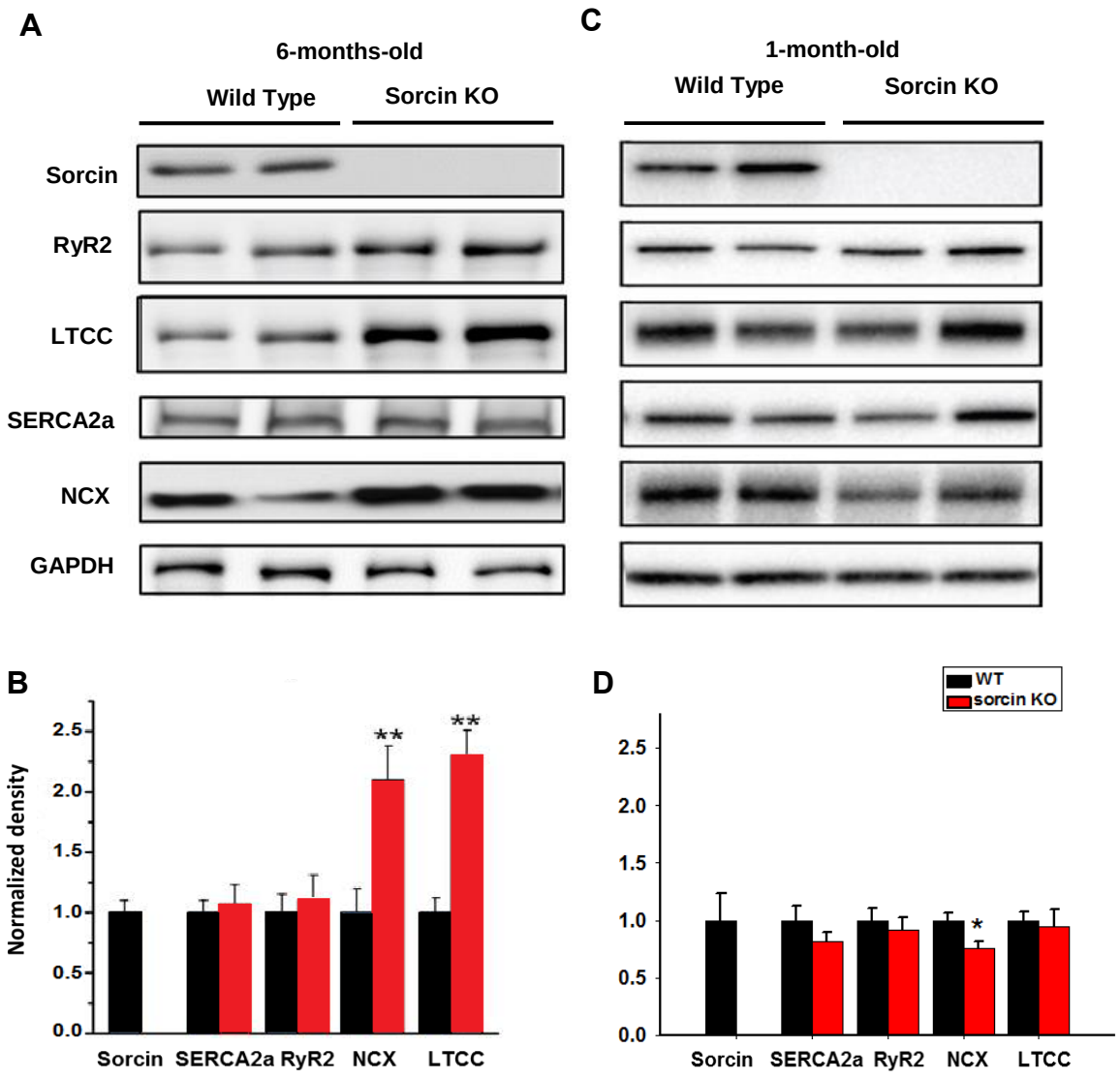

Figure 16. Expression of Ca^{2+} regulatory proteins. (A-B) Representative western blots (A) and quantification (B) for sorcin, SERCA2a, RyR2, NCX, and LTCC expression in 6-month old WT and sorcin KO hearts. (C-D) Representative western blots (C) and quantification (D) for protein expression in 1-month old WT and sorcin KO hearts. N=5 in each group. *, $p<0.05$ vs. WT; ** $p<0.01$ vs. WT (t-test).

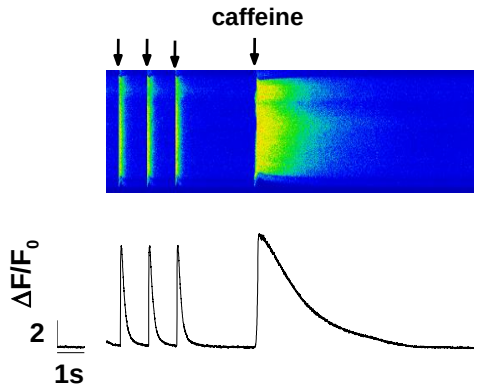

Figure 17. Caffeine fully opens RyR2 and releases SR Ca^{2+} to cytosol. The cardiomyocyte was loaded by Fluo-4 AM and was paced by 1Hz field stimulation (arrow). After pacing, 10 mM caffeine was perfused to the cell to deplete SR Ca^{2+}. The decay rate of caffeine-induced Ca^{2+} transient reflects NCX pumping rate.

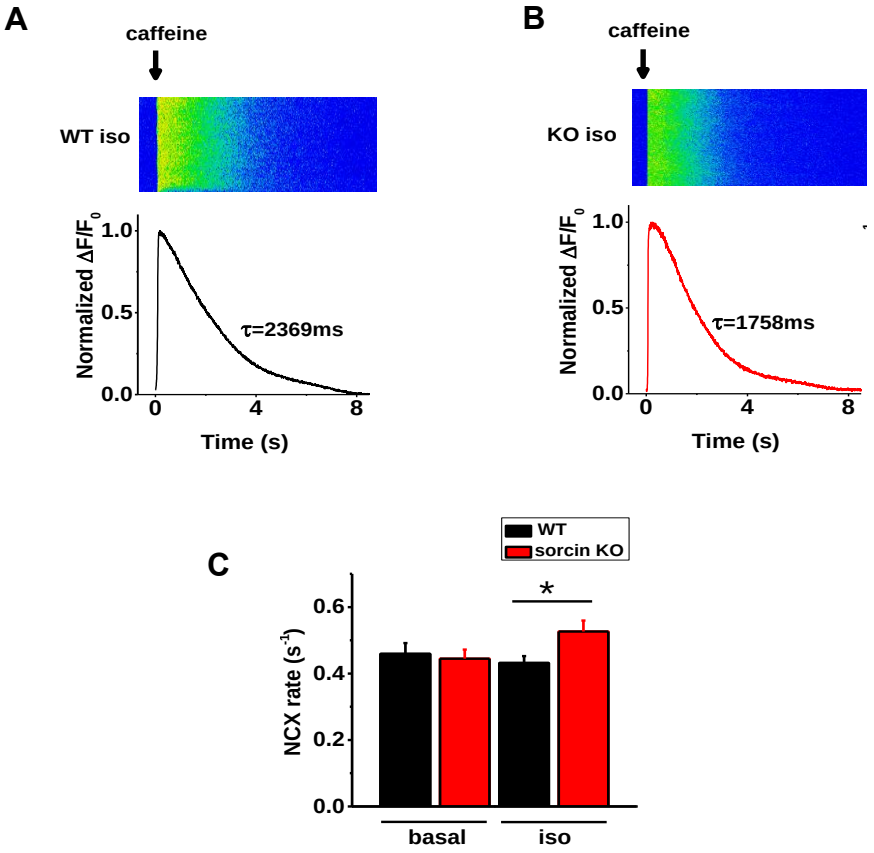

Figure 18. NCX activity of 6-month-old cardiomyocytes evaluated by caffeine-induced Ca^{2+} transient. (A-B). Representative Ca^{2+} imaging and plot of caffeine-induced Ca^{2+} transient of WT (A) and sorcin KO cardiomyocyte (B). WT τ_{caff}= 2369 ms, KO τ_{caff}= 1758 ms. (C) NCX rate (K_{NCX}) of WT and sorcin KO cardiomyocytes under basal conditions and isoproterenol stimulation. WT-basal n=10, KO-basal n=9; WT-iso n=12, KO-iso n=13. *, p<0.05 vs. WT (t-test).

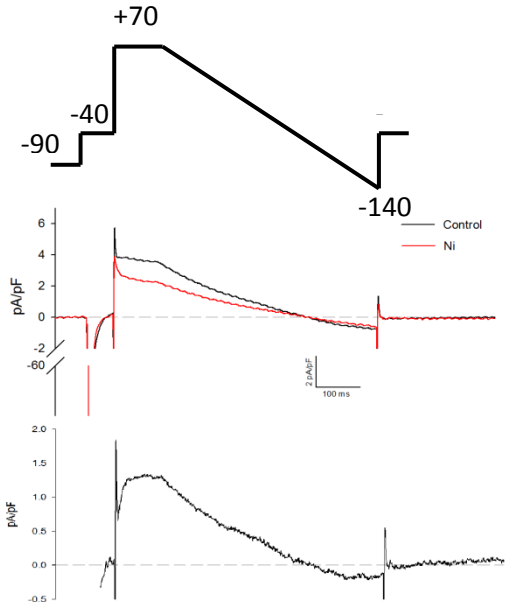

Figure 19. I_{NCX} recording. Upper: voltage protocol for recording I_{NCX}. Middle: Currents recorded before (black) and after (red) Ni^{2+} perfusion. Under: I_{NCX} obtained by subtracting the second current from the first one.

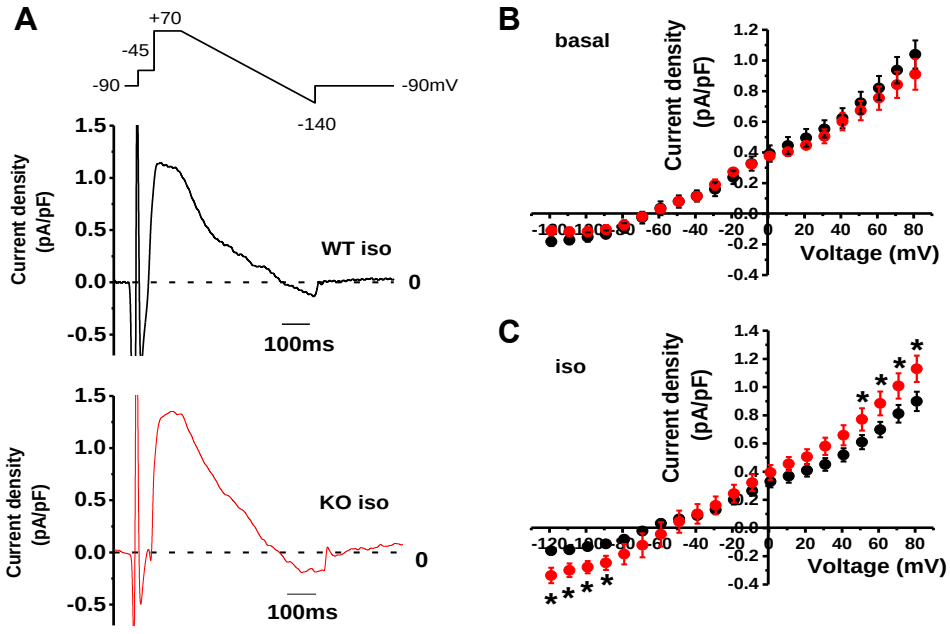

Figure 20. I_{NCX} of 6-month-old WT and sorcin KO cardiomyocytes under basal conditions and isoproterenol stimulation. (A) representative I_{NCX} of WT and sorcin KO cardiomyocytes under isoproterenol stimulation. (B) I-V curve of I_{NCX} under basal conditions. WT-basal n=9, KO-basal n=8. (C) I-V curve of I_{NCX} under isoproterenol stimulation. WT-iso n=9, KO-iso n=9. *, p<0.05 vs. WT (Two-way RM ANOVA).

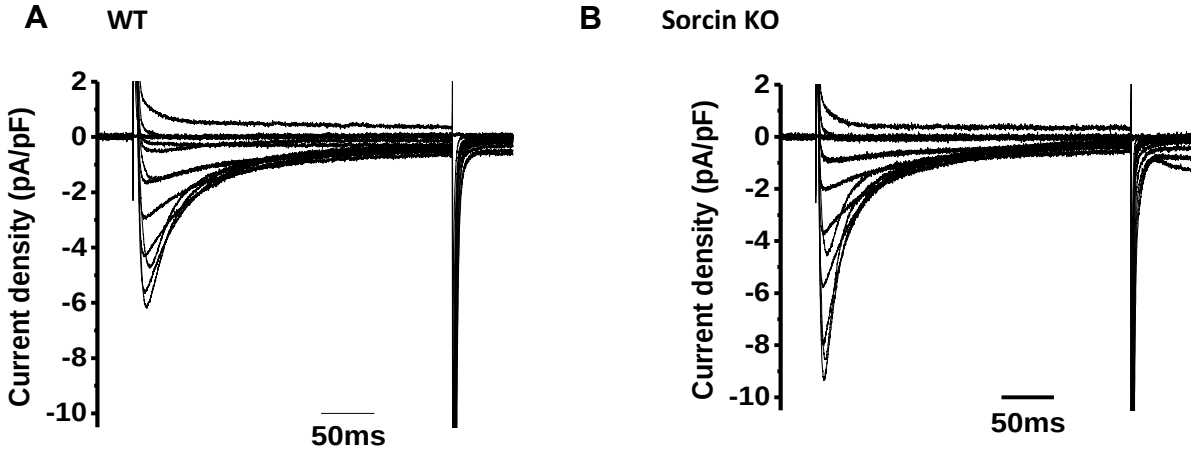

Figure 21. I_{Ca} of 6-month-old WT and sorcin KO cardiomyocytes under basal conditions. (A-B) A representative recording of I_{Ca} of a WT cardiomyocyte (A) and a sorcin KO cardiomyocyte (B) under basal conditions.

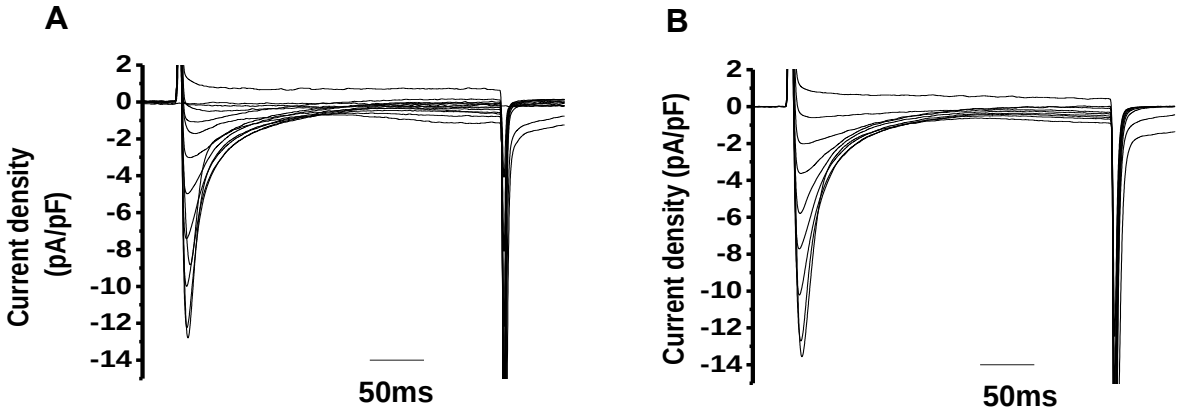

Figure 22. I_{Ca} of 6-month-old WT and sorcin KO cardiomyocytes under isoproterenol stimulation. (A-B) A representative recording of I_{Ca} of a WT cardiomyocyte (A) and a sorcin KO cardiomyocyte (B) under isoproterenol stimulation.

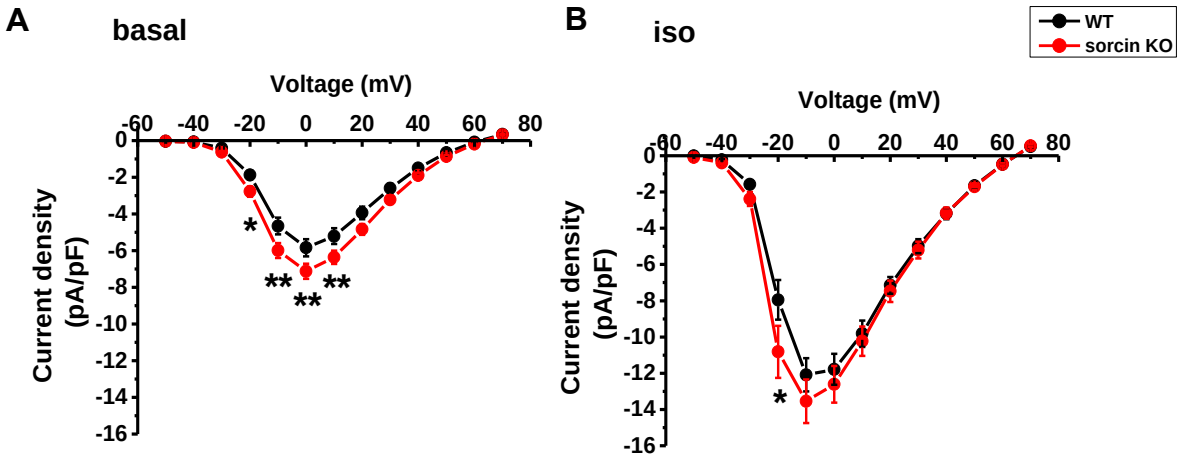

Figure 23. I-V curve of I_{Ca} of 6-month-old cardiomyocytes. (A) I-V curve of I_{Ca} of WT and sorcin KO cardiomyocytes under basal conditions. Two-way RM ANOVA p<0.05. (B) I-V curve of I_{Ca} of WT and sorcin KO cardiomyocytes under isoproterenol stimulation. WT-basal n=11, KO-basal n=14, WT-iso n=10, KO-iso n=10. *, Holm-Sidak test p<0.05 vs. WT; **, Holm-Sidak test p<0.01 vs. WT (Two-way RM ANOVA).

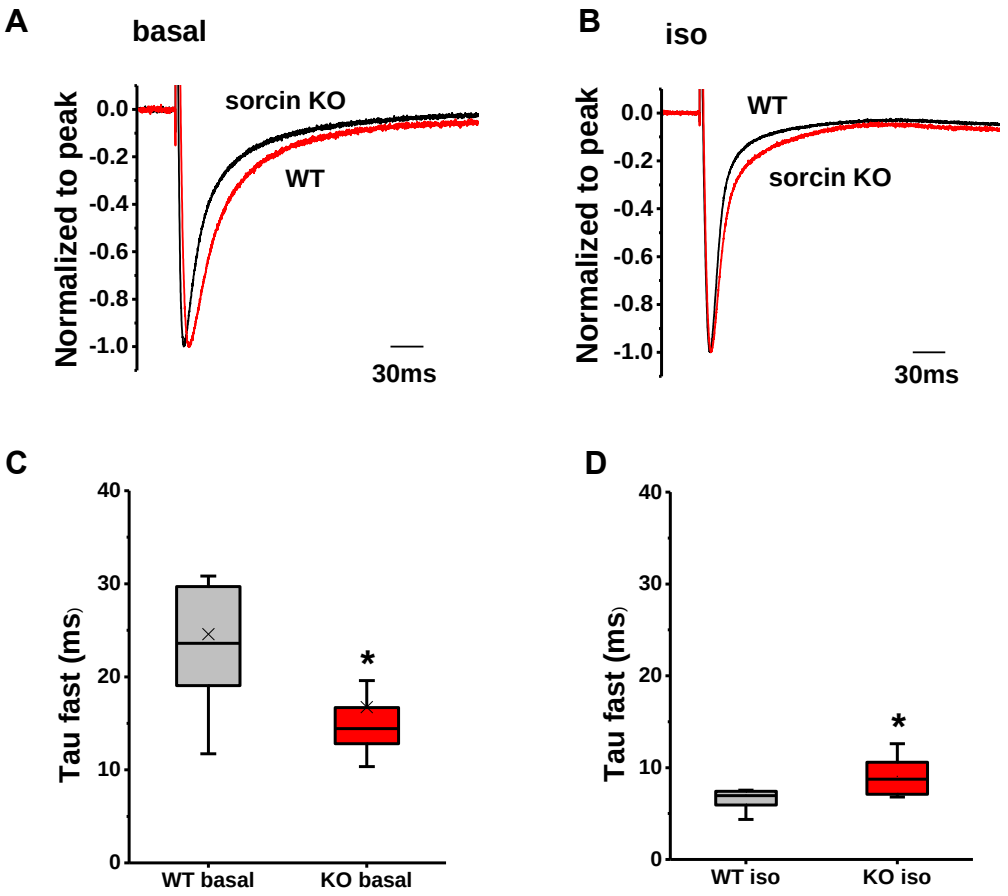

Figure 24. Inactivation of I_{Ca} of 6-month-old cardiomyocytes. (A) Representative curves of I_{Ca} at 0 mV under basal conditions. (B) Representative curves of I_{Ca} at -10 mV under isoproterenol stimulation. Currents are normalized to the peak value. (C) Ca^{2+}-dependent inactivation (τ_{fast}) of I_{Ca} inactivation at 0 mV under basal conditions. (D) τ_{fast} of I_{Ca} inactivation at -10 mV under isoproterenol stimulation. WT-basal n=11, KO-basal n=14, WT-iso n=10, KO-iso n=10. *, $p<0.05$ vs. WT (Rank-sum test).

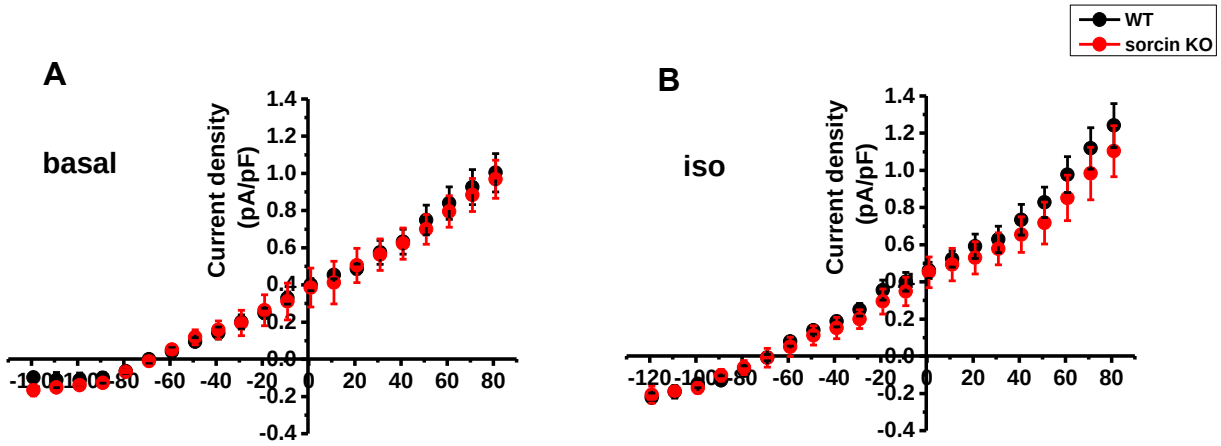

Figure 25. I-V curve of I_{NCX} of 1-month-old cardiomyocytes. (A) I-V curve of I_{NCX} of WT and sorcin KO cardiomyocytes under basal conditions. (B) I-V curve of I_{NCX} of WT and sorcin KO cardiomyocytes under isoproterenol stimulation. WT-basal n=7, KO-basal n=8, WT-iso n=8, KO-iso n=7 (Two-way RM ANOVA).

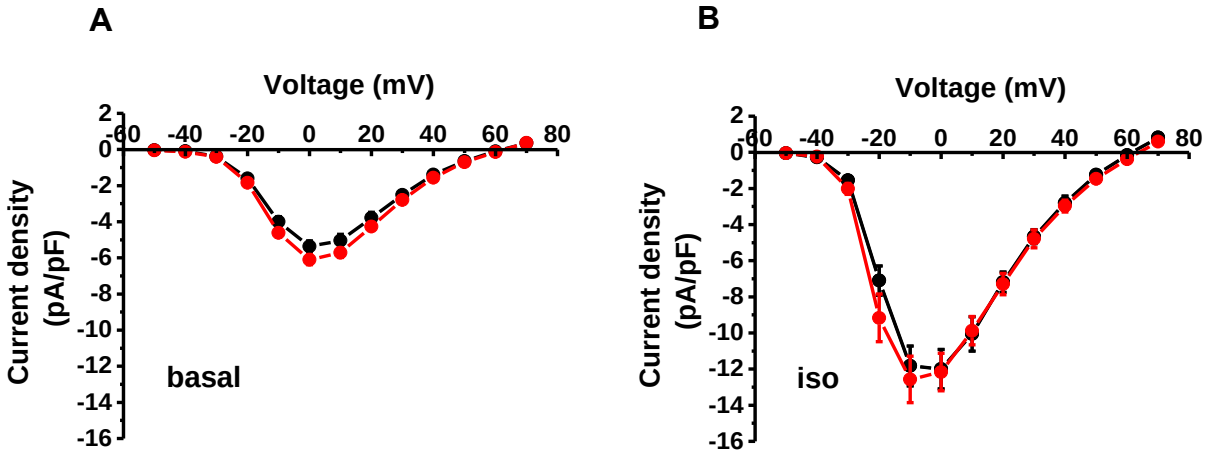

Figure 26. I-V curve of I_{Ca} of 1-month-old cardiomyocytes. (A) I-V curve of I_{Ca} of WT and sorcin KO cardiomyocytes under basal conditions. (B) I-V curve of I_{Ca} of WT and sorcin KO cardiomyocytes under isoproterenol stimulation. WT-basal n=11, KO-basal n=15, WT-iso n=10, KO-iso n=14 (Two-way RM ANOVA).

CHAPTER VII

Ca^{2+} leak in sorcin KO cardiomyocytes

7.1 Introduction

As introduced before, the RyR2 is likely the most important target of sorcin. In single channel recordings, recombinant sorcin added in the *cis* (cytosolic) side can significantly decrease the bursting frequency and increase the mean closed time of RyR2 in a dose-dependent manner (EC_{50} = 480 nM) (88). The onset of this inhibitory effect is fast (less than 20 ms), which enables sorcin to act on a beat-to-beat basis (86). Due to the inhibitory effect of sorcin on RyR2, sorcin (1 μM) added in the bath solution is able to prevent Ca^{2+} sparks in permeabilized cardiomyocytes.

In this chapter, I investigated whether *endogenous* sorcin in cardiomyocytes plays a role in decreasing SR Ca^{2+} leak by stabilizing RyR2s. Ca^{2+} sparks and RyR2-mediated diastolic Ca^{2+} leak flux were measured in sorcin KO cardiomyocytes.

7.2 Ca^{2+} sparks in sorcin KO cardiomyocytes

In resting cardiomyocytes, the stochastic release of Ca^{2+} from a CRU to a local area can be observed as a Ca^{2+} spark. Although random Ca^{2+} sparks are common in healthy cardiomyocytes, abnormal high frequency of Ca^{2+} sparks could lead to extra contractions and the depletion of SR Ca^{2+} load, which are detrimental to the heart

function. Therefore, the frequency and kinetics of Ca^{2+} sparks reflect RyR2 activity and cardiomyocyte stability.

To record Ca^{2+} sparks, cardiomyocytes were loaded with 10 μM Fluo-4 AM. Ca^{2+} images were collected by the unidirectional line scan of the long axis of the cell, at a speed of 3.072 ms/line. The cell was paced at 1Hz by field stimulation for 20 times and then left in resting state for 20 s to observe Ca^{2+} sparks. For β-adrenergic stimulation, 300 nM isoproterenol was added in the bath solution. Ca^{2+} spark frequency = number of Ca^{2+} sparks · cell $width^{-1}$ · $time^{-1}$.

Under basal conditions, both WT and sorcin KO cardiomyocytes had few Ca^{2+} sparks (KO 0.13±0.07 vs. WT 0.22±0.09 sparks/100 $\mu m^{-1} \bullet s^{-1}$). Notably, however, sorcin KO cells exhibited significantly higher frequency of Ca^{2+} sparks under isoproterenol stimulation (KO 1.43±0.29 vs. WT 0.51±0.15 sparks •100 $\mu m^{-1} \bullet s^{-1}$, $p<0.05$) (Fig. 27).

I then evaluated the kinetics of Ca^{2+} sparks that appeared under isoproterenol stimulation. The amplitude of Ca^{2+} sparks was evaluated by normalizing the peak fluorescence (F) to background level (F_0). Full width at half maximum (FWHM) was used to describe the spatial width of Ca^{2+} sparks. Full duration at half maximum (FDHM) was used to express the duration of the spark from rising to elimination, and half decay time was used to evaluate the decay rate of the spark.

Sorcin KO cardiomyocytes presented no significant difference in FWHM compared with WT (KO 2.11±0.04 vs. WT 2.12±0.06 μm, graph not shown). However, the spark amplitude, FDHM, and half decay time were all strikingly higher in sorcin KO cardiomyocytes compared with WT ($p<0.001$) (Fig. 28). The result suggests that RyR2s

in sorcin KO cardiomyocytes are more active, leading to increased Ca^{2+} spark frequency with greater spark amplitude and duration.

7.3 Increased diastolic Ca^{2+} leak in sorcin KO cardiomyocytes

Besides visible Ca^{2+} sparks, there is also diastolic SR Ca^{2+} leak flux in resting cardiomyocytes. The diastolic Ca^{2+} leak flux, together with a reversed SR Ca^{2+} pump back flux (110, 111), counteract forward Ca^{2+} uptake by SR Ca^{2+} pump, forming a pump-leak balance in cardiomyocytes (112, 113). To ascertain RyR2 activity without the influence of LTCC and NCX, I measured RyR2-mediated diastolic SR Ca^{2+} leak by an alternative method, as described by Shannon *et al.* (114). The cardiomyocyte was perfused with $0Na^{+}$-$0Ca^{2+}$ solution (step 1), which blocked LTCC and NCX and stopped Ca^{2+} exchange between extracellular and intracellular compartments. Then, tetracaine (1 mM) was added to block RyR2 (step 2). As there was no longer SR Ca^{2+} leak flux through RyR2 after tetracaine perfusion, $[Ca^{2+}]_i$ drops and $[Ca^{2+}]_{SR}$ increases until a new equilibrium state is achieved. The fluorescence difference between step 1 and 2 reflected diastolic Ca^{2+} leak. At the end, 10 mM caffeine was perfused to the cell to measure SR Ca^{2+} load (Fig. 29A, B).

Under basal conditions, sorcin KO cardiomyocytes had diastolic SR Ca^{2+} leak flux comparable to WT. However, under isoproterenol stimulation, sorcin KO cardiomyocytes displayed higher diastolic SR Ca^{2+} leak than WT (Fig. 29C). The difference was maintained after the Ca^{2+} leak was normalized to the SR Ca^{2+} load (Fig. 29D). Isoproterenol stimulation decreased the diastolic Ca^{2+} leak flux in both WT and sorcin KO cardiomyocyte. This may be because PKA-mediated phosphorylation of

RyR2 accelerates adaptation of channel to Ca^{2+}, leading to a lower P_o after adaptation (38).

7.4 Summary

In this experiment, we found that sorcin KO cardiomyocytes presented increased Ca^{2+} sparks and diastolic Ca^{2+} leak flux. The Ca^{2+} leak in sorcin KO cardiomyocytes was still higher after being normalized to SR Ca^{2+} load (Fig. 29D), suggesting RyR2 hyperactivity in KO cells. This phenotype can only be observed in the presence of isoproterenol, suggesting sorcin's Ca^{2+} regulatory effect is more prominent under β-adrenergic stimulation (will be further discussed in Chapter IX and X). In the following experiments, I will investigate whether SR Ca^{2+} leak may trigger cell-wide Ca^{2+} waves in sorcin KO cardiomyocytes.

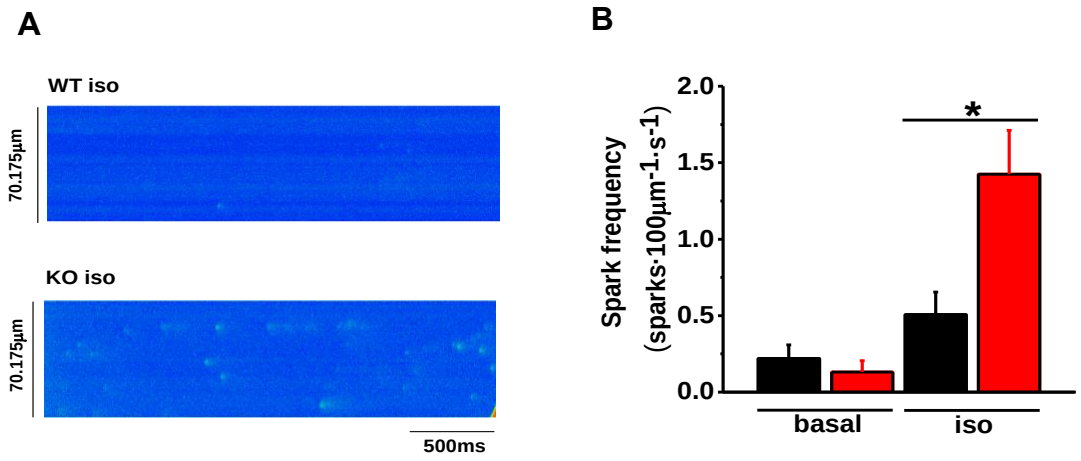

Figure 27. Ca^{2+} spark frequency in cardiomyocytes. (A) Representative recording of Ca^{2+} sparks of WT and sorcin KO cardiomyocytes under isoproterenol stimulation. Sparks were measured after 20 times of 1Hz pacing. (B) Ca^{2+} spark frequency of cardiomyocytes under basal conditions and isoproterenol stimulation. WT-basal n=16, KO-basal n=16, WT-iso n=16, KO-iso n=32 cells. *, $p<0.05$ vs. WT (t-test).

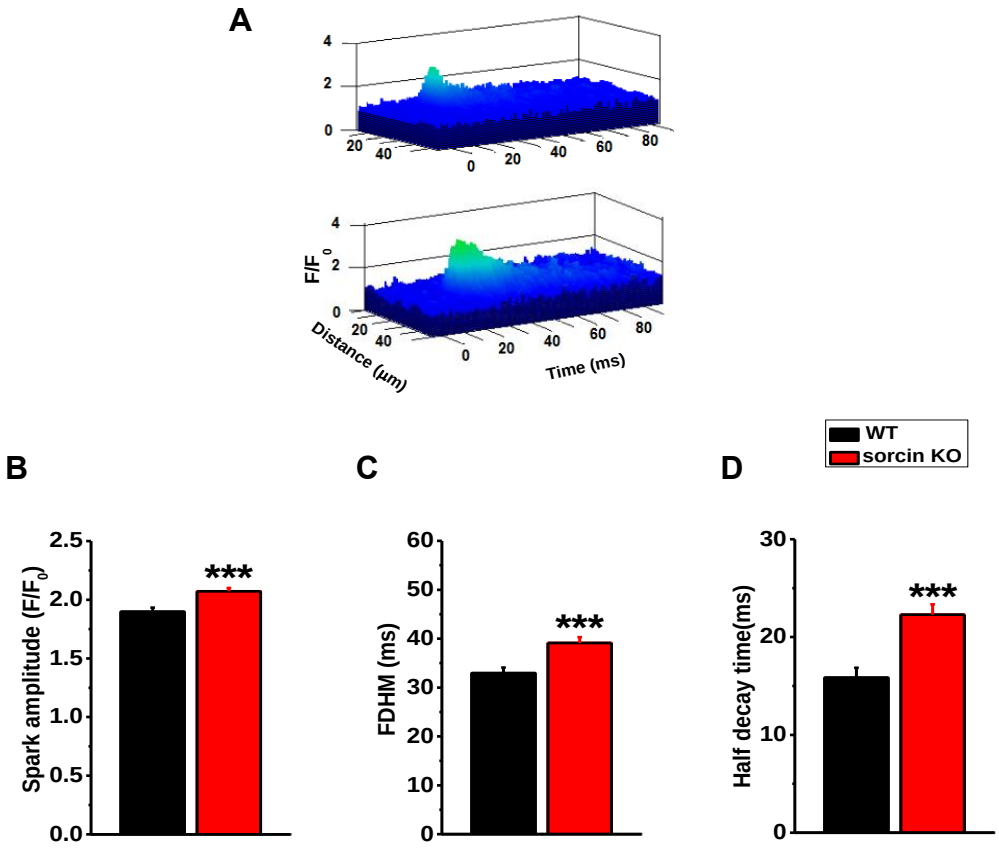

Figure 28. Kinetics of Ca^{2+} sparks. (A) 3D plots of representative Ca^{2+} sparks of WT and sorcin KO cardiomyocytes. (B-D) Ca^{2+} sparks amplitude (B), full duration at half maximum (FDHM) (C), and half decay time (D) under isoproterenol stimulation. WT-basal n=16, KO-basal n=16, WT-iso n=16, KO-iso n=32 cells. ***, $p<0.001$ (t-test).

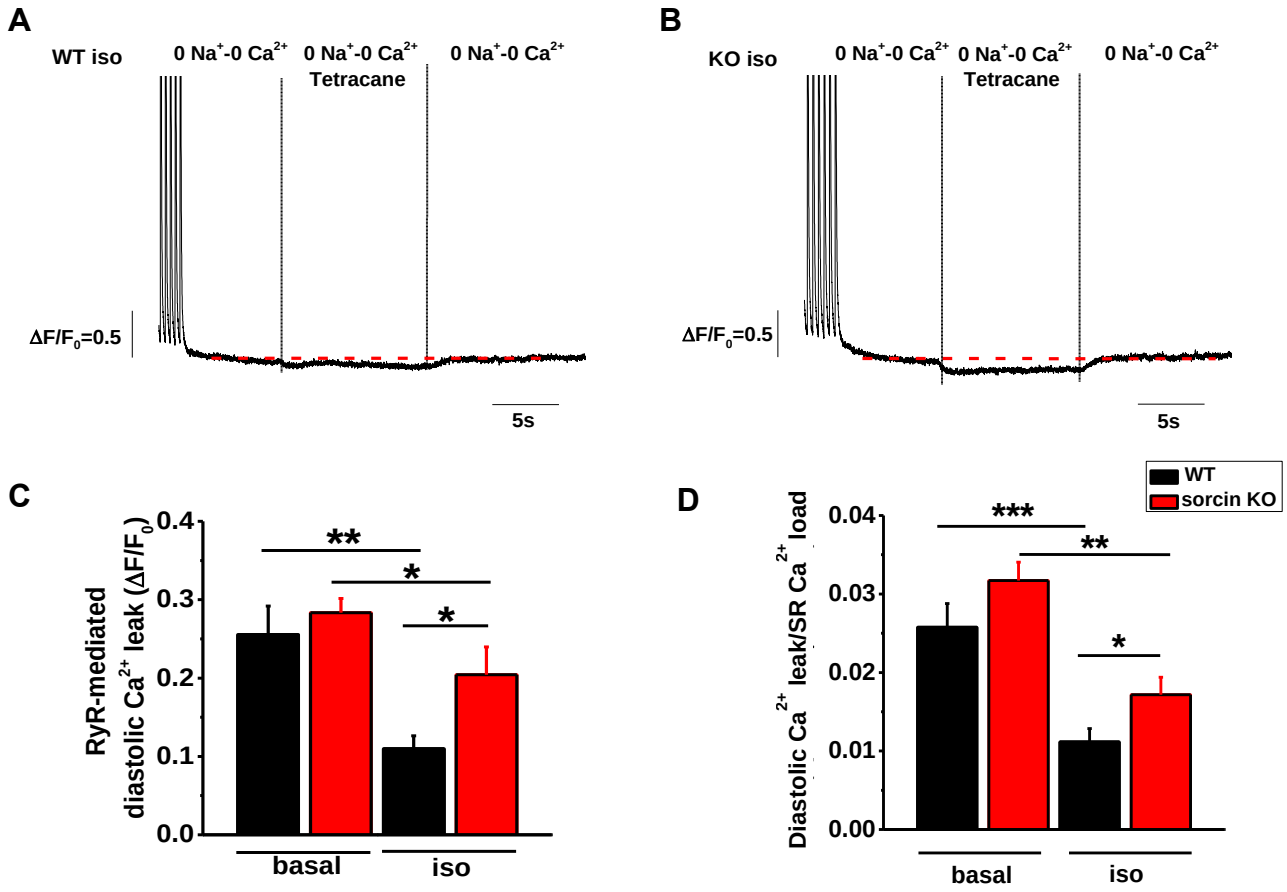

Figure 29. RyR2-mediated diastolic Ca^{2+} leak. (A-B) Representative plots of RyR2-mediated SR Ca^{2+} leak of WT (A) and sorcin KO (B) cardiomyocytes under isoproterenol stimulation. Cardiomyocytes were perfused in $0Na^{+}$-$0Ca^{2+}$ solution. Then, tetracaine (1 mM) was added to block Ca2+ leak through RyR2. After 10s, tetracaine was washed out by $0Na^{+}$-$0Ca^{2+}$ solution. The fluorescence difference before and after tetracaine application (marked by red dashed line) reflects RyR-mediated diastolic Ca^{2+} leak. (C) RyR2-mediated diastolic SR Ca^{2+} leak under basal conditions and isoproterenol stimulation. (D) RyR2-mediated diastolic SR Ca^{2+} leak normalized to SR Ca^{2+} load under basal conditions and isoproterenol stimulation. WT-basal n=11, KO-basal n=15; WT-iso n=12, KO-iso n=12 cells. *, p<0.05, **, p<0.01, ***, p<0.001 (t-test).

CHAPTER VIII

Ca^{2+} transient amplitude and SR Ca^{2+} load in sorcin KO cardiomyocytes

8.1 Introduction

In Chapter VII, I found increased SR Ca^{2+} leak in sorcin KO cardiomyocytes, which put the cell at risk of having decreased SR Ca^{2+} load and Ca^{2+} transient amplitude. However, Langendorff perfusion experiments showed that 1-month-old, but not 6-month-old sorcin KO mice, presented decreased heart contractility under isoproterenol stimulation (Chapter V). To investigate if there are corresponding changes in Ca^{2+} transient amplitude and SR Ca^{2+} load, I conducted Ca^{2+} imaging on 6-month and 1-month-old sorcin KO cardiomyocytes.

8.2 Preserved Ca^{2+} transient amplitude and SR Ca^{2+} load in 6-month-old sorcin KO cardiomyocytes

Fluo-4 loaded cardiomyocyte was paced 20 times by 1Hz field stimulation, and 10 mM caffeine was perfused to the cell after pacing to deplete SR Ca^{2+} load. The amplitude of the Ca^{2+} transient was defined as the $(F-F_0)/F_0$ ($\Delta F/F_0$) of the twitch Ca^{2+} transient, and SR Ca^{2+} load was $\Delta F/F_0$ of caffeine-induced Ca^{2+} transient (Fig. 30A). During pacing, Ca^{2+} transient amplitude gradually decreased until SR Ca^{2+} reached a steady level. The

average peak value of the last 10 Ca^{2+} transients of a train of stimulation was used to represent Ca^{2+} transient amplitude.

Under basal conditions, 6-month-old sorcin KO cardiomyocytes presented modest but statistically higher Ca^{2+} transient amplitude than WT. Under isoproterenol stimulation, both WT and sorcin KO cardiomyocytes presented significantly increased Ca^{2+} transient amplitude, and there was no significant difference between the two groups (Fig. 30B). SR Ca^{2+} load, measured as caffeine-induced Ca^{2+} release after pacing, was not different between 6-month-old sorcin KO and WT cardiomyocytes (Fig. 30C).

8.3 Decreased Ca^{2+} transient amplitude and SR Ca^{2+} load in 1-month-old sorcin KO cardiomyocytes

I then measured Ca^{2+} transients and SR Ca^{2+} load of 1-month-old sorcin KO cardiomyocytes. 1-month-old sorcin KO cardiomyocytes had comparable Ca^{2+} transient amplitude and SR Ca^{2+} load as WT cells under basal conditions, but displayed significantly lower Ca^{2+} transient amplitude and SR Ca^{2+} load ($p<0.001$) under isoproterenol stimulation (Fig. 31). The result, at the cellular level, confirms that young sorcin KO heart has decreased contractility than WT under isoproterenol stimulation due to SR Ca^{2+} depletion. With increase of age, the phenotype is rescued such that no difference is observed between adult WT and sorcin KO hearts.

8.4 Decreased SERCA pumping rate in sorcin KO cardiomyocytes

To investigate the influence of SERCA activity on SR Ca^{2+} load, I evaluated SERCA pumping rate of 6-month-old sorcin KO cardiomyocytes by analyzing the decay of twitch

$[Ca^{2+}]_i$ transient. The decay of twitch $[Ca^{2+}]_i$ (shown as $\Delta F/F_0$) was fitted to the formula $Ca(t) = A + Ca_0 \cdot e^{-\frac{t}{\tau}}$, in which Ca_0 was the apex of the Ca^{2+} transient. *K*, defined as $1/\tau$, was used to describe the decay rate of the Ca^{2+} transient. During pacing, the decay of the twitch $[Ca^{2+}]_i$ transient depended on both NCX and SERCA, so $K_{SERCA} = K_{twitch} - K_{NCX}$ (115). K_{NCX} was calculated by analyzing the decay of the caffeine-induced $[Ca^{2+}]_i$ transient,.

Sorcin KO cardiomyocytes presented slower Ca^{2+} pumping rate by SERCA under isoproterenol stimulation (Fig. 32), which bodes well with previous results showing that sorcin stimulates SERCA function (89).

8.5 Summary

In this experiment, I found decreased Ca^{2+} transient amplitude and SR Ca^{2+} load in 1-month-old sorcin KO cardiomyocytes under isoproterenol stimulation (Fig. 31). In accordance with the *in vitro* result, the left ventricular contractility of 1-month-old sorcin KO hearts was significantly lower than WT ~5 min after isoproterenol stimulation (Fig. 15). The observation agrees with the hypothesis that the increased SR Ca^{2+} leak would bring negative effects on heart contractility.

However, as sorcin KO mice entered into adulthood, 6-month-old sorcin KO cardiomyocytes presented modest but statistically higher Ca^{2+} transient amplitude than WT under basal conditions (Fig. 30B). The stroke volume and fractional shortening of adult sorcin KO heart, which were recorded by echocardiogram, presented a tendency of increase (Fig. 14E, F, non-banded) compared to WT (the Langendorff perfusion

cannot measure differences in contractility under basal conditions, as the baseline left ventricular pressure was manually set at ~70 mmHg by adjusting the size of the pressure balloon (Fig. 13). Under isoproterenol stimulation, 6-month-old sorcin KO cardiomyocytes did not present significant decrease in Ca^{2+} transient amplitude and SR Ca^{2+} load than WT (Fig. 30B), and KO hearts had comparable heart contractility as WT.

Therefore, both *in vivo* and *in vitro* experiments demonstrate that there is impaired heart contractility in young sorcin KO mice but preserved contractility in adult mice. The observed phenomenon leads to the question: how Ca^{2+} transient amplitude and SR Ca^{2+} load are maintained in adult sorcin KO heart, even though there are increased spontaneous Ca^{2+} release events and decreased SERCA pumping rate? We believe that the electrophysiological remodeling of I_{Ca} and I_{NCX} may be important compensatory mechanisms. As the increased SR Ca^{2+} leak and decreased SERCA pumping eventually deplete SR Ca^{2+}, sorcin KO cardiomyocytes become more dependent on external Ca^{2+} to activate contractions and reload the SR. Hence, sorcin KO cells must increase their pool and/or their activity of LTCC. The increased Ca^{2+} influx (Ca^{2+} in, Na^{+} out) through overexpressed NCX (Fig. 16, 18, 20) during the upstroke of the action potential also may contribute to maintaining SR Ca^{2+} release. Since a larger Ca^{2+} entry and SR Ca^{2+} leak cannot be sustained without a comparable Ca^{2+} extrusion mechanism, the 2.2-fold increase in the density of sarcolemmal NCX, who works in forward mode (Ca^{2+} out, Na^{+} in) during diastole, represents such concomitant Ca^{2+} extrusion mechanism.

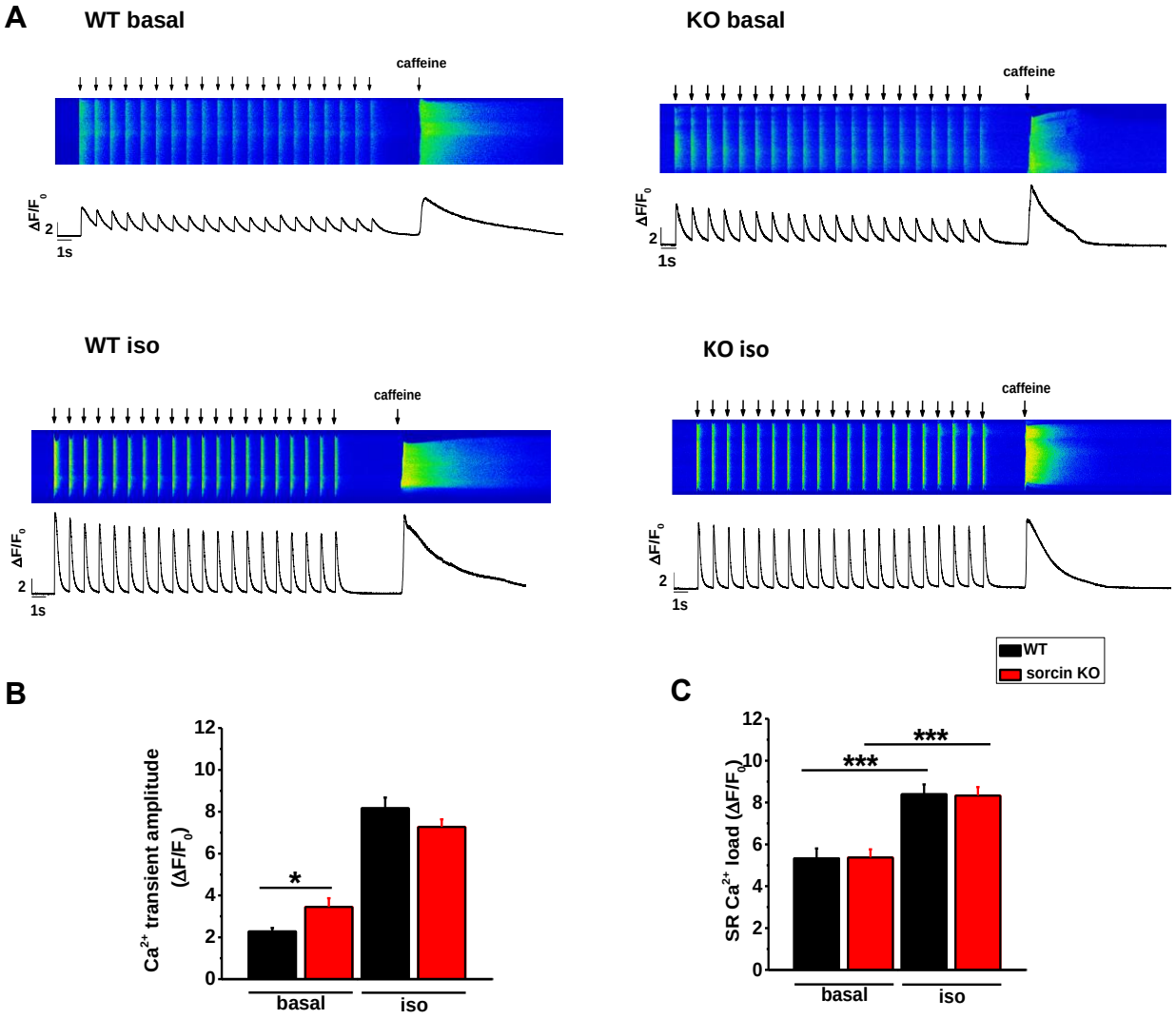

Figure 30. Intracellular Ca^{2+} transients and SR Ca^{2+} load of 6-month-old sorcin KO cardiomyocytes. (A) Representative recordings of Ca^{2+} transients and SR Ca^{2+} load of WT and sorcin KO cardiomyocytes under basal conditions and isoproterenol stimulation. Cardiomyocytes were paced 20 times and 10 mM caffeine was perfused to the cell after pacing to measure SR Ca^{2+} load. (B-C) Ca^{2+} transient amplitude (B), SR Ca^{2+} load (C) of 6-month-old WT and sorcin KO cardiomyocytes under basal conditions and isoproterenol stimulation. WT-basal n=13, KO-basal n=14, WT-iso n=13, KO-iso n=16. *, $p<0.05$ vs. WT; ***, $p<0.001$ (t-test).

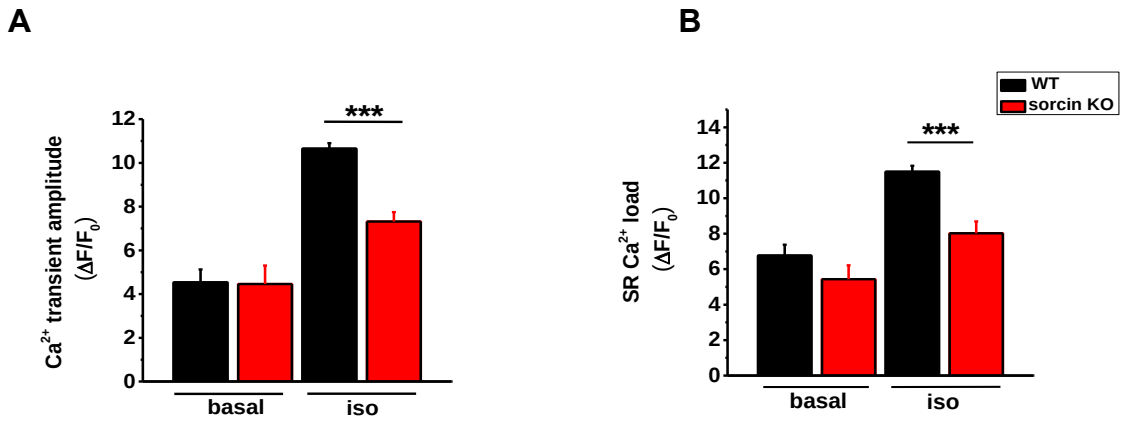

Figure 31. Intracellular Ca^{2+} transients and SR Ca^{2+} load of 1-month-old sorcin KO cardiomyocytes. (A-B) Ca^{2+} transient amplitude (A) and SR Ca^{2+} load (B) of 1-month-old WT and sorcin KO cardiomyocytes under basal conditions and isoproterenol stimulation. Both WT and sorcin KO cardiomyocytes presented significant increase of Ca^{2+} transient amplitude and SR Ca^{2+} load after isoproterenol stimulation. WT basal n=12, KO basal n=8, WT iso n=14, KO iso n=13. ***, p<0.001 vs. WT (t-test).

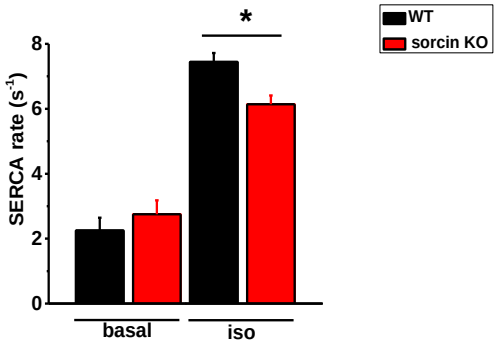

Figure 32. SERCA rate. SERCA rate of adult WT and sorcin KO cardiomyocytes under basal conditions and isoproterenol stimulation. WT-basal n=13, KO-basal n=14, WT-iso n=13, KO-iso n=16. *, p<0.05 vs. WT (t-test).

CHAPTER IX

Prolonged action potential duration, early and delayed afterdepolarizations in adult sorcin KO cardiomyocytes

9.1 Introduction

It has been demonstrated that spontaneous Ca^{2+} sparks could trigger cell-wide Ca^{2+} waves, leading to -aftercontractions between two normal beatings (Chapter I, 1.6) (43). In accordance with this notion, 1-month and 6-month-old sorcin KO mice presented ventricular arrhythmias under acute stress, suggesting that the ablation of sorcin *per se* predisposes mice to arrhythmias. Nonetheless, young sorcin KO mice presented short ventricular arrhythmia episodes (19.15±4.44s), whereas adult sorcin KO mice presented stable, long-lasting ventricular tachyarrhythmias (356±151s, rank-sum test $p<0.05$ vs. young ones). Based on this observation, we propose that the electrophysiological remodeling of I_{Ca} and I_{NCX}, although could bring beneficial compensatory effects, may also provide a substrate for sustained ventricular arrhythmias because: 1) The enhanced inward I_{NCX} can lead to membrane depolarization and further, may trigger arrhythmogenic DADs if fired by spontaneous Ca^{2+} release events (116); 2) both increased I_{Ca} and I_{NCX} may prolong AP repolarization and induce early afterdepolarizations (EADs) (117, 118). To investigate if the electrophysiological remodeling described above brings about arrhythmogenic events in sorcin KO

cardiomyocytes, I recorded action potentials (APs) and Ca^{2+} transients simultaneously (119) in 6-month-old sorcin KO cardiomyocytes.

9.2 Stochastic early afterdepolarizations and prolonged action potential duration in 6-month-old sorcin KO cardiomyocytes under basal conditions.

Action potential and Ca^{2+} activities were recorded simultaneously by using the combined technique of patch clamp and confocal microscopy. In current clamp mode, action potentials were triggered by the 3-6 ms current injection of 400 pA at 1 Hz for 20 times. 0.2 mM fluo-4 pentapotassium salt was dialysed into the cell via pipette solution to record Ca^{2+} activities simultaneously. Ca^{2+} images were collected by unidirectional line scan at the speed of 10 μs/pixel. After pacing, the cell was left in resting state to observe spontaneous Ca^{2+} release events.

Unlike the human cardiac action potential that presents a plateau phase during repolarization, the mouse cardiac action potential has a fast repolarization phase due to the strong effect of I_{to} (120) and other repolarizing currents. The APD of mice ventricular cardiomyocytes is around 100ms, which has important meaning to the fast heart rate in mice. Under basal conditions, cardiomyocytes had resting potential at around -70 mV. When stimulated by 1 Hz current injection, most (11 of 13) of WT cardiomyocytes presented normal triangle-shaped action potential, which triggered synchronized Ca^{2+} transients and cell contraction at 1 Hz frequency (Fig. 33).

Under basal conditions, 8 out of 12 KO cardiomyocytes had normal APs and Ca^{2+} transients as WT. Four out of 12 sorcin KO cells presented EADs, which were

accompanied by spontaneous Ca^{2+} release events between pacing. However, because 1 out of 11 WT cardiomyocytes also presented EADs, EAD frequency was not statistically different between sorcin KO and WT cardiomyocytes (p=0.128) (Fig. 34, 35).

The APD was analyzed by measuring the time at which the membrane potential was 25, 30, 50, 70, 75, 80, and 90 percentage repolarized. Among 12 sorcin KO cells, 6 had APD90 longer than 300 ms, including 4 that presented EADs and 2 that did not. The rest of 6 sorcin KO cells had APD90 that were less than 200 ms (Fig. 36). Although the variability of APD was large, the APD at 70, 75, 80, 90 percentage of repolarization were significantly increased in sorcin KO cells compared with WT (Two-way RM ANOVA $p<0.001$).

In summary, most of sorcin KO cardiomyocytes presented normal APs and Ca^{2+} transients under basal conditions. Although some sorcin KO cardiomyocytes presented EADs and extremely long APD, the incidence did not reach statistical significance and so the KO mice did not present ventricular arrhythmias nor long Q-T interval at baseline (WT 0.0253±0.0042 vs. KO 0.0237±0.0034 s). Nonetheless, the phenomenon might be a sign of disturbed Ca^{2+} homeostasis in sorcin KO cardiomyocytes.

9.3 Ca^{2+} waves, delayed afterdepolarizations and triggered activities in 6-month-old sorcin KO cardiomyocytes under isoproterenol stimulation

Under isoproterenol stimulation, sorcin KO cardiomyocytes had significantly higher frequency of spontaneous Ca^{2+} waves than WT. Seventy-eight percent (47/60) of spontaneous Ca^{2+} waves in sorcin KO cardiomyocytes led to membrane depolarizations

that were of sufficient amplitude to reach threshold for I_{Na} activation, thus triggering full-blown DADs and synchronized full-cell-width Ca^{2+} transients, which were called triggered activities. By contrast, only 35% (6/17) of spontaneous Ca^{2+} waves developed into triggered activities in WT cardiomyocytes, while the rest only led to mild (<20 mV) membrane depolarization (Fig. 37). As sorcin KO cardiomyocytes had higher incidence of spontaneous Ca^{2+} waves, and their Ca^{2+} waves led to APs more readily, the frequency of triggered activities in sorcin KO cardiomyocytes was dramatically higher than WT (Fig. 38).

Although sorcin KO cardiomyocytes had very few EADs during pacing under isoproterenol stimulation, they still presented significantly longer APDs at 70, 80, and 90 percent of repolarization compared with WT (Fig. 39).

9.4 Chelation of $[Ca^{2+}]_i$ prevented triggered activities in sorcin KO cardiomyocytes

To evaluate if $[Ca^{2+}]_i$ is required to trigger EADs and DADs in sorcin KO cardiomyocytes, we added Ca^{2+} chelators in the pipette solution to buffer free $[Ca^{2+}]_i$. We first dialyzed 10 mM 1,2-bis(o-aminophenoxy)ethane-N,N,N',N'-tetraacetic acid (BAPTA) in cells, which completely quenched Ca^{2+}-induced Ca^{2+} release in paced cells, and significantly decreased APD (Fig. 40, 41). Under isoproterenol stimulation, zero out of 7 sorcin KO cardiomyocytes dialyzed with BAPTA developed DADs (Fig. 40A, 42).

We then tested the slower Ca^{2+} chelator, EGTA. EGTA also significantly decreased APD in sorcin KO cardiomyocytes (Fig. 41). Since the buffering rate of EGTA is ~100 times slower than that of BAPTA, cells dialyzed with EGTA presented "Ca^{2+} spikes"

(121) of lower amplitude than normal Ca^{2+} transients when initially paced, and then decreased in amplitude later in time. Resting $[Ca^{2+}]_i$ slightly increased with pacing as the Ca^{2+}-binding capacity of EGTA reached saturation. Among 8 cardiomyocytes dialyzed with EGTA, 3 presented DADs after pacing, which were accompanied with Ca^{2+} spikes (Fig. 40B, 42). The results suggests that $[Ca^{2+}]_i$ is necessary to trigger electrical alterations in the sarcolemma of sorcin KO cardiomyocytes.

9.5 Summary

The electrophysiological remodelings, although beneficial in maintaining heart contractility, may alter the shape of the action potential and trigger focal activity. Under basal conditions, 6 out of 12 sorcin KO cardiomyocytes presented significantly prolonged APD 90, and 4 presented EADs (Fig. 35, 36). The significantly enhanced I_{Ca} in sorcin KO cardiomyocytes under basal conditions led to the prolongation of the action potential, which provided a favorable condition for the reactivation of I_{Ca} during the plateau phase of the action potential. Other factors, like reactivation of I_{Na}, may also contribute to the initiation of EADs (122). Although a fraction of sorcin KO cardiomyocytes had severe EAD events, the majority of KO cells presented normal AP and Ca^{2+} transients, so the incidence of EADs in sorcin KO cardiomyocytes was not significantly higher than that of WT (Fig. 35). Accordingly, sorcin KO mice did not show alteration in QT interval and arrhythmias under basal conditions.

Under isoproterenol stimulation, resting sorcin KO cardiomyocytes presented increased Ca^{2+} sparks and Ca^{2+} waves due to RyR2-hyperactivity. As SERCA rate was decreased in sorcin KO cardiomyocytes, the contribution of NCX on $[Ca^{2+}]_i$ extrusion increased.

The inward I_{NCX}, however, led to membrane depolarization that may trigger DADs. The increase of I_{NCX} in sorcin KO cardiomyocytes is $[Ca^{2+}]_i$ independent, as KO cardiomyocytes presented increased I_{NCX} when $[Ca^{2+}]_i$ of both WT and sorcin KO cardiomyocytes was set at 210 nM (Fig. 20). Thus, although WT cardiomyocytes also had some spontaneous Ca^{2+} release events under isoproterenol stimulation, the Ca^{2+} release-induced I_{NCX} was not large enough to depolarize the membrane potential to the threshold of firing (Fig. 37A). The complete quenching of Ca^{2+} propagation by the fast Ca^{2+} chelator, BAPTA, fully prevented DADs in sorcin KO cardiomyocytes, suggesting $[Ca^{2+}]_i$ is prerequisite for triggering DADs in sorcin KO cells.

The electrophysiological remodeling of adult sorcin KO cardiomyocytes provides a substrate for sustained ventricular arrhythmias. When spontaneous Ca^{2+} release events appear as a trigger, sorcin KO cardiomyocytes are more readily to have focal activities and DAD-induced ventricular arrhythmias. In accordance with the *in vitro* recording, adult sorcin KO mice presented long-lasting ventricular arrhythmias, cardiac arrest, and sudden death after the injection of an arrhythmogenic cocktail. Our project, for the first time, illustrates that the loss of sorcin is associated with lethal ventricular arrhythmias.

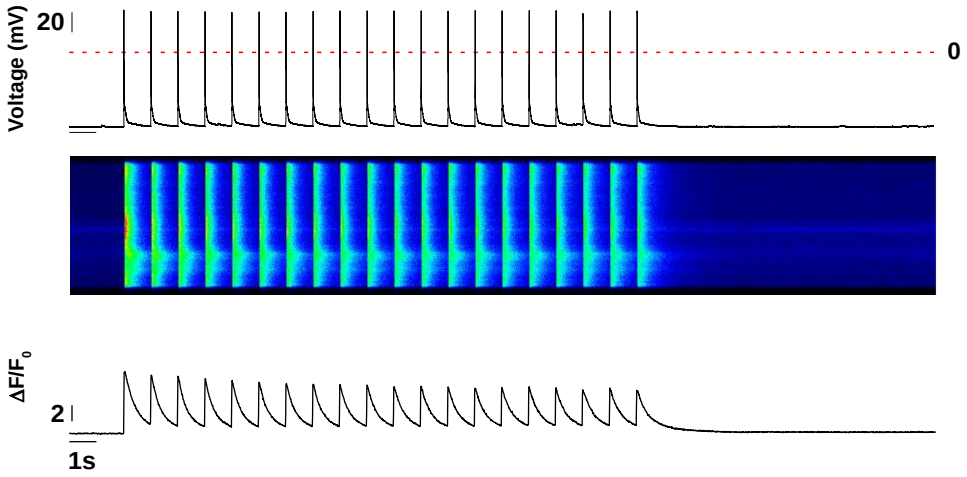

Figure 33. A representative recording of action potential and Ca^{2+} transient in a WT cardiomyocyte under basal conditions. Action potential was triggered by the 3-6ms current injection of 400pA at 1Hz for 20 times. 0.2 mM fluo-4 pentapotassium salt was dialysed into the cell via pipette solution to record Ca^{2+} activities. Upper panel: action potential; arrows indicate the time when the electrical stimulus was applied; middle panel: fluorescent recording of Ca^{2+} transient; under panel: line plot of Ca^{2+} transient.

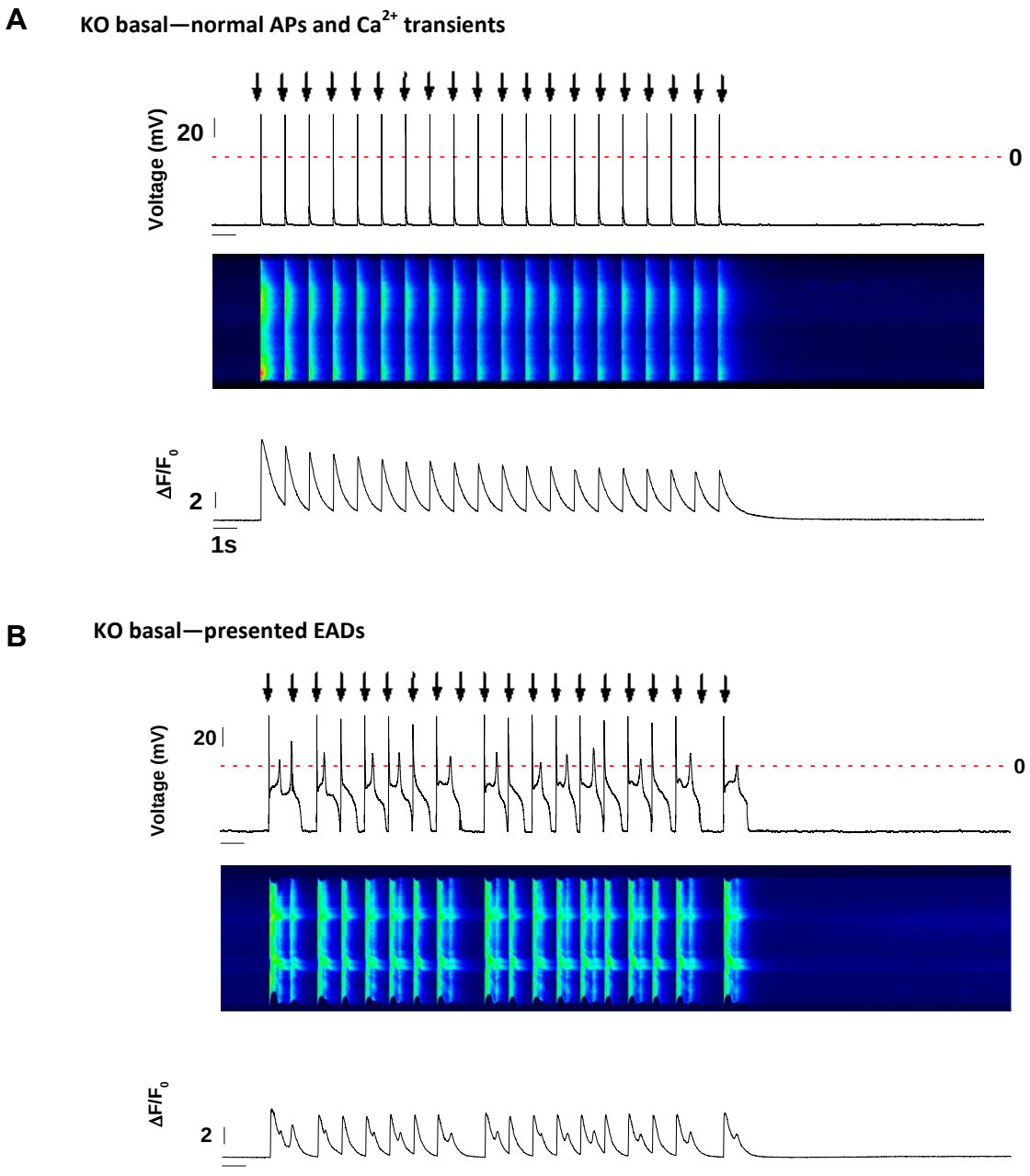

Figure 34. Representative recordings of action potential and Ca^{2+} transient in sorcin KO cardiomyocytes under basal conditions. (A) A sorcin KO cardiomyocyte presented normal action potentials and Ca^{2+} transients under basal conditions. (B) A sorcin KO cardiomyocyte presented EADs, which were accompanied with spontaneous Ca^{2+} waves between pacing. APD was prolonged due to appearance of EADs. Arrows indicate the time when the electrical stimulus was applied.

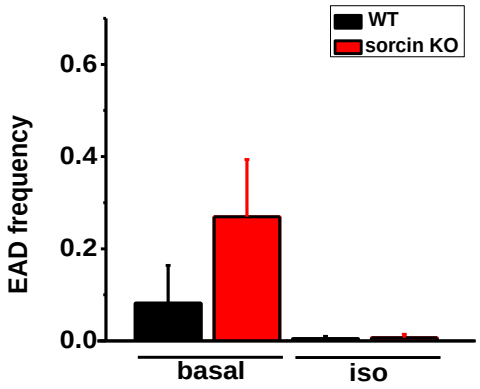

Figure 35. EAD frequency of WT and sorcin KO cardiomyocytes under basal conditions and isoproterenol stimulation. WT-basal n=11, KO-basal n=12, WT-iso n=10, KO-iso n=14 (Rank-sum test).

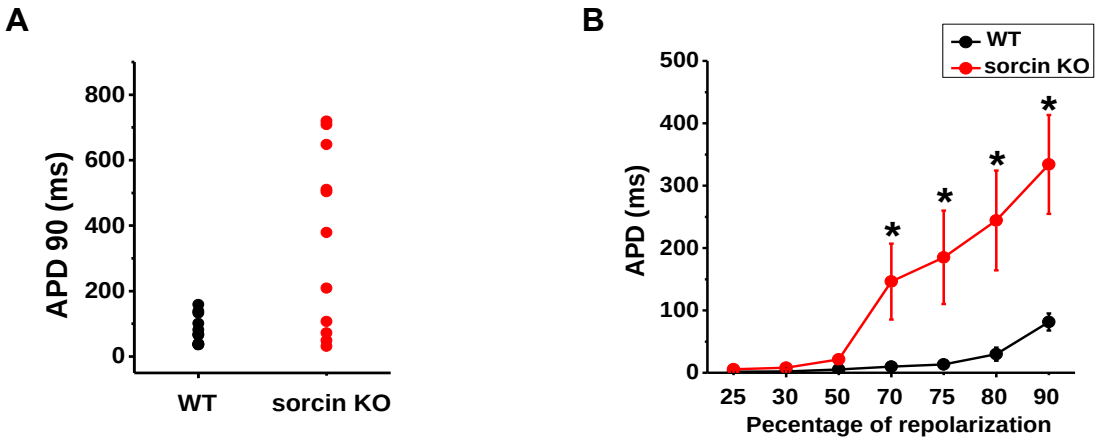

Figure 36. Action potential duration under basal conditions. (A) Scatter plot of APD90 under basal conditions. 6 of 12 sorcin KO cells presented APD 90 that was longer than 200ms. (F) APD at indicated percent of repolarization under basal conditions. WT-basal n=11, KO-basal n=12. *, p<0.05 vs. WT (Two-way RM ANOVA).

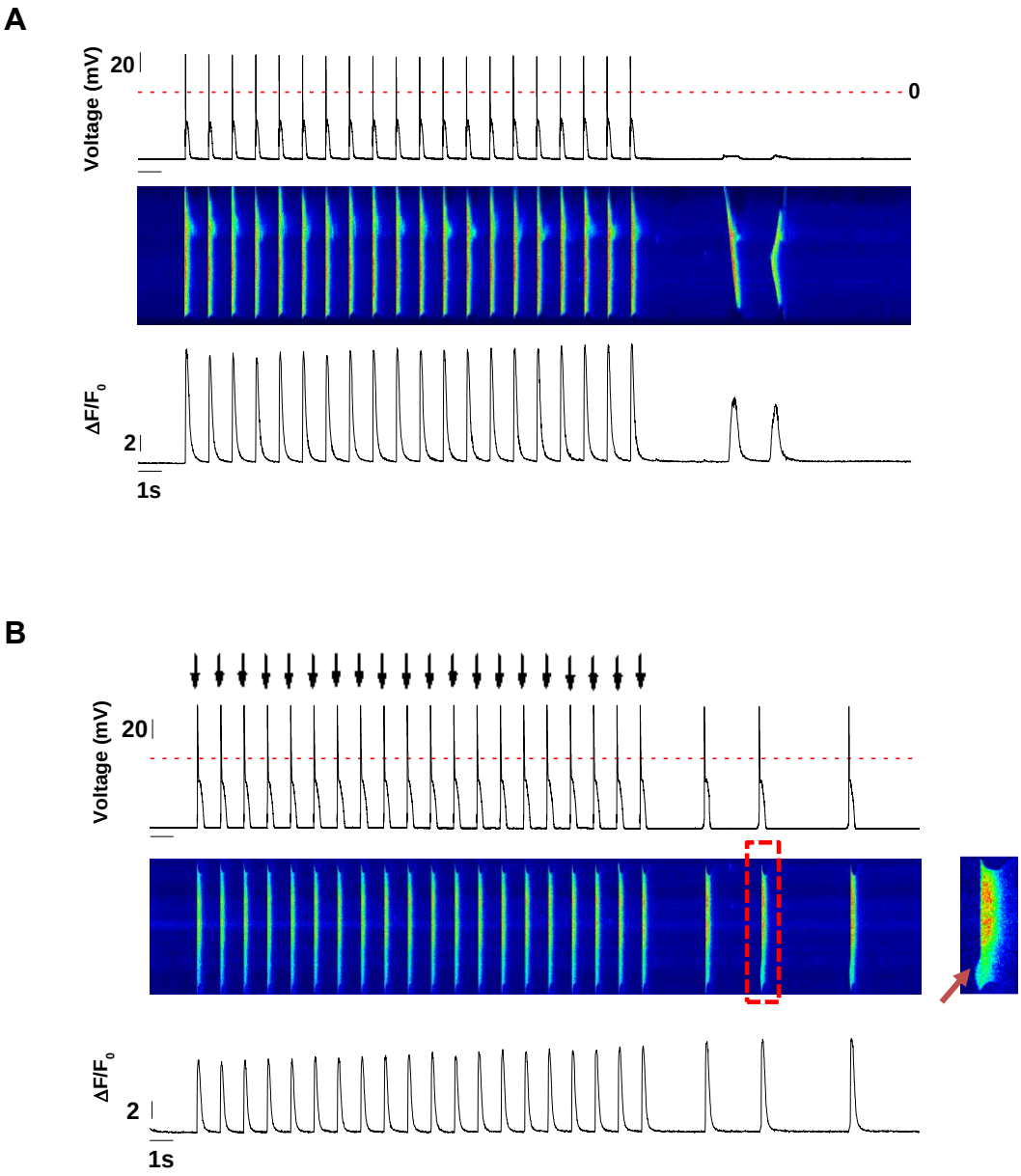

Figure 37. Action potential and Ca^{2+} transients under isoproterenol stimulation. (A) Representative WT cardiomyocyte that presented spontaneous Ca^{2+} release events but not triggered activity after pacing. (B) Representative sorcin KO cardiomyocyte that presented triggered activities after pacing. Insert at right: expanded image of the spontaneous Ca^{2+} wave in the red frame, showing how a localized Ca^{2+} release (arrow) ignited a full Ca^{2+} transient and triggered activity. Arrows indicate the time when the electrical stimulus was applied.

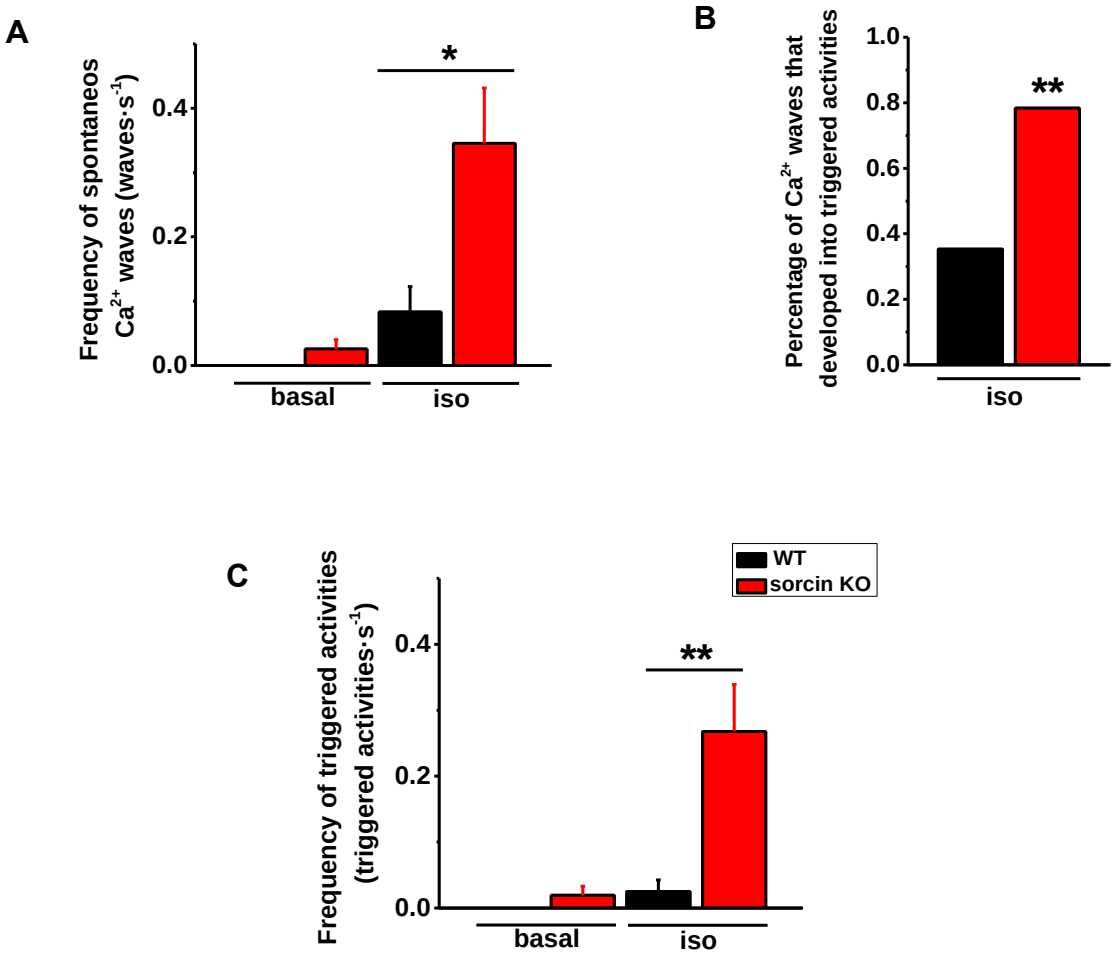

Figure 38. Frequency of Ca^{2+} waves and triggered activities. (A) Frequency of spontaneous Ca^{2+} waves in quiescent state. (B) Percentage of spontaneous Ca^{2+} waves that developed into triggered activity under isoproterenol stimulation: 3 out of 14 and 47 out of 60 spontaneous Ca^{2+} waves in WT and sorcin KO cardiomyocytes, respectively, developed into triggered activities. (C) Frequency of triggered activities in quiescent state. WT-basal n=11, WT-iso n=12, KO basal n=10, KO-iso n=14 cells. *, $p<0.05$ vs. WT; **, $p<0.01$ vs. WT (t-test, rank-sum test).

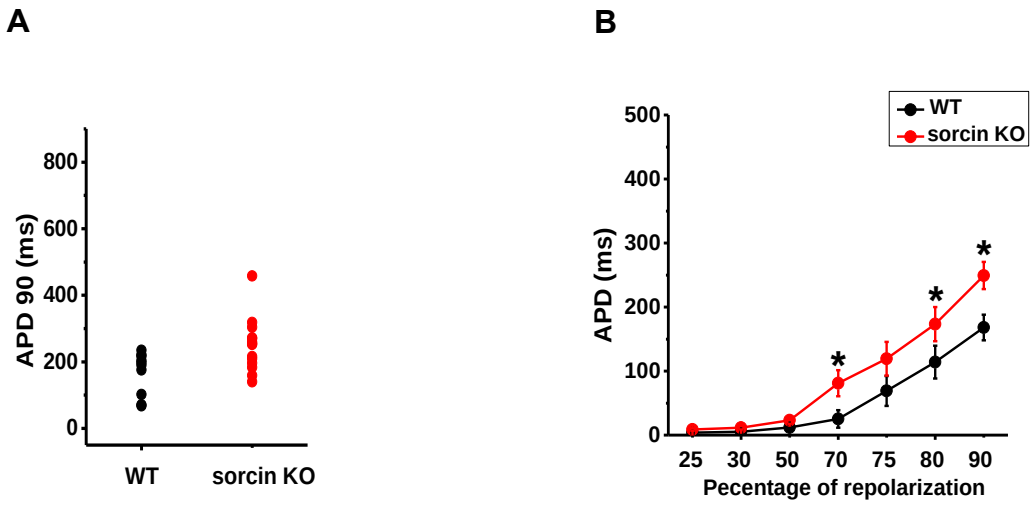

Figure 39. Action potential duration under isoproterenol stimulation. (A) Scatter plot of APD90 under isoproterenol stimulation. Each dot represents a different cell. (B) APD at indicated percent of repolarization under isoproterenol stimulation. WT-basal n=11, WT-iso n=12, KO basal n=10, KO-iso n=14 cells. *, $p<0.05$ vs (Two-way RM ANOVA).

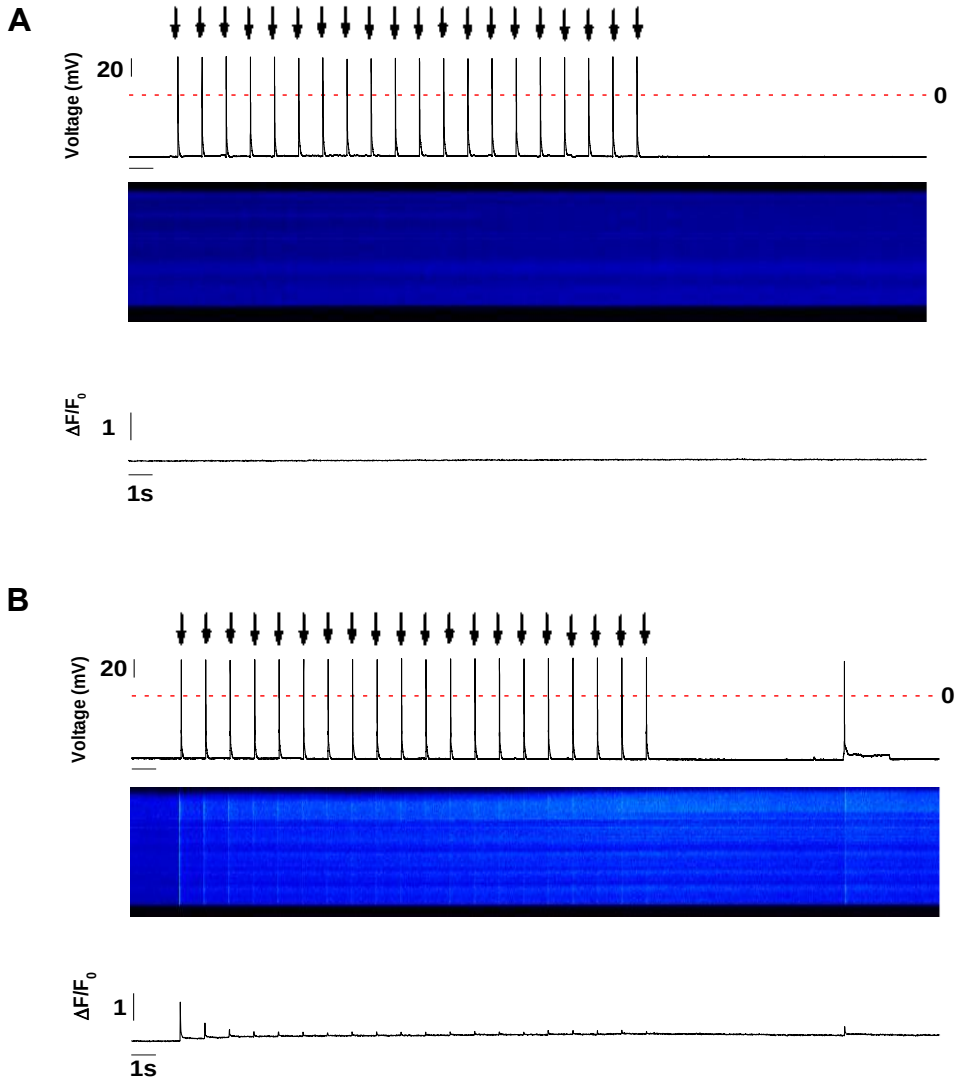

Figure 40. Effects of Ca^{2+} chelators on action potential and Ca^{2+} transient. (A) Representative recording of action potential and Ca^{2+} activity in a sorcin KO cardiomyocyte dialyzed with 10 mM BAPTA under isoproterenol stimulation. (B) Representative recording of action potential and Ca^{2+} activity in a sorcin KO cardiomyocyte dialyzed with 10 mM EGTA under isoproterenol stimulation. Arrows indicate the time when the electrical stimulus was applied.

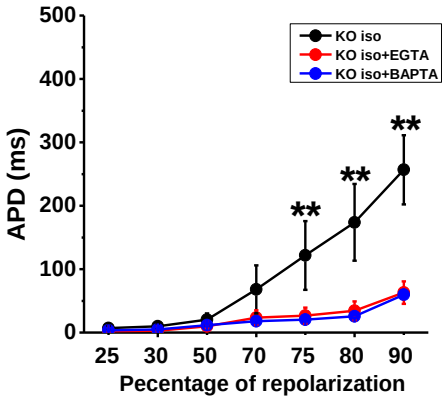

Figure 41. Effects of Ca^{2+} chelators on action potential duration. APDs of sorcin KO control, KO-EGTA, and KO-BAPTA cardiomyocytes. KO-iso n=6, KO-iso + EGTA n=8, KO-iso + BAPTA n=7 cells. **, p<0.01 vs. KO-iso + EGTA and KO-iso + BAPTA cardiomyocytes (Two-way RM ANOVA).

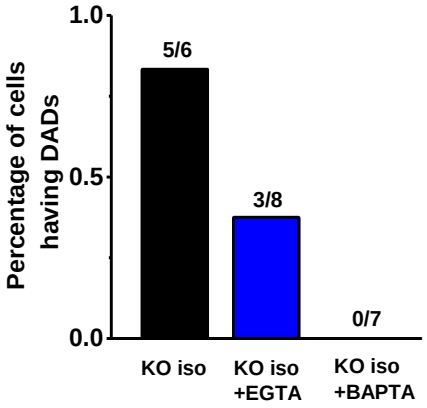

Figure 42. Percentage of cells that presented triggered activities under isoproterenol stimulation. KO-iso n=6, KO-iso + EGTA n=8, KO-iso + BAPTA n=7 cells.

CHAPTER X

Discussion

Sorcin, a 21.6-kDa Ca^{2+} binding protein originally discovered in multi-drug resistance cells, is also expressed in ventricular cardiomyocytes of mammalian species, including humans (81, 104). This basic observation compels a fundamental question: *what does sorcin do in cardiac cells?* We previously found that the majority of sorcin (but not all) is localized in bands of high intensity running along the width of the cardiomyocyte, interspaced at about ~1.7 μm, and overlapping with RyR2 located in *z*-lines (78). Thus, a great portion of sorcin appears localized in the dyadic junction, where crucial steps of e-c coupling occur. Using single RyR2 channel or isolated ventricular cells, we have found that sorcin rapidly binds to RyR2 and directly inhibits single channel activity. In cardiomyocytes, sorcin translocates from cytosol to membrane-bound protein targets in a Ca^{2+}-dependent manner, and attenuates Ca^{2+} sparks and Ca^{2+} transients (86). These and other findings affirmed a role for sorcin in modulation of Ca^{2+} release by RyR2s, but its integral role in Ca^{2+} homeostasis and e-c coupling of the heart remained unclear. Here, we generated a mouse line with genetic ablation of *Sri,* the gene encoding for sorcin in humans and animal. These mice were born without heart structural remodeling, and propagated at the expected Mendelian ratio (Fig. 8). However, hearts of young (1-month-old) sorcin KO mice, although showing no apparent electrical remodeling, quickly presented impaired contractility and transient tachyarrhythmias upon β-adrenergic

stimulation (Fig. 12, 15), indicating that sorcin absence *per se* predisposes mice to decreased heart function and arrhythmias. As sorcin KO mice developed into adulthood, an increase in LTCC and NCX expression (Fig. 16) and activity (Fig.18, 20, 23) suggests cardiac contractions become increasingly dependent on sarcolemma Ca^{2+} entry and extrusion. Thus, the prolonged absence of sorcin plus its resultant electrical remodeling appears to lead the adult sorcin KO mice to a precarious condition, because a) stress tests promptly induced aberrant cardiac electrical activity (sustained ventricular tachyarrhythmias and sudden cardiac arrest) (Fig. 10, 11), b) at 7 months, their survival rate was lower than WT even under resting conditions (Fig. 9A), c) aortic banding that was tolerated by WT mice caused significantly more attrition in sorcin KO mice (Fig. 9B). All these results, therefore, support the hypothesis that sorcin is a relevant component of the e-c coupling machinery of the heart, independent of or in addition to other roles that it may play in other cells.

10.1 Sorcin KO phenotype and resemblance to CPVT

Sorcin ablation brings about significant alterations in Ca^{2+} homeostasis of ventricular myocytes, and this becomes more apparent under β-adrenergic stimulation: isolated cardiomyocytes stimulated with isoproterenol displayed Ca^{2+} oscillations, aftercontractions, and DAD-elicited triggered activity (Fig. 37, 38), whereas SR Ca^{2+} leak and Ca^{2+} sparks were also especially increased under adrenergic stimulation (Fig. 27, 28, 29). All these alterations are typically associated with hyperactive or “sensitized” RyR2 channels, and the general features of the sorcin KO phenotype are strikingly similar to those of CPVT, an arrhythmogenic syndrome linked to hyperactive RyR2

channels. In both cases, a cardiac phenotype is “silent” functionally and structurally and goes unnoticed until sympathetic stimulation triggers catastrophic Ca^{2+} release and life-threatening arrhythmias. Bidirectional ventricular tachycardia, characteristic of Ca^{2+}-overloaded cells and a hallmark sign of CPVT (43), is also present in sorcin KO mice (Fig. 10, 12). We postulate, therefore, that RyR2 channels are among the most prominent molecular targets of sorcin and the most affected by its absence.

10.2 Amplification of sorcin effect by sympathetic stimulation

During normal β-adrenergic stimulation, RyR2s are especially active due to increased I_{Ca} and higher SR Ca^{2+} load. Ca^{2+} release from a cluster of RyR2s into the dyadic nanospace could theoretically increase local [Ca^{2+}] to up to ~100 μM(123, 124), which is sufficient to translocate sorcin to SR membrane targets. By decreasing RyR2 activity, sorcin conceivably attenuates Ca^{2+}-induced Ca^{2+} release and helps prevent Ca^{2+}-triggered membrane depolarization. On the other hand, sorcin has been shown to be PKA-phosphorylated at residue S178 (80, 88, 89), and others (89) and we (unpublished data) have shown that phosphorylation facilitates translocation of sorcin from cytosolic to membrane compartments. Therefore, the high [Ca^{2+}] in the dyadic space and sorcin phosphorylation during β-adrenergic stimulation amplify sorcin’s regulatory effect on RyR2, its key target.

10.3 Hypothesis for an integrated role of sorcin in e-c coupling

While initial experiments to elucidate sorcin’s role in the heart demonstrate that sorcin inhibits Ca^{2+} release by RyR2 channels, equally compelling are the findings that sorcin

increases NCX activity (90, 91), accelerates LTCC inactivation (87, 125), and stimulates SERCA2a Ca^{2+} uptake (89). All these effects are congruent with the general hypothesis that in normal ventricular myocytes, sorcin forms macromolecular complexes with at least four key players of e-c coupling, with its overall effect being that of a “cytosolic Ca^{2+} sweeper”. By summing the individual effects exerted by sorcin on the above-mentioned Ca^{2+} transporters, it seems obvious that the unified role for sorcin in cardiac cells is to restrict I_{Ca}-triggered RyR2 activity, prevent diastolic SR Ca^{2+} leak, and avoid Ca^{2+} accumulation in cytosolic compartments. However, what is not immediately obvious is that such an integrated effect is not possible in the long run, because it would eventually deplete cardiac cells of Ca^{2+} by restricting Ca^{2+} entry and release and stimulating Ca^{2+} extrusion. In a delimited and finely regulated system such as a ventricular cell, inward and outward Ca^{2+} fluxes must be equal, and in this zero-sum game, small disturbances are rapidly counteracted, lest profound alterations in electrical excitability, e-c coupling and signal conduction ensue (126). Therefore, a process that mitigates adrenergic-induced Ca^{2+} buildup is necessary, and we propose that sorcin is an integral part of such a process. Sorcin’s Ca^{2+} removal role may be especially active during β-adrenergic stimulation of the heart, right after cardiac cells have transitioned to Ca^{2+} overload due to a rapid surge of plasmalemmal Ca^{2+} entry. It is during this time window that Ca^{2+} fluxes are briefly unbalanced and cardiac cells are in a precarious equilibrium because the β adrenergic-induced Ca^{2+} overload, while maximizing contractions, promotes also the generation of DADs (by spontaneous Ca^{2+} release) and EADs (by prolonging APD). If removal of adrenergic-induced Ca^{2+} buildup by sorcin is indeed necessary, then sorcin KO mice should develop arrhythmias mainly during β-

adrenergic stimulation, or under stress. In favor of this hypothesis, others and we find that adrenergic stimulation of ventricular cells increases translocation of sorcin from cytosolic to membrane-bound targets (89) and that sorcin KO hearts and living mice are readily thrown into tachyarrhytmias under sympathetic simulation. Besides preventing Ca^{2+} overload during systole, sorcin also prevents spontaneous Ca^{2+} leak during diastole. In the absence of sorcin, cardiomyocytes presented increased diastolic Ca^{2+} leak, which negatively affects SR Ca^{2+} and Ca^{2+} transient amplitude (1-month-old). Thus, the overall hypothesis that emerges from this and previous studies is that sorcin "sweeps" cytosolic compartments from excess Ca^{2+} during systole and diastole.

10.4 General model to explain heart contractility and rhythm in young and adult sorcin KO mice

From the above, we propose a *model* that integrates the major mechanisms governing the induction of arrhythmias/impaired heart contractility in young and adult sorcin KO mice. First, the model must consider fundamental differences in e-c coupling between immature (neonatal and young mice) and adult ventricular cells, with the former relying more on external Ca^{2+} entry due to incompletely formed T-tubules and dyads (127), while the latter obtaining from the SR (by CICR) most of the Ca^{2+} needed for contractions (29). Second, the model must also consider data showing increased LTCC and NCX density in adult, but not in young, sorcin KO cardiomyocytes, as observed here (Fig. 16). In both cases, however, β-adrenergic stimulation increases contractility by increasing Ca^{2+} cycling. Hence, in the absence of sorcin, a modulator that normally decreases Ca^{2+} entry, promotes Ca^{2+} extrusion, stimulates SR Ca^{2+} reuptake, and

decreases SR Ca^{2+} fluxes, the most plausible mechanism to induce ventricular arrhythmias in the *immature* hearts is one in which the adrenergically-stimulated cytosolic Ca^{2+} surges generate an inward depolarizing current of sufficient magnitude to bring membrane potential to threshold, generating DADs and subsequent triggered activity. This mechanism would be akin to that postulated to occur in CPVT (43) and does not require electrical remodeling (normal expression of e-c coupling proteins). On the other hand, abnormal expression of e-c coupling proteins in the *mature* sorcin KO hearts suggests gradual adaptation of the e-c coupling machinery to the absence of sorcin: the increased SR Ca^{2+} leak and decreased SERCA pumping may eventually depleting SR Ca^{2+}, prompting sorcin KO cardiomyocytes to become more dependent on external Ca^{2+} to activate contractions and reload SR Ca^{2+}. Hence, KO cells must increase their pool and/or their activity of LTCC (Fig. 16, 23). The increased Ca^{2+} influx (Ca^{2+} in, Na^{+} out) through overexpressed NCX (Fig. 16, 20) during the upstroke of action potential also makes contribution to maintaining SR Ca^{2+} release. Since a larger Ca^{2+} entry and SR Ca^{2+} leak cannot be sustained without a comparable Ca^{2+} extrusion mechanism, the 2.2-fold increase in the density of sarcolemmal NCX (Fig. 16), who works in forward mode (Ca^{2+} out, Na^{+} in) during diastole, represents such concomitant Ca^{2+} extrusion mechanism (Fig. 18, 20). In this hypothetical scheme, adult sorcin KO ventricular cells appear to tilt the balance between sarcolemmal and SR Ca^{2+} fluxes to maintain a pseudo-equilibrium that is stable under basal conditions but favors sustained ventricular arrhythmias under adrenergic stimulation (Fig. 43).

10.5 Limitations of our study and future plan

Our general hypothesis above, while viable and accommodating of our major observations here, requires further testing and experimentation that go beyond the scope of this thesis. First, as it happens with most transgenic animals, ablation of a single gene seldom results in “clean” knockout of the target protein, because such targeted gene and protein interact with a variety of (known and unknown) partners that constitute an indivisible functional network. In the case of the sorcin KO, we performed a *targeted* analysis of what we considered the most relevant sorcin-interacting proteins and found alterations in some, but not all, binding partners. Wider changes in protein expression would not be surprising, and they may even force key revisions of our hypothesis. Second, sorcin is encoded by a single gene (*Sri*) and expressed in several tissues, therefore, it is possible that the cardiac arrhythmias or the decreased lifespan of sorcin KO mice reported here may have extra-cardiac origins. For example, we previously reported that the absence of sorcin in pancreatic β-cells triggers ER stress (77), and it is possible that the resultant glucose intolerance may have impacted cardiac function (128). Even though our experiments using isolated, Langendorff-perfused hearts indicate that cardiac arrhythmias are present in the absence of autonomic nerve system or hormonal input, we cannot completely discard this possibility. Lastly, the majority of sorcin localizes in immunocytochemical experiments to the dyadic space and near RyR2 (86, 87), but a small portion (~18%) does not. The first study describing expression of sorcin in cardiac cells (76) found anti-sorcin reactivity in mitochondria. The potential impact of mitochondria dysfunction to the cardiac arrhythmias described here, if any, requires an in-depth study of its own.

In the future, we would like to expand our scope to other potential target proteins of sorcin. A promising target could be $Na_v1.5$, which is a member of the voltage-gated Na^+ channel family. Mutations in *SCN5A*, the encoding gene of Na_v 1.5, are related to the long QT syndrome and Brugada syndrome. We would like to investigate whether sorcin has a direct interaction with Na_v 1.5, and how this interaction may influence the membrane excitability and the action potential duration.

Because part of sorcin is expressed in mitochondria, we are also interested in knowing the role of sorcin in mitochondria function. It has been demonstrated that the high concentration of mitochondria Ca^{2+} would trigger bursts of reactive oxygen species (ROS), named superoxide flashes, in the matrix of single mitochondria (129). Therefore, we would like to investigate whether sorcin, as a Ca^{2+} regulator, may influence mitochondrial ROS production and further induce heart diseases.

10.6 Summary

In summary, data here and published studies make it increasingly evident that sorcin modulates e-c coupling in the heart, at the very least through its well-established effect on RyR2 channels, but also through newly-found molecular targets. Although our general hypothesis may require further testing, data obtained here with the sorcin KO mouse does lay some solid foundations to postulate a unified role for sorcin in cardiac cells: sorcin is a Ca^{2+}-dependent molecular switch that is activated during cytosolic Ca^{2+} surges, especially during β-adrenergic stimulation and, by binding to at least four key e-c coupling proteins, it removes Ca^{2+} from cytosolic compartments, guarantees efficient SR Ca^{2+} release, and avoids Ca^{2+}-dependent arrhythmias (130).

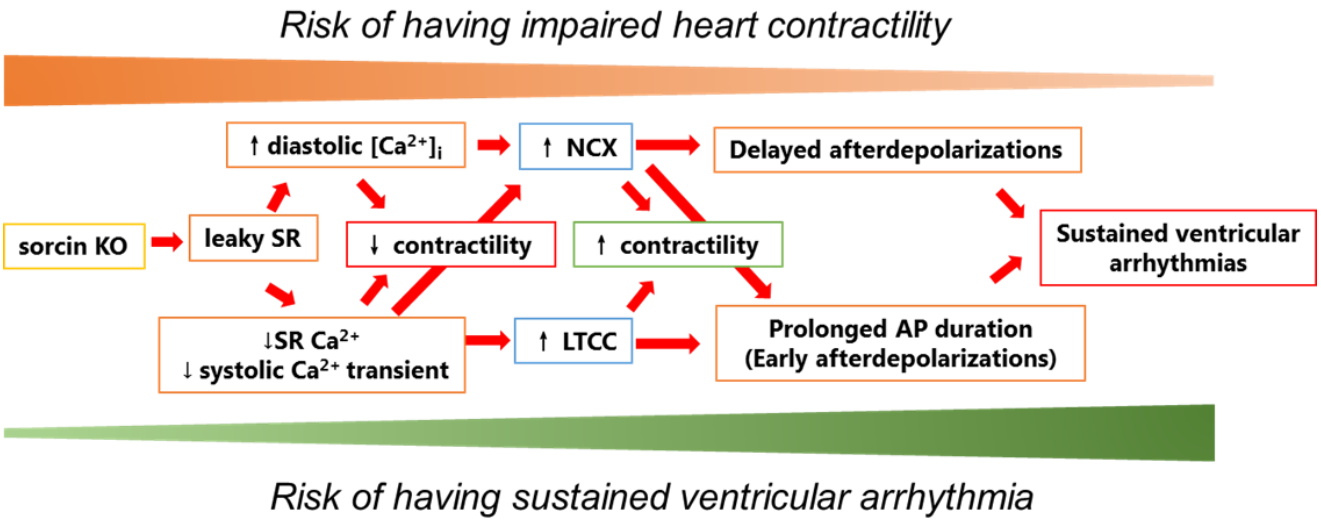

Figure 43. General model to explain heart contractility and rhythm of young and adult sorcin KO mice. At early age of the sorcin KO mouse, the increased SR Ca^{2+} leak and decreased SERCA pumping eventually deplete SR Ca^{2+}, leading to decreased heart contractility under isoproterenol stimulation. As time pass by, sorcin KO heart gradually develops electrophysiological remodeling of I_{NCX} and I_{Ca}, which helps preserving heart contractility. Although the ablation of sorcin *per se* could predispose mice to ventricular arrhythmias, the electrophysiological remodeling provides favorable substrate for DADs and EADs, leading to long-lasting ventricular arrhythmia, cardiac arrest and sudden death in adult sorcin KO mouse.

CHAPTER XI

Materials and methods

Generation of sorcin knockout mice The generation of sorcin KO mice are described in Chapter III. Briefly, the sorcin KO targeting vector was generated by homologous recombination of endogenous *Sri* and a vector containing *LoxP*-flanked exon 3 of *Sri* and Neo-cassette. The targeting vector was electroporated into mouse 129S1/SvImJ ES cells to generate a chimeric male founder. The excision of Neo cassette and *Sri* exon 3 was achieved by crossing FloxNeo$^{-/+}$ mouse in F_1 generation with EIIa-Cre transgenic mice. The *Sri*$^{+/-}$ mouse were backcrossed to 129S1/SvImJ mice for 10 generations to eliminate Cre recombinase and then used for breeding. Sorcin KO and their age-matched WT littermates were maintained and studied according to the protocol approved by the University Committee on Use and Care of Animals (UCUCA) and by the Association for Assessment and Accreditation of Laboratory Care International.

Western blot Whole heart homogenates were prepared as described before (35). Heart frozen in liquid nitrogen was pulverized by pestle, and homogenized in lysis buffer containing 0.9% NaCl, 10 mM Tris-HCl pH 6.8, 20 mM NaF, 2 µM leupeptin, 100 µM phenylmethylsulphonyl fluoride, 500 µM benzamidine, 100 nM aprotinin at 4°C. The sample was centrifuged at 1000 xg for 10 minutes, and the supernatant was collected. The protein concentration was measured by Bradford method. For western blots, 50 µg

of lysate suspended in Laemmlii buffer was separated by SDS-PAGE in 4-20% TGX or AnyKD precast gels (Bio-Rad). Proteins were transferred to PVDF membranes at 25V for 16-18h at 4°C. Then, membranes were blocked in PBS-T containing (mM) 3 KH_2PO_4, 10 Na_2HPO_4, 150 NaCl, pH 7.2–7.4, 0.1% Tween 20) plus 5% dried skim milk. Proteins were probed with the following primary antibodies: sorcin (1:2000 custom), SERCA (1:1000, ab2861, Abcam), NCX (1:200, ab6495, Abcam), Cav1.2 (1:200, ACC-003, Alomone), RyR2 (1:2000, MA3-925, ThermoFisher). After the membrane was washed three times by PBS-T, membranes were incubated with goat anti-mouse-HRP (1:1000, 31437, Thermo) or goat anti-rabbit-HRP (1:2000, 31463, Thermo). Protein-antibody reactions were detected by using SuperSignal Femto ECL reagent (Thermo), and imaged by the ChemiDoc MP apparatus (Bio-Rad). Band intensity was analyzed by the ImageLab software (Bio-Rad).

Translocation of endogenous sorcin Translocation of endogenous sorcin was measured as described before (86). Briefly, isolated mouse cardiomyocytes were centrifuged for 2 min at 2,500 rpm. Cell pellets were collected and re-suspended in bath solution containing 0.01% saponin (to permeabilize the cell) and 1 or 10 μM Ca^{2+}, with or without 300 nM isoproterenol. After ~1 min, cells were centrifuged for 5 min at 14,000 rpm and the pellets were re-suspended in Ca^{2+}-free bath solution. The cell suspensions then went through glass fiber size C (GF-C) Whatman filter placed in a vacuum-suctioned cell harvester. Membrane components were obtained by suspension of the filter in Laemmli buffer that contained (in mM): 250 Tris-HCl, 400 dithiothreitol, 8% SDS, 0.04% bromphenol blue, 50% glycerol, pH=6.8. The protein suspension was subject to western blot for sorcin as described above.

Histological staining Hearts explanted from mice were perfused with PBS and fixed in 10% neutral buffered formalin. Hearts were cut transversely, embedded in paraffin and stained with Masson's trichrome.

Mouse ventricular cell isolation Mouse ventricular cells were isolated as described before (119). Mice of 5-6 months were anesthetized by peritoneal injection of urethane (1g/kg). After deep anesthetize was achieved, sternotomy was performed and the heart was quickly excised and cannulated on a Langendorff-perfusion system by aorta. The heart was first perfused with perfusion buffer containing (mM) 10 HEPES, 0.6 Na_2HPO_4, 113 NaCl, 4.7 KCl, 12 $NaHCO_3$, 0.6 KH_2PO_4, 1.2 $MgSO_4$-$7H_2O$, 10 $KHCO_3$, 30 Taurine, 500 mM 2,3-Butanedione monoxime, 5.5 mM Glucose, pH 7.46 at 37℃ at the speed of 3ml/min. Then the heart was switched to digestion buffer which contained 773.48 u/ml Collagenase Type II, 0.14 mg/ml Trypsin, and 12.5 μM $CaCl_2$. After the heart turning soft, the ventricle was cut off from the heart and cut into pieces in the stopping buffer, which added 10% FBS and 12.5 μM $CaCl_2$ in perfusion buffer. Tissue pieces were gently suspended and the single cell supernatant was transferred to a clean tube. Ca^{2+} was reintroduced to 1.0 mM step by step and cells were finally transferred to bath solution containing (mM) 135 NaCl, 4 KCl, 1.0 $CaCl_2$, 1 $MgCl_2$, 10

Hepes, 1.2 NaH_2PO_4, and 10 glucose, pH 7.40 with NaOH.

Confocal Ca^{2+} imaging Ca^{2+} activities, including Ca^{2+} spark, field stimulation-stimulated Ca^{2+} transient, SR Ca^{2+} load, and RyR2-mediated diastolic Ca^{2+} leak, were recorded by the LSM510 Meta inverted confocal microscope (Carl Zeiss) with a 40×/1.2 N.A water immerse objective. Cardiomyocytes were incubated in bath solution with

10μM Fluo-4 AM at 37℃ for 5min, and then washed and kept in fresh bath solution. For β-adrenergic stimulation, 300 nM isoproterenol was applied in bath solution. Ca^{2+} images were collected by the unidirectional line scan of the long axis of cell, at the speed of 3.072ms/line. Fluorescence was excited at the wavelength of 488 nm and recorded at wavelength >505 nm. For Ca^{2+} spark measurement, cardiomyocytes were paced 20 times by 1Hz field stimulation (54V, 2ms duration). After pacing, Ca^{2+} sparks were recorded in quiescent state for 10s. The criterion for the fluorescence amplitude of spark was set at 1.32 (F/F_0). Ca^{2+} spark frequency, full duration at half maximum (FDHM), full width at half maximum (FWHM), and half decay time were analyzed by a self-written program based on IDL 5.5. For Ca^{2+} transient and SR Ca^{2+} load, cardiomyocytes were paced 20 times by 1Hz field stimulation, and 10 mM caffeine was perfused to the cell after pacing to deplete SR. Ca^{2+} transient amplitude was defined as the $(F-F_0)/F_0$ ($\Delta F/F_0$) of the twitch Ca^{2+} transient, and SR Ca^{2+} load was $\Delta F/F_0$ of caffeine-induced Ca^{2+} transient. The RyR2-mediated diastolic Ca^{2+} leak was measured as described before (114). Briefly, after pacing, the cardiomyocyte was perfused with $0Na^{+}$-$0Ca^{2+}$ solution containing (mM): 135 LiCl, 4 KCl, 1 $MgCl{\cdot}6H_2O$,10 Hepes, 10 EGTA, 10 Glucose, pH 7.40 with LiOH. As LTCC and NCX of the cardiomyocyte were blocked by $0Na^{+}$-$0Ca^{2+}$ solution, there was no Ca^{2+} exchange between extracellular and intracellular environment (step 1). After 10s, solution was switched to $0Na^{+}$-$0Ca^{2+}$ with 1 mM RyR2 blocker tetracaine for 30s. Tetracaine blocked diastolic Ca^{2+} leak through RyR2 so the fluorescence difference between Step 1 and 2 reflected diastolic Ca^{2+} leak (step 2). Finally the cell was perfused with 10 mM caffeine to measure the SR Ca^{2+} load (Step 3). To evaluate NCX and SERCA activity, caffeine induced Ca^{2+} transient and

twitch Ca^{2+} transient were analyzed by the following method: The $[Ca^{2+}]_i$ (shown as $\Delta F/F_0$) is fitted to the formula $Ca(t) = A + Ca_0 \cdot e^{-\frac{t}{\tau}}$, in which Ca_0 is the apex of Ca^{2+} transient. K, defined as $1/\tau$, is used to describe the decay rate of Ca^{2+} transient. During caffeine perfusion, Ca^{2+} continues to be released from the SR through open RyR2s so the decline of $[Ca^{2+}]_i$ only depends on NCX, thus $K_{caffeine}=K_{NCX}$. In normal twitching, the decay of twitch Ca^{2+} transient depends on both NCX and SERCA, so $K_{SERCA}= K_{twitch}-K_{NCX}$ (115).

For Ca^{2+} imaging with patch clamp, cardiomyocytes were dialyzed with 0.2 mM fluo-4 pentapotassium salt via pipette solution. Ca^{2+} activity was recorded by the Olympus IX51 inverted microscopy system with a 40× oil immerse objective. Ca^{2+} images were collected by the unidirectional line scan at the speed of 10μs/pixel.

Patch clamp Whole-cell patch clamp experiments were conducted by using an Axopatch 700B and a Digidata 1440A digitizer (Axon Instruments) at room temperature. For L-type Ca^{2+} current recording, cardiomyocytes were incubated in bath solution plus 30 μM TTX and 10 mM 4-aminopyridine to inhibit I_{Na} and I_{to}. The pipette solution contains (mM): 110 CsCl, 6 $MgCl_2$, 5 Na_2ATP, 0.3 Na_2GTP, 10 Hepes, and 15 TEA·Cl, pH 7.2 with CsOH. The cell was clamped at -50 mV and depolarized from -50 mV to +70 mV with an increment of 10 mV. For NCX current recording, cardiomyocytes were bathed in bath solution containing (mM) 130 NaCl, 5 CsCl, 1.2 $MgSO_4$, 1.2 $NaH_2PO_4{\cdot}H_2O$, 10 Hepes, 10 Glucose, 0.01 Nifedipine, 1 Ouabain·$8H_2O$, 0.01 Niflumic Acid, 1.0 $CaCl_2$, pH 7.40 with CsOH. Pipette solution contains (mM): 100 $CsOH{\cdot}H_2O$, 100 Glutamic Acid, 7.25 Na^+-Hepes, 1 $MgCl_2.6H_2O$, 12.75 Hepes, 2.5 Na_2ATP, 10

EGTA, 6 $CaCl_2.2H_2O$, pH 7.2 with CsOH. Once the whole-cell configuration formed, cardiomyocytes were perfused with bath solution. The cell was depolarized to -40 mV to inactivate I_{Na} and go through a ramp from +70 mV to -140 mV to induce remaining current. Then the perfusion solution was switched to bath solution plus 2.5 mM $NiCl_2$ for 30s, and the current recording protocol was repeated. NCX current—a Ni^{2+} sensitive current, was obtained by subtracting the second current from the first one. For action potential recording, cardiomyocytes were incubated in regular bath solution. The pipette solution contains (mM): 120 K-aspartate, 20 KCl, $1MgCl_2$, 4 Na_2ATP, 0.1GTP, 10 HEPES, 10 glucose, pH 7.2 with KOH. At current clamp mode, action potential was triggered by the 3-6ms current injection of 400 pA at 1Hz for 20 times, and Ca^{2+} transient was recorded by confocal microscopy at the same time. After pacing, the cell was left in quiescent state to observe DADs and Ca^{2+} waves for 10s. To quench Ca^{2+} release and propagation, 10 mM EGTA or 10 mM 5,5'-dibromo BAPTA tetrapotassium salt was added in pipette solution. When adding BAPTA in pipette solution, K-aspartate was adjusted to 80 mM.

Electrocardiography Mice were anesthetized by 5% isoflurane inhalation vaporized in oxygen at a flow rate of 0.8-1 L/min, and maintained at anesthetized state by 1.5-2% isoflurane. Mice were placed in a supine position on a heating pad of 37 ˚C, and needle ECG electrodes were placed under skin to record leads I and II ECG. After 10 min of baseline ECG recording, acute stress will be induced by intraperitoneal injection of epinephrine 2 mg/kg + caffeine 120 mg/kg. ECG was analyzed as described before (Loaiza et al., 2013). After recording, mice were sacrificed by cervical dislocation.

Transverse aortic constriction Transverse aortic constriction was conducted as described before (108). Briefly, mice were anesthetized by 5% isoflurane inhalation at the speed of 0.8-1 L/min, and maintained at anesthetized state by 1.5-2% isoflurane. During surgery, mice were kept ventilated at a respiration rate of 80-120/min, tidal volume 0.15ml. The transverse aorta was dissected, and a piece of 27½ gauge blunt needle was tied to transvers aorta by knots. Then, the needle was removed promptly to leave a 0.4 mm constriction. After surgery, mice were recovered in a clean cage with water and food, being monitored every 5-10 minutes and then returned to animal room. For analgesia, 5mg/kg Carprofen (Rimadyl) was administrated by i.p. injection preemptively and every 24 hours after surgery.

Langendorff perfusion Langendorff perfusion was conducted as described before (18). Briefly, the mouse was sacrificed by cervical dislocation, and the heart was quickly excised and cannulated on a Langendorff-perfusion system by aorta. The heart was perfused with 95% O_2+5% CO_2 gassed Krebs-Henseleit Buffer containing (mM): 118.5 NaCl, 4.7 KCl, 1.2 KH_2PO_4, 1.2 $MgSO_4$, 11 Glucose, 25 $NaHCO_3$, 1.8 $CaCl_2$. A water-filled balloon connected to the pressure transducer was placed in the left ventricle to record left ventricular pressure. Size of the balloon was adjusted to make the end diastolic pressure under basal conditions around 10 mmHg. Two electrodes were attached to the atria and apex of the heart to record ECG (AD Instruments, Colorado Springs, CO). After stabilization, ECG and left ventricular pressure of the heart were recorded at basal condition for 10min. Following, the heart was perfused with the KH solution containing 300 nM isoproterenol. ECG and left ventricular pressure under isoproterenol stimulation were recorded for another 10min. Arrhythmic behavior, end

diastolic left ventricular pressure, left ventricular developed pressure (maximum systolic pressure-end diastolic pressure), and max dp/dt were analyzed by LabChart 8.

Echocardiography Transthoracic echocardiography (Echo) was performed using a Vevo 2100 system with a 22-55 MHz transducer (MS550D; Visual Sonics), as described previously (35). Mice were anesthetized by 5% isoflurane inhalation at the speed of 0.8-1 L/min, and maintained at anesthetized state by 1.5-2% isoflurane. Two-dimensionally guided M-mode images of the left ventricle (LV) were acquired at the tip of the papillary muscles. Posterior and anterior wall during systole and diastole, stroke volume, and heart rate were measured. Left ventricular mass was calculated by the formula [1.05 x ((Posterior $Wall_{diastole}$+Anterior $Wall_{diastole}$+LV $diameter_{diastole}$)^3 – (LV $diameter_{diastole}$)^3)]; fractional shortening was calculated by the formula [(LV $diameter_{diastole}$ –LV $diameter_{systole}$)/LV $diameter_{diastole}$] x 100.

Statistics All data are presented as mean$\pm$SEM. Student t test, rank-sum test, two-way repeated-measures ANOVA, Holm-Sidak test, χ^2 test, Kaplan-Meier test were carried when appropriate to determine statistical significance. $p < 0.05$ was considered statistically significant.

REFERENCE

1. Venes, D. 2009. *Taber's cyclopedic medical dictionary*: Davis Company, F. A.

2. Page, E. 1978. Quantitative ultrastructural analysis in cardiac membrane physiology. *Am J Physiol* 235:C147-158.

3. Page, E., McCallister, L.P., and Power, B. 1971. Sterological measurements of cardiac ultrastructures implicated in excitation-contraction coupling. *Proc Natl Acad Sci U S A* 68:1465-1466.

4. Kawai, M., Hussain, M., and Orchard, C.H. 1999. Excitation-contraction coupling in rat ventricular myocytes after formamide-induced detubulation. *Am J Physiol* 277:H603-609.

5. Levin, K.R., and Page, E. 1980. Quantitative studies on plasmalemmal folds and caveolae of rabbit ventricular myocardial cells. *Circ Res* 46:244-255.

6. Anderson, R.G. 1993. Caveolae: where incoming and outgoing messengers meet. *Proc Natl Acad Sci U S A* 90:10909-10913.

7. Catterall, W.A. 2000. Structure and regulation of voltage-gated Ca2+ channels. *Annu Rev Cell Dev Biol* 16:521-555.

8. Bers, D.M. 2001. *Excitation-Contraction Coupling and Cardiac Contractile Force*: Kluwer Academic Publishers.

9. Richard, S., Perrier, E., Fauconnier, J., Perrier, R., Pereira, L., Gomez, A.M., and Benitah, J.P. 2006. 'Ca(2+)-induced Ca(2+) entry' or how the L-type Ca(2+) channel remodels its own signalling pathway in cardiac cells. *Prog Biophys Mol Biol* 90:118-135.

10. Nayler, W.G., Daile, P., Chipperfield, D., and Gan, K. 1970. Effect of ryanodine on calcium in cardiac muscle. *Am J Physiol* 219:1620-1626.

11. Meissner, G. 1986. Ryanodine activation and inhibition of the Ca2+ release channel of sarcoplasmic reticulum. *J Biol Chem* 261:6300-6306.

12. Peng, W., Shen, H., Wu, J., Guo, W., Pan, X., Wang, R., Chen, S.R., and Yan, N. 2016. Structural basis for the gating mechanism of the type 2 ryanodine receptor RyR2. *Science* 354.

13. des Georges, A., Clarke, O.B., Zalk, R., Yuan, Q., Condon, K.J., Grassucci, R.A., Hendrickson, W.A., Marks, A.R., and Frank, J. 2016. Structural Basis for Gating and Activation of RyR1. *Cell* 167:145-157 e117.

14. Yan, Z., Bai, X., Yan, C., Wu, J., Li, Z., Xie, T., Peng, W., Yin, C., Li, X., Scheres, S.H.W., et al. 2015. Structure of the rabbit ryanodine receptor RyR1 at near-atomic resolution. *Nature* 517:50-55.

15. Fill, M., and Copello, J.A. 2002. Ryanodine receptor calcium release channels. *Physiol Rev* 82:893-922.

16. Capes, E.M., Loaiza, R., and Valdivia, H.H. 2011. Ryanodine receptors. *Skelet Muscle* 1:18.

17. Meissner, G., Rios, E., Tripathy, A., and Pasek, D.A. 1997. Regulation of skeletal muscle Ca2+ release channel (ryanodine receptor) by Ca2+ and monovalent cations and anions. *J Biol Chem* 272:1628-1638.

18. Loaiza, R., Benkusky, N.A., Powers, P.P., Hacker, T., Noujaim, S., Ackerman, M.J., Jalife, J., and Valdivia, H.H. 2013. Heterogeneity of ryanodine receptor dysfunction in a mouse model of catecholaminergic polymorphic ventricular tachycardia. *Circ Res* 112:298-308.

19. Fernandez-Velasco, M., Rueda, A., Rizzi, N., Benitah, J.P., Colombi, B., Napolitano, C., Priori, S.G., Richard, S., and Gomez, A.M. 2009. Increased Ca2+ sensitivity of the ryanodine receptor mutant RyR2R4496C underlies catecholaminergic polymorphic ventricular tachycardia. *Circ Res* 104:201-209, 212p following 209.

20. Jiang, D., Wang, R., Xiao, B., Kong, H., Hunt, D.J., Choi, P., Zhang, L., and Chen, S.R. 2005. Enhanced store overload-induced Ca2+ release and channel sensitivity to luminal Ca2+ activation are common defects of RyR2 mutations linked to ventricular tachycardia and sudden death. *Circ Res* 97:1173-1181.

21. Fabiato, A. 1985. Time and calcium dependence of activation and inactivation of calcium-induced release of calcium from the sarcoplasmic reticulum of a skinned canine cardiac Purkinje cell. *J Gen Physiol* 85:247-289.

22. Nabauer, M., and Morad, M. 1990. Ca2(+)-induced Ca2+ release as examined by photolysis of caged Ca2+ in single ventricular myocytes. *Am J Physiol* 258:C189-193.

23. Varro, A., Negretti, N., Hester, S.B., and Eisner, D.A. 1993. An estimate of the calcium content of the sarcoplasmic reticulum in rat ventricular myocytes. *Pflugers Arch* 423:158-160.

24. Shannon, T.R., Guo, T., and Bers, D.M. 2003. Ca2+ scraps: local depletions of free [Ca2+] in cardiac sarcoplasmic reticulum during contractions leave substantial Ca2+ reserve. *Circ Res* 93:40-45.

25. Tang, Y., Tian, X., Wang, R., Fill, M., and Chen, S.R. 2012. Abnormal termination of Ca2+ release is a common defect of RyR2 mutations associated with cardiomyopathies. *Circ Res* 110:968-977.

26. MacLennan, D.H., and Chen, S.R. 2009. Store overload-induced Ca2+ release as a triggering mechanism for CPVT and MH episodes caused by mutations in RYR and CASQ genes. *J Physiol* 587:3113-3115.

27. Ikemoto, N., Ronjat, M., Meszaros, L.G., and Koshita, M. 1989. Postulated role of calsequestrin in the regulation of calcium release from sarcoplasmic reticulum. *Biochemistry* 28:6764-6771.

28. Terentyev, D., Viatchenko-Karpinski, S., Gyorke, I., Volpe, P., Williams, S.C., and Gyorke, S. 2003. Calsequestrin determines the functional size and stability of cardiac intracellular calcium stores: Mechanism for hereditary arrhythmia. *Proc Natl Acad Sci U S A* 100:11759-11764.

29. Bers, D.M. 2002. Cardiac excitation-contraction coupling. *Nature* 415:198-205.

30. Zhou, P., Zhao, Y.T., Guo, Y.B., Xu, S.M., Bai, S.H., Lakatta, E.G., Cheng, H., Hao, X.M., and Wang, S.Q. 2009. Beta-adrenergic signaling accelerates and synchronizes cardiac ryanodine receptor response to a single L-type Ca2+ channel. *Proc Natl Acad Sci U S A* 106:18028-18033.

31. Shan, J., Kushnir, A., Betzenhauser, M.J., Reiken, S., Li, J., Lehnart, S.E., Lindegger, N., Mongillo, M., Mohler, P.J., and Marks, A.R. 2010. Phosphorylation of the ryanodine receptor mediates the cardiac fight or flight response in mice. *J Clin Invest* 120:4388-4398.

32. Wehrens, X.H., Lehnart, S.E., Reiken, S., Vest, J.A., Wronska, A., and Marks, A.R. 2006. Ryanodine receptor/calcium release channel PKA phosphorylation: a critical mediator of heart failure progression. *Proc Natl Acad Sci U S A* 103:511-518.

33. Marx, S.O., Reiken, S., Hisamatsu, Y., Jayaraman, T., Burkhoff, D., Rosemblit, N., and Marks, A.R. 2000. PKA phosphorylation dissociates FKBP12.6 from the calcium release channel (ryanodine receptor): defective regulation in failing hearts. *Cell* 101:365-376.

34. Lehnart, S.E., Terrenoire, C., Reiken, S., Wehrens, X.H., Song, L.S., Tillman, E.J., Mancarella, S., Coromilas, J., Lederer, W.J., Kass, R.S., et al. 2006. Stabilization of cardiac ryanodine receptor prevents intracellular calcium leak and arrhythmias. *Proc Natl Acad Sci U S A* 103:7906-7910.

35. Benkusky, N.A., Weber, C.S., Scherman, J.A., Farrell, E.F., Hacker, T.A., John, M.C., Powers, P.A., and Valdivia, H.H. 2007. Intact beta-adrenergic response and unmodified progression toward heart failure in mice with genetic ablation of a major protein kinase A phosphorylation site in the cardiac ryanodine receptor. *Circ Res* 101:819-829.

36. MacDonnell, S.M., Garcia-Rivas, G., Scherman, J.A., Kubo, H., Chen, X., Valdivia, H., and Houser, S.R. 2008. Adrenergic regulation of cardiac contractility does not involve phosphorylation of the cardiac ryanodine receptor at serine 2808. *Circ Res* 102:e65-72.

37. Alvarado, F.J., Chen, X., and Valdivia, H.H. 2017. Ablation of the cardiac ryanodine receptor phospho-site Ser2808 does not alter the adrenergic response or the progression to heart failure in mice. Elimination of the genetic background as critical variable. *J Mol Cell Cardiol* 103:40-47.

38. Valdivia, H.H., Kaplan, J.H., Ellis-Davies, G.C., and Lederer, W.J. 1995. Rapid adaptation of cardiac ryanodine receptors: modulation by Mg2+ and phosphorylation. *Science* 267:1997-2000.

39. Ginsburg, K.S., and Bers, D.M. 2004. Modulation of excitation-contraction coupling by isoproterenol in cardiomyocytes with controlled SR Ca2+ load and Ca2+ current trigger. *J Physiol* 556:463-480.

40. Ai, X., Curran, J.W., Shannon, T.R., Bers, D.M., and Pogwizd, S.M. 2005. Ca2+/calmodulin-dependent protein kinase modulates cardiac ryanodine receptor phosphorylation and sarcoplasmic reticulum Ca2+ leak in heart failure. *Circ Res* 97:1314-1322.

41. Curran, J., Hinton, M.J., Rios, E., Bers, D.M., and Shannon, T.R. 2007. Beta-adrenergic enhancement of sarcoplasmic reticulum calcium leak in cardiac myocytes is mediated by calcium/calmodulin-dependent protein kinase. *Circ Res* 100:391-398.

42. Valdivia, H.H. 2012. Ryanodine receptor phosphorylation and heart failure: phasing out S2808 and "criminalizing" S2814. *Circ Res* 110:1398-1402.

43. Priori, S.G., and Chen, S.R. 2011. Inherited dysfunction of sarcoplasmic reticulum Ca2+ handling and arrhythmogenesis. *Circ Res* 108:871-883.

44. Morotti, S., Grandi, E., Summa, A., Ginsburg, K.S., and Bers, D.M. 2012. Theoretical study of L-type Ca(2+) current inactivation kinetics during action potential repolarization and early afterdepolarizations. *J Physiol* 590:4465-4481.

45. Wehrens, X.H., Lehnart, S.E., Reiken, S.R., Deng, S.X., Vest, J.A., Cervantes, D., Coromilas, J., Landry, D.W., and Marks, A.R. 2004. Protection from cardiac arrhythmia through ryanodine receptor-stabilizing protein calstabin2. *Science* 304:292-296.

46. Lehnart, S.E., Mongillo, M., Bellinger, A., Lindegger, N., Chen, B.X., Hsueh, W., Reiken, S., Wronska, A., Drew, L.J., Ward, C.W., et al. 2008. Leaky Ca2+ release channel/ryanodine receptor 2 causes seizures and sudden cardiac death in mice. *J Clin Invest* 118:2230-2245.

47. Jiang, D., Xiao, B., Yang, D., Wang, R., Choi, P., Zhang, L., Cheng, H., and Chen, S.R. 2004. RyR2 mutations linked to ventricular tachycardia and sudden death reduce the threshold for store-overload-induced Ca2+ release (SOICR). *Proc Natl Acad Sci U S A* 101:13062-13067.

48. Yamamoto, T., Yano, M., Xu, X., Uchinoumi, H., Tateishi, H., Mochizuki, M., Oda, T., Kobayashi, S., Ikemoto, N., and Matsuzaki, M. 2008. Identification of target domains of the cardiac ryanodine receptor to correct channel disorder in failing hearts. *Circulation* 117:762-772.

49. Faggioni, M., Kryshtal, D.O., and Knollmann, B.C. 2012. Calsequestrin mutations and catecholaminergic polymorphic ventricular tachycardia. *Pediatr Cardiol* 33:959-967.

50. Liu, N., and Priori, S.G. 2008. Disruption of calcium homeostasis and arrhythmogenesis induced by mutations in the cardiac ryanodine receptor and calsequestrin. *Cardiovasc Res* 77:293-301.

51. Kubalova, Z., Terentyev, D., Viatchenko-Karpinski, S., Nishijima, Y., Gyorke, I., Terentyeva, R., da Cunha, D.N., Sridhar, A., Feldman, D.S., Hamlin, R.L., et al. 2005. Abnormal intrastore calcium signaling in chronic heart failure. *Proc Natl Acad Sci U S A* 102:14104-14109.

52. George, C.H. 2008. Sarcoplasmic reticulum Ca2+ leak in heart failure: mere observation or functional relevance? *Cardiovasc Res* 77:302-314.

53. Marks, A.R. 2002. Ryanodine receptors, FKBP12, and heart failure. *Front Biosci* 7:d970-977.

54. Lehnart, S.E., Wehrens, X.H., Reiken, S., Warrier, S., Belevych, A.E., Harvey, R.D., Richter, W., Jin, S.L., Conti, M., and Marks, A.R. 2005. Phosphodiesterase 4D deficiency in the ryanodine-receptor complex promotes heart failure and arrhythmias. *Cell* 123:25-35.

55. Respress, J.L., van Oort, R.J., Li, N., Rolim, N., Dixit, S.S., deAlmeida, A., Voigt, N., Lawrence, W.S., Skapura, D.G., Skardal, K., et al. 2012. Role of RyR2 phosphorylation at S2814 during heart failure progression. *Circ Res* 110:1474-1483.

56. Currie, S., Elliott, E.B., Smith, G.L., and Loughrey, C.M. 2011. Two candidates at the heart of dysfunction: The ryanodine receptor and calcium/calmodulin protein kinase II as potential targets for therapeutic intervention-An in vivo perspective. *Pharmacol Ther* 131:204-220.

57. Bers, D.M. 2012. Ryanodine receptor S2808 phosphorylation in heart failure: smoking gun or red herring. *Circ Res* 110:796-799.

58. Yang, J., Rothermel, B., Vega, R.B., Frey, N., McKinsey, T.A., Olson, E.N., Bassel-Duby, R., and Williams, R.S. 2000. Independent signals control expression of the calcineurin inhibitory proteins MCIP1 and MCIP2 in striated muscles. *Circ Res* 87:E61-68.

59. Lu, J., McKinsey, T.A., Nicol, R.L., and Olson, E.N. 2000. Signal-dependent activation of the MEF2 transcription factor by dissociation from histone deacetylases. *Proc Natl Acad Sci U S A* 97:4070-4075.

60. Gomez, A.M., Schuster, I., Fauconnier, J., Prestle, J., Hasenfuss, G., and Richard, S. 2004. FKBP12.6 overexpression decreases Ca2+ spark amplitude but enhances [Ca2+]i transient in rat cardiac myocytes. *Am J Physiol Heart Circ Physiol* 287:H1987-1993.

61. Gellen, B., Fernandez-Velasco, M., Briec, F., Vinet, L., LeQuang, K., Rouet-Benzineb, P., Benitah, J.P., Pezet, M., Palais, G., Pellegrin, N., et al. 2008. Conditional FKBP12.6 overexpression in mouse cardiac myocytes prevents triggered ventricular tachycardia through specific alterations in excitation-contraction coupling. *Circulation* 117:1778-1786.

62. Kettlewell, S., Most, P., Currie, S., Koch, W.J., and Smith, G.L. 2005. S100A1 increases the gain of excitation-contraction coupling in isolated rabbit ventricular cardiomyocytes. *J Mol Cell Cardiol* 39:900-910.

63. Most, P., Seifert, H., Gao, E., Funakoshi, H., Volkers, M., Heierhorst, J., Remppis, A., Pleger, S.T., DeGeorge, B.R., Jr., Eckhart, A.D., et al. 2006. Cardiac S100A1 protein levels determine contractile performance and propensity toward heart failure after myocardial infarction. *Circulation* 114:1258-1268.

64. Walsh, M.P. 1994. Calmodulin and the regulation of smooth muscle contraction. *Mol Cell Biochem* 135:21-41.

65. Protasi, F. 2002. Structural interaction between RYRs and DHPRs in calcium release units of cardiac and skeletal muscle cells. *Front Biosci* 7:d650-658.

66. Alvarado, F.J. 2017. Mechanisms of Ryanodine Receptor 2 Regulation in Cardiac Pathophysiology.

67. Fauci, A.S., Kasper, D.L., Braunwald, E., Hauser, S.L., Longo, D.L., Jameson, J.L., and Loscalzo, J. *Harrison's Principles of Internal Medicine, 17th Edition*.

68. Van der Bliek, A.M., Baas, F., Van der Velde-Koerts, T., Biedler, J.L., Meyers, M.B., Ozols, R.F., Hamilton, T.C., Joenje, H., and Borst, P. 1988. Genes amplified and overexpressed in human multidrug-resistant cell lines. *Cancer Res* 48:5927-5932.

69. Deng, L., Su, T., Leng, A., Zhang, X., Xu, M., Yan, L., Gu, H., and Zhang, G. 2010. Upregulation of soluble resistance-related calcium-binding protein (sorcin) in gastric cancer. *Med Oncol* 27:1102-1108.

70. Maddalena, F., Laudiero, G., Piscazzi, A., Secondo, A., Scorziello, A., Lombardi, V., Matassa, D.S., Fersini, A., Neri, V., Esposito, F., et al. 2011. Sorcin induces a drug-resistant phenotype in human colorectal cancer by modulating Ca(2+) homeostasis. *Cancer Res* 71:7659-7669.

71. Dabaghi, M., Rahgozar, S., Moshtaghian, J., Moafi, A., Abedi, M., and Pourabutaleb, E. 2016. Overexpression of SORCIN is a Prognostic Biomarker for Multidrug-Resistant Pediatric Acute Lymphoblastic Leukemia and Correlates with Upregulated MDR1/P-gp. *Genet Test Mol Biomarkers* 20:516-521.

72. Van der Bliek, A.M., Meyers, M.B., Biedler, J.L., Hes, E., and Borst, P. 1986. A 22-kd protein (sorcin/V19) encoded by an amplified gene in multidrug-resistant cells, is homologous to the calcium-binding light chain of calpain. *EMBO J* 5:3201-3208.

73. Colotti, G., Poser, E., Fiorillo, A., Genovese, I., Chiarini, V., and Ilari, A. 2014. Sorcin, a calcium binding protein involved in the multidrug resistance mechanisms in cancer cells. *Molecules* 19:13976-13989.

74. He, Q., Zhang, G., Hou, D., Leng, A., Xu, M., Peng, J., and Liu, T. 2011. Overexpression of sorcin results in multidrug resistance in gastric cancer cells with up-regulation of P-gp. *Oncol Rep* 25:237-243.

75. Kawakami, M., Nakamura, T., Okamura, N., Komoto, C., Markova, S., Kobayashi, H., Hashimoto, N., Okumura, K., and Sakaeda, T. 2007. Knock-down of sorcin induces up-regulation of MDR1 in HeLa cells. *Biol Pharm Bull* 30:1065-1073.

76. Meyers, M.B., Pickel, V.M., Sheu, S.S., Sharma, V.K., Scotto, K.W., and Fishman, G.I. 1995. Association of sorcin with the cardiac ryanodine receptor. *J Biol Chem* 270:26411-26418.

77. Marmugi, A., Parnis, J., Chen, X., Carmichael, L., Hardy, J., Mannan, N., Marchetti, P., Piemonti, L., Bosco, D., Johnson, P., et al. 2016. Sorcin Links Pancreatic beta-Cell Lipotoxicity to ER Ca2+ Stores. *Diabetes* 65:1009-1021.

78. Rueda, A., Song, M., Toro, L., Stefani, E., and Valdivia, H.H. 2006. Sorcin modulation of Ca2+ sparks in rat vascular smooth muscle cells. *J Physiol* 576:887-901.

79. Gracy, K.N., Clarke, C.L., Meyers, M.B., and Pickel, V.M. 1999. N-methyl-D-aspartate receptor 1 in the caudate-putamen nucleus: ultrastructural localization and co-expression with sorcin, a 22,000 mol. wt calcium binding protein. *Neuroscience* 90:107-117.

80. Ilari, A., Johnson, K.A., Nastopoulos, V., Verzili, D., Zamparelli, C., Colotti, G., Tsernoglou, D., and Chiancone, E. 2002. The crystal structure of the sorcin calcium binding domain provides a model of Ca2+-dependent processes in the full-length protein. *J Mol Biol* 317:447-458.

81. Ilari, A., Fiorillo, A., Poser, E., Lalioti, V.S., Sundell, G.N., Ivarsson, Y., Genovese, I., and Colotti, G. 2015. Structural basis of Sorcin-mediated calcium-dependent signal transduction. *Sci Rep* 5:16828.

82. Maki, M., Kitaura, Y., Satoh, H., Ohkouchi, S., and Shibata, H. 2002. Structures, functions and molecular evolution of the penta-EF-hand Ca2+-binding proteins. *Biochim Biophys Acta* 1600:51-60.

83. Xie, X., Dwyer, M.D., Swenson, L., Parker, M.H., and Botfield, M.C. 2001. Crystal structure of calcium-free human sorcin: a member of the penta-EF-hand protein family. *Protein Sci* 10:2419-2425.

84. Zamparelli, C., Ilari, A., Verzili, D., Vecchini, P., and Chiancone, E. 1997. Calcium- and pH-linked oligomerization of sorcin causing translocation from cytosol to membranes. *FEBS Lett* 409:1-6.

85. Colotti, G., Zamparelli, C., Verzili, D., Mella, M., Loughrey, C.M., Smith, G.L., and Chiancone, E. 2006. The W105G and W99G sorcin mutants demonstrate the role of the D helix in the Ca(2+)-dependent interaction with annexin VII and the cardiac ryanodine receptor. *Biochemistry* 45:12519-12529.

86. Farrell, E.F., Antaramian, A., Rueda, A., Gomez, A.M., and Valdivia, H.H. 2003. Sorcin inhibits calcium release and modulates excitation-contraction coupling in the heart. *J Biol Chem* 278:34660-34666.

87. Meyers, M.B., Fischer, A., Sun, Y.J., Lopes, C.M., Rohacs, T., Nakamura, T.Y., Zhou, Y.Y., Lee, P.C., Altschuld, R.A., McCune, S.A., et al. 2003. Sorcin regulates excitation-contraction coupling in the heart. *J Biol Chem* 278:28865-28871.

88. Lokuta, A.J., Meyers, M.B., Sander, P.R., Fishman, G.I., and Valdivia, H.H. 1997. Modulation of cardiac ryanodine receptors by sorcin. *J Biol Chem* 272:25333-25338.

89. Matsumoto, T., Hisamatsu, Y., Ohkusa, T., Inoue, N., Sato, T., Suzuki, S., Ikeda, Y., and Matsuzaki, M. 2005. Sorcin interacts with sarcoplasmic reticulum Ca(2+)-ATPase and modulates excitation-contraction coupling in the heart. *Basic Res Cardiol* 100:250-262.

90. Seidler, T., Miller, S.L., Loughrey, C.M., Kania, A., Burow, A., Kettlewell, S., Teucher, N., Wagner, S., Kogler, H., Meyers, M.B., et al. 2003. Effects of adenovirus-mediated sorcin overexpression on excitation-contraction coupling in isolated rabbit cardiomyocytes. *Circ Res* 93:132-139.

91. Zamparelli, C., Macquaide, N., Colotti, G., Verzili, D., Seidler, T., Smith, G.L., and Chiancone, E. 2010. Activation of the cardiac Na(+)-Ca(2+) exchanger by sorcin via the interaction of the respective Ca(2+)-binding domains. *J Mol Cell Cardiol* 49:132-141.

92. Fowler, M.R., Colotti, G., Chiancone, E., Smith, G.L., and Fearon, I.M. 2008. Sorcin modulates cardiac L-type Ca2+ current by functional interaction with the alpha1C subunit in rabbits. *Exp Physiol* 93:1233-1238.

93. Fowler, M.R., Colotti, G., Chiancone, E., Higuchi, Y., Seidler, T., and Smith, G.L. 2009. Complex modulation of L-type Ca(2+) current inactivation by sorcin in isolated rabbit cardiomyocytes. *Pflugers Arch* 457:1049-1060.

94. Suarez, J., Belke, D.D., Gloss, B., Dieterle, T., McDonough, P.M., Kim, Y.K., Brunton, L.L., and Dillmann, W.H. 2004. In vivo adenoviral transfer of sorcin reverses cardiac contractile abnormalities of diabetic cardiomyopathy. *Am J Physiol Heart Circ Physiol* 286:H68-75.

95. Frank, K.F., Bolck, B., Ding, Z., Krause, D., Hattebuhr, N., Malik, A., Brixius, K., Hajjar, R.J., Schrader, J., and Schwinger, R.H. 2005. Overexpression of sorcin enhances cardiac contractility in vivo and in vitro. *J Mol Cell Cardiol* 38:607-615.

96. Takahashi, K., Ishikawa, T., Makita, N., Takefuta, K., Nabeshima, T., and Nakayashiro, M. 2017. A novel de novo calmodulin mutation in a 6-year-old boy who experienced an aborted cardiac arrest. *HeartRhythm Case Rep* 3:69-72.

97. Rohde, D., Busch, M., Volkert, A., Ritterhoff, J., Katus, H.A., Peppel, K., and Most, P. 2015. Cardiomyocytes, endothelial cells and cardiac fibroblasts: S100A1's triple action in cardiovascular pathophysiology. *Future Cardiol* 11:309-321.

98. Song, L., Alcalai, R., Arad, M., Wolf, C.M., Toka, O., Conner, D.A., Berul, C.I., Eldar, M., Seidman, C.E., and Seidman, J.G. 2007. Calsequestrin 2 (CASQ2) mutations increase expression of calreticulin and ryanodine receptors, causing catecholaminergic polymorphic ventricular tachycardia. *J Clin Invest* 117:1814-1823.

99. Yamaguchi, N., Takahashi, N., Xu, L., Smithies, O., and Meissner, G. 2007. Early cardiac hypertrophy in mice with impaired calmodulin regulation of cardiac muscle Ca release channel. *J Clin Invest* 117:1344-1353.

100. Medeiros-Domingo, A., Bhuiyan, Z.A., Tester, D.J., Hofman, N., Bikker, H., van Tintelen, J.P., Mannens, M.M., Wilde, A.A., and Ackerman, M.J. 2009. The RYR2-encoded ryanodine receptor/calcium release channel in patients diagnosed previously with either catecholaminergic polymorphic ventricular tachycardia or genotype negative, exercise-induced long QT syndrome: a comprehensive open reading frame mutational analysis. *J Am Coll Cardiol* 54:2065-2074.

101. Smith, G.L., Elliott, E.E., Kettlewell, S., Currie, S., and Quinn, F.R. 2006. Na(+)/Ca(2+) exchanger expression and function in a rabbit model of myocardial infarction. *J Cardiovasc Electrophysiol* 17 Suppl 1:S57-S63.

102. Franceschini, S., Ilari, A., Verzili, D., Zamparelli, C., Antaramian, A., Rueda, A., Valdivia, H.H., Chiancone, E., and Colotti, G. 2008. Molecular basis for the impaired function of the natural F112L sorcin mutant: X-ray crystal structure, calcium affinity, and interaction with annexin VII and the ryanodine receptor. *FASEB J* 22:295-306.

103. Valdivia, H.H., Farrell, E.F., Antaramian, A., Benkusky, N., Zhu, X., Rueda, A., and Gomez, A.M. 2004. Sorcin and ryanodine receptors in heart failure. *J Muscle Res Cell Motil* 25:605-607.

104. Suarez, J., McDonough, P.M., Scott, B.T., Suarez-Ramirez, A., Wang, H., Fricovsky, E.S., and Dillmann, W.H. 2013. Sorcin modulates mitochondrial Ca(2+) handling and reduces apoptosis in neonatal rat cardiac myocytes. *Am J Physiol Cell Physiol* 304:C248-256.

105. Wilkins, B.J., Dai, Y.S., Bueno, O.F., Parsons, S.A., Xu, J., Plank, D.M., Jones, F., Kimball, T.R., and Molkentin, J.D. 2004. Calcineurin/NFAT coupling participates in pathological, but not physiological, cardiac hypertrophy. *Circ Res* 94:110-118.

106. Chen, X., Valdivia, R.C., Weber, C., Riva, G.G., Powers, P.A., and Valdivia, H.H. 2014. Enhanced sodium-calcium exchanger current, prolonged action potential duration, and early/delayed-afterdepolarization in sorcin knockout heart. *Circulation* 130:A13891-A13891.

107. Chen, X., Valdivia, R.C., Weber, C., Riva, G.G., Powers, P.A., and Valdivia, H.H. 2013. Increased spontaneous Ca2+ release events and Na+-Ca2+ exchanger activity induce ventricular arrhythmias in sorcin-knockout mice under beta-adrenergic stimulation. *Circulation* 128:A11390-A11390.

108. deAlmeida, A.C., van Oort, R.J., and Wehrens, X.H. 2010. Transverse aortic constriction in mice. *J Vis Exp*.

109. Cerrone, M., Colombi, B., Santoro, M., di Barletta, M.R., Scelsi, M., Villani, L., Napolitano, C., and Priori, S.G. 2005. Bidirectional ventricular tachycardia and fibrillation elicited in a knock-in mouse model carrier of a mutation in the cardiac ryanodine receptor. *Circ Res* 96:e77-82.

110. Takenaka, H., Adler, P.N., and Katz, A.M. 1982. Calcium fluxes across the membrane of sarcoplasmic reticulum vesicles. *J Biol Chem* 257:12649-12656.

111. Feher, J.J., and Briggs, F.N. 1984. Undirectional calcium and nucleotide fluxes in cardiac sarcoplasmic reticulum. II. Experimental results. *Biophys J* 45:1135-1144.

112. Bassani, R.A., and Bers, D.M. 1995. Rate of diastolic Ca release from the sarcoplasmic reticulum of intact rabbit and rat ventricular myocytes. *Biophys J* 68:2015-2022.

113. Shannon, T.R., Ginsburg, K.S., and Bers, D.M. 2000. Reverse mode of the sarcoplasmic reticulum calcium pump and load-dependent cytosolic calcium decline in voltage-clamped cardiac ventricular myocytes. *Biophys J* 78:322-333.

114. Shannon, T.R. 2002. Quantitative Assessment of the SR Ca2+ Leak-Load Relationship. *Circulation Research* 91:594-600.

115. Rodriguez, J.S., Velez Rueda, J.O., Salas, M., Becerra, R., Di Carlo, M.N., Said, M., Vittone, L., Rinaldi, G., Portiansky, E.L., Mundina-Weilenmann, C., et al. 2014. Increased Na(+)/Ca(2)(+) exchanger expression/activity constitutes a point of inflection in the progression to heart failure of hypertensive rats. *PLoS One* 9:e96400.

116. Schlotthauer, K., and Bers, D.M. 2000. Sarcoplasmic reticulum Ca(2+) release causes myocyte depolarization. Underlying mechanism and threshold for triggered action potentials. *Circ Res* 87:774-780.

117. Weiss, J.N., Garfinkel, A., Karagueuzian, H.S., Chen, P.S., and Qu, Z. 2010. Early afterdepolarizations and cardiac arrhythmias. *Heart Rhythm* 7:1891-1899.

118. Madhvani, R.V., Angelini, M., Xie, Y., Pantazis, A., Suriany, S., Borgstrom, N.P., Garfinkel, A., Qu, Z., Weiss, J.N., and Olcese, R. 2015. Targeting the late component of the cardiac L-type Ca2+ current to suppress early afterdepolarizations. *J Gen Physiol* 145:395-404.

119. Zhao, Y.T., Valdivia, C.R., Gurrola, G.B., Powers, P.P., Willis, B.C., Moss, R.L., Jalife, J., and Valdivia, H.H. 2015. Arrhythmogenesis in a catecholaminergic polymorphic ventricular tachycardia mutation that depresses ryanodine receptor function. *Proc Natl Acad Sci U S A* 112:E1669-1677.

120. Nerbonne, J.M., Nichols, C.G., Schwarz, T.L., and Escande, D. 2001. Genetic manipulation of cardiac K(+) channel function in mice: what have we learned, and where do we go from here? *Circ Res* 89:944-956.

121. Xu, M., Zhou, P., Xu, S.M., Liu, Y., Feng, X., Bai, S.H., Bai, Y., Hao, X.M., Han, Q., Zhang, Y., et al. 2007. Intermolecular failure of L-type Ca2+ channel and ryanodine receptor signaling in hypertrophy. *PLoS Biol* 5:e21.

122. Edwards, A.G., Grandi, E., Hake, J.E., Patel, S., Li, P., Miyamoto, S., Omens, J.H., Heller Brown, J., Bers, D.M., and McCulloch, A.D. 2014. Nonequilibrium reactivation of Na+ current drives early afterdepolarizations in mouse ventricle. *Circ Arrhythm Electrophysiol* 7:1205-1213.

123. Cannell, M.B., Kong, C.H., Imtiaz, M.S., and Laver, D.R. 2013. Control of sarcoplasmic reticulum Ca2+ release by stochastic RyR gating within a 3D model of the cardiac dyad and importance of induction decay for CICR termination. *Biophys J* 104:2149-2159.

124. Zhao, Y.T., and Valdivia, H.H. 2014. Ca2+ nanosparks: shining light on the dyadic cleft but missing the intensity of its signal. *Circ Res* 114:396-398.

125. Meyers, M.B., Puri, T.S., Chien, A.J., Gao, T., Hsu, P.H., Hosey, M.M., and Fishman, G.I. 1998. Sorcin associates with the pore-forming subunit of voltage-dependent L-type Ca2+ channels. *J Biol Chem* 273:18930-18935.

126. Ter Keurs, H.E., and Boyden, P.A. 2007. Calcium and arrhythmogenesis. *Physiol Rev* 87:457-506.

127. Snopko, R.M., Ramos-Franco, J., Di Maio, A., Karko, K.L., Manley, C., Piedras-Renteria, E., and Mejia-Alvarez, R. 2008. Ca2+ sparks and cellular distribution of ryanodine receptors in developing cardiomyocytes from rat. *J Mol Cell Cardiol* 44:1032-1044.

128. Giles, T.D., and Sander, G.E. 2004. Diabetes mellitus and heart failure: basic mechanisms, clinical features, and therapeutic considerations. *Cardiol Clin* 22:553-568.

129. Jian, C., Hou, T., Yin, R., Cheng, H., and Wang, X. 2014. Regulation of superoxide flashes by transient and steady mitochondrial calcium elevations. *Sci China Life Sci* 57:495-501.

130. Chen, X., Weber, C., Farrell, E.T., Alvarado, F.J., Zhao, Y.T., Gomez, A.M., and Valdivia, H.H. 2017. Sorcin ablation plus beta-adrenergic stimulation generate an arrhythmogenic substrate in mouse ventricular myocytes. *J Mol Cell Cardiol* 114:199-210.